INFORMATION TO USERS

This manuscript has been reproduced from the microfilm master. UMI films the text directly from the original or copy submitted. Thus, some thesis and dissertation copies are in typewriter face, while others may be from any type of computer printer.

The quality of this reproduction is dependent upon the quality of the copy submitted. Broken or indistinct print, colored or poor quality illustrations and photographs, print bleedthrough, substandard margins, and improper alignment can adversely affect reproduction.

In the unlikely event that the author did not send UMI a complete manuscript and there are missing pages, these will be noted. Also, if unauthorized copyright material had to be removed, a note will indicate the deletion.

Oversize materials (e.g., maps, drawings, charts) are reproduced by sectioning the original, beginning at the upper left-hand corner and continuing from left to right in equal sections with small overlaps. Each original is also photographed in one exposure and is included in reduced form at the back of the book.

Photographs included in the original manuscript have been reproduced xerographically in this copy. Higher quality 6" x 9" black and white photographic prints are available for any photographs or illustrations appearing in this copy for an additional charge. Contact UMI directly to order.

Role of atomic hydrogen during hot filament assisted chemical vapor deposition of diamond

Tankala, Kanishka, Ph.D.

The Pennsylvania State University, 1994

The Pennsylvania State University

The Graduate School

Department of Materials Science and Engineering

ROLE OF ATOMIC HYDROGEN DURING HOT FILAMENT
ASSISTED CHEMICAL VAPOR DEPOSITION OF DIAMOND

A Thesis in

Metals Science and Engineering

by

Kanishka Tankala

Submitted in Partial Fulfillment
of the Requirements
for the Degree of

Doctor of Philosophy

May 1994

We approve the thesis of Kanishka Tankala.

Date of signature

Tarasankar DebRoy
Tarasankar DebRoy
Professor of Materials Science and Engineering
Thesis Advisor
Chair of Committee

21 March 1994

Lee Cuddy
Lee Cuddy
Associate Professor of Metallurgy

21 March 1994

Russell Messier
Russell Messier
Professor of Engineering Science and Mechanics
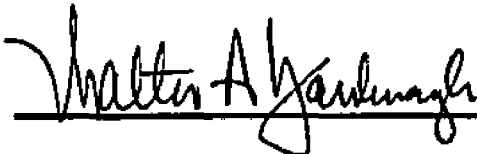
21 March 1994

Walter A. Yarbrough
Walter A. Yarbrough
Assistant Professor of Ceramics Science and Engineering

21 March 1994

Donald A. Koss
Donald A. Koss
Professor of Metallurgy
In Charge of Graduate Programs in
    Metals Science and Engineering

March 21, 1994

ABSTRACT

The importance of atomic hydrogen in the chemical vapor deposition of diamond has been well recognized. Much of the previous work on the role of atomic hydrogen in low pressure diamond growth has been focussed on its formation on various refractory filaments, its reaction in the gas phase and its role in the growth mechanism. In this work, the role of atomic hydrogen in heat transfer and in influencing the stability of diamond and graphite surfaces has been examined.

In hot filament assisted chemical vapor deposition of diamond, the mechanism of heat transfer is unique. In addition to conduction, convection and radiation, filament to substrate heat transfer takes place by dissociation of molecular hydrogen at the filament and recombination of atomic hydrogen at the substrate surface. The temperature and atomic hydrogen concentration profiles in a hot filament type diamond deposition reactor were determined experimentally and theoretically to demonstrate that the reaction of atomic hydrogen on the substrate surface plays an important role in the heating of the substrate. For a given filament temperature, the substrate temperature in helium was significantly lower than that in pure hydrogen or 1% methane-hydrogen atmospheres. The presence of small amounts of methane did not have any significant effect in influencing the shape of the atomic hydrogen concentration profile. In the space between the filament and the substrate, the concentration field is established primarily due to diffusive mixing of atomic hydrogen with molecular hydrogen and other species in the gas phase. Homogeneous chemical reactions in the gas phase do not significantly affect the spatial distribution of atomic hydrogen.

Experiments were done in a hot filament diamond deposition reactor to examine the effect of various process parameters on the atomic hydrogen generation rate and the substrate temperature. A mathematical model to calculate fluid flow and heat transfer in the reactor taking into account substrate heating due to atomic hydrogen recombination in addition to conduction, convection and radiation from the filament has been developed. Model predictions of the substrate temperature have been experimentally verified. The results indicate that the dissociation of molecular hydrogen to atomic hydrogen does not attain equilibrium at the filament. Furthermore, in hot filament diamond deposition reactors, system geometry, filament temperature and pressure are the most important factors in determining the substrate temperature distribution.

The free energies of bulk diamond and graphite do not explain the formation of diamond, with simultaneous gasification of graphite, at low pressures and temperatures encountered in chemical vapor deposition. Since the structure and composition of diamond and graphite surfaces are significantly different from the bulk, and diamond growth occurs at the gas-solid interface in the presence of atomic hydrogen, the stability of diamond relative to graphite was examined using surface free energies of formation rather than bulk free energies of formation. The enthalpies and entropies of formation of diamond and graphite surfaces were estimated from principles of group additivity and bond energy contributions. The influence of atomic hydrogen on the stability of diamond and graphite surfaces was examined. The results indicate that a super-equilibrium concentration of atomic hydrogen at the substrate stabilizes the diamond surface relative to graphite surface. The predictions are consistent with several experimentally observed trends in low pressure diamond growth.

TABLE OF CONTENTS

LIST OF FIGURES

Figure   Page

LIST OF TABLES

ACKNOWLEDGMENTS

I am extremely grateful to my thesis advisor, Dr. Tarasankar DebRoy, for his valuable guidance, encouragement and suggestions during the course of this investigation. I deeply appreciate the valuable advice and suggestions of Drs. W. A. Yarbrough and R. Messier. I wish to thank Dr. L. Cuddy for the time, effort and advice while serving on my thesis committee. I also wish to thank the faculty, staff and fellow students for their help and support. My sincere thanks to my parents, brothers and other members of my family for their love and guidance throughout my life. My special thanks to Kamlesh Mundra for his friendly advice and support.

Chapter 1

INTRODUCTION

1.1 Chemical Vapor Deposition of Diamond

The pioneering efforts of Eversole [1], Angus et al. [2, 3], Deryagin and others [4, 5] have led to the deposition of well crystallized diamond at low pressures from the vapor phase. Although chemical vapor deposition (CVD) of diamond was demonstrated by these scientists, the early synthetic routes, involving hydrocarbon gases, resulted in the formation of diamond with a poor crystallinity and significant co-deposition of non-diamond carbon. Furthermore, the continued growth of diamond required alternating the deposition step with an etching step to remove the graphitic co-deposits. In subsequent work, Deryagin and co-workers [4] demonstrated that the use of dilute mixtures of methane in hydrogen as feed gas and activating the gas prior to deposition, to produce significant concentrations of atomic hydrogen, markedly increased the deposition rates. In addition, the co-deposition of non-diamond carbon was substantially reduced allowing continuous deposition of diamond.

In the last decade, several methods such as plasma assisted CVD, hot filament CVD, reactive vapor deposition and various combinations of these, have been used to deposit polycrystalline diamond films from dilute mixtures of hydrocarbons in hydrogen [6-10]. Each method employs a unique technique of gas phase activation to achieve considerable production of radical species, notably atomic hydrogen. Although there is some controversy over the nature of the hydrocarbon species [11-13] important for growth, there

is a general consensus in recognizing the importance of atomic hydrogen in the growth process. To date, most of the methods for diamond deposition depend on a supply of atomic hydrogen. However, researchers at Rice University showed in recent experiments [14] that diamond can be deposited from fluorine, hydrogen and various hydrocarbons, without any significant production of atomic hydrogen. In a later experiment [15], they also showed that diamond can also be deposited from carbon disulfide and fluorine without the use of hydrogen in any form. However, these techniques have not yet yielded films whose quality is comparable to other contemporary CVD techniques, and all popular deposition methods still rely on the production of significant concentrations of atomic hydrogen to achieve good quality diamond films at practical rates.

1.2 Hot Filament Assisted Chemical Vapor Deposition

Among the various techniques employed to deposit diamond films, the hot filament assisted chemical vapor deposition (HFCVD) has received world wide attention due to its relative simplicity and low set-up cost. In HFCVD, the activation of the gas, i.e. the generation of hydrocarbon radicals and atomic hydrogen, is achieved by heating refractory metal filaments such as W, Ta or Re to temperatures in excess of 2000 °C. Although the use of W filaments for the generation of atomic hydrogen was mentioned by Deryagin and co-workers [4], Matsumoto et al. [16, 17] were the first to document a detailed description of the hot filament technique. These papers provided information on the effect of various process parameters on the growth rate and quality of diamond films and became the basis of all future hot filament work.

In a typical hot filament system, shown in Figure 1.1, the filament is heated to a temperature in the range of 2000-2300 °C. The substrate to be coated is placed within a centimeter of the filament and is maintained within a temperature range of 800-1000 °C. The diamond films are deposited on the substrates from dilute mixtures of hydrocarbons in hydrogen at a system pressure of the order of tens of Torr. Typically, the substrates are pretreated by scratching the surface with sub-micron size diamond grit to facilitate nucleation [18]. A variety of hydrocarbon gases have been used to deposit diamond films with comparable success [19], indicating that the nature of the hydrocarbon in the feed gas is relatively unimportant. Addition of small amounts of oxygen in the form of pure oxygen [20], oxygen containing hydrocarbons [21] and water vapor [22] has been shown to improve the quality as well as growth rate of the diamond films. However, only a small concentration of oxygen can be introduced without oxidation of the filament. The oxygen addition experiments are better suited to plasma assisted CVD processes for preparing diamond.

Although the hot filament technique is relatively simple to use and can be scaled up to obtain uniform deposits over large areas, it has its share of problems. First, diamond films deposited by HFCVD have small amounts of filament material which is undesirable particularly, for optical and electronic applications. In one attempt to overcome this problem carbon rods have been used in place of refractory metal filaments to grow diamond [23]. However, when carbon rods were used the generation of atomic hydrogen and diamond growth rates were lower than when metal filaments were used [23]. Second, at high temperatures the filaments do not hold their shape very well. Furthermore, most refractory metals in contact with carbonaceous gases at elevated temperatures form carbides [24]. This results in some volume expansion and embrittlement of the filament which leads to

THERMOCOUPLE

PUMP

46

QUARTZ SAMPLE
HOLDER

27

GRAPHITE
SUSCEPTOR

10

SILICON
SUBSTRATE

Ta RING
φ18

260

6

CH$_4$ + H$_2$

50

PRESSURE GAUGE
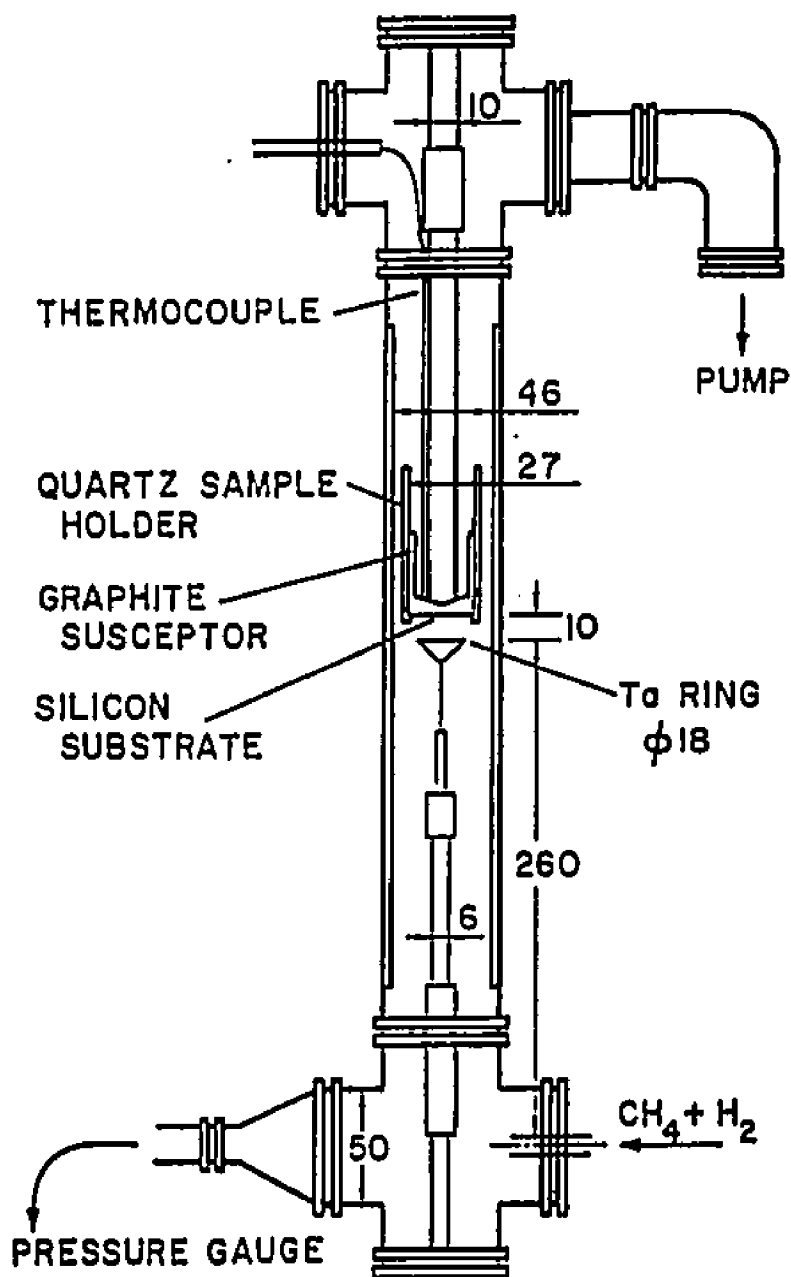
Fig. 1.1 Schematic diagram of a hot filament assisted chemical vapor deposition reactor for
diamond growth. Typical diamond deposition conditions are 30 Torr pressure, 2500 K
filament temperature, 1200 K substrate temperature, 200 sccm gas flow rate, 1% CH$_4$-H$_2$
feed gas composition and 10 mm filament to substrate distance.

subsequent warpage and breakage. In addition, the filament to substrate distance may change and become spatially non-uniform during the process, causing ill-defined growth conditions. Several practical improvements to the hot filament system, such as spring loading the filament to accommodate expansion and warpage, have been used to alleviate the problem.

Various methods are now available for the deposition of good quality diamond films. However, it is believed that the methods differ only in the technique used for gas activation, and there is a common mechanism for the growth process [6]. Unlike plasma assisted processes, where the growth environment consists of ions, electrons, excited species, neutral radicals, atoms and molecules, the growth environment in a hot filament reactor has primarily neutral radicals, atoms and molecules. Thus, at least in this respect, the hot filament system is less complex and has been widely used to understand the growth mechanism and various physical and chemical phenomena occurring during the growth process. By combining carefully designed experiments with fluid flow, heat transfer and chemical kinetic models significant insight has been gained into the diamond CVD process.

1.3 Role of Atomic Hydrogen in Diamond CVD

A major breakthrough in developing the science and technology of low pressure diamond synthesis occurred when Deryagin and co-workers [4] discovered that using excess hydrogen in the deposition gas and activating the gas prior to deposition resulted in significant reduction in the co-deposition of non-diamond carbon and higher growth rates. Several factors have been suggested to explain the role of hydrogen dilution. First, and probably the most popular, is the preferential etching of graphite over diamond by

hydrogen atoms [2, 5, 9, 25, 26]. Deryagin and Fedoseev [4] proposed that the presence of a super-equilibrium concentration of atomic hydrogen at the growth surface is responsible for the reduction in the co-deposition of non-diamond phases. Their studies of the relative etch rates of diamond and graphite showed that the etching of graphite by activated hydrogen was orders of magnitude larger than that for diamond. Angus et al. [2] also showed that molecular hydrogen would thermally etch graphite about 500 times faster than diamond.

The second frequently discussed [9, 25] effect of hydrogen is that it satisfies the dangling bonds of surface carbon atoms during growth, keeping them in sp^3 configuration and thus preventing the diamond surface from reconstructing into graphitic, sp^2 or carbynic, sp, structures. Atomic hydrogen is also believed to aid in the formation of various hydrocarbon species, such as CH_3 and C_2H_2, which are considered to be important for diamond growth [11-13]. Hydrogen molecules suppress the formation of polycyclic aromatic hydrocarbons in the gas phase which otherwise leads to the deposition of non-diamond carbon phases [27]. Atomic hydrogen also helps in generating new growth sites, where hydrocarbon species can be added, by abstracting hydrogen atoms bonded to surface carbon atoms [9]. Although various roles have been assigned to atomic hydrogen, significant amount of work is still underway to fully understand its importance in the growth process.

The formation of atomic hydrogen at the filament surface is highly endothermic. Atomic hydrogen readily recombines on solid surfaces to form molecular hydrogen and the recombination reaction is highly exothermic. Thus, atomic hydrogen acts as a carrier of heat from the filament to the growth surface. In the previous work, the concentrations of

atomic hydrogen and hydrocarbon species such as CH_3 and C_2H_2 in the gas phase have been measured by various techniques such as infrared absorption spectroscopy [28], laser induced fluorescence [29], mass spectroscopy [30-32] and catalytic probes [33]. Much of the work was undertaken to develop a better understanding of the role of atomic hydrogen in gas phase chemistry, gas surface reactions and growth mechanism. However, none of the previous work was aimed at the investigation of the role of atomic hydrogen in affecting the substrate temperature.

1.4 Stability of Diamond vs. Graphite

Since 1797, when Tennant first established experimentally that diamond is a crystalline form of carbon [34] there has been significant interest in determining the thermodynamic stability of diamond and to synthesize diamond in the laboratory. Many of the early attempts to synthesize diamond involved simulation of the high temperature and pressure conditions encountered in the earth's crust where diamond forms naturally. For a historical perspective of the events that led to the development of the pressure-temperature phase diagram of carbon and the current high pressure and high temperature (HPHT) synthesis of diamond, the reader is referred to an excellent review article by Bundy, Strong and Wentorf [34].

Figure 1.2 shows the pressure temperature phase diagram of elemental carbon as understood today [34]. The solid line at lower temperatures and relatively low pressures represents the graphite-diamond equilibrium line determined from the experimentally measured heats of formation of diamond and graphite [35]. The dashed line is the Berman-Simon linear extrapolation [36] of the equilibrium line. The "V-notch" regions in Fig. 1.2
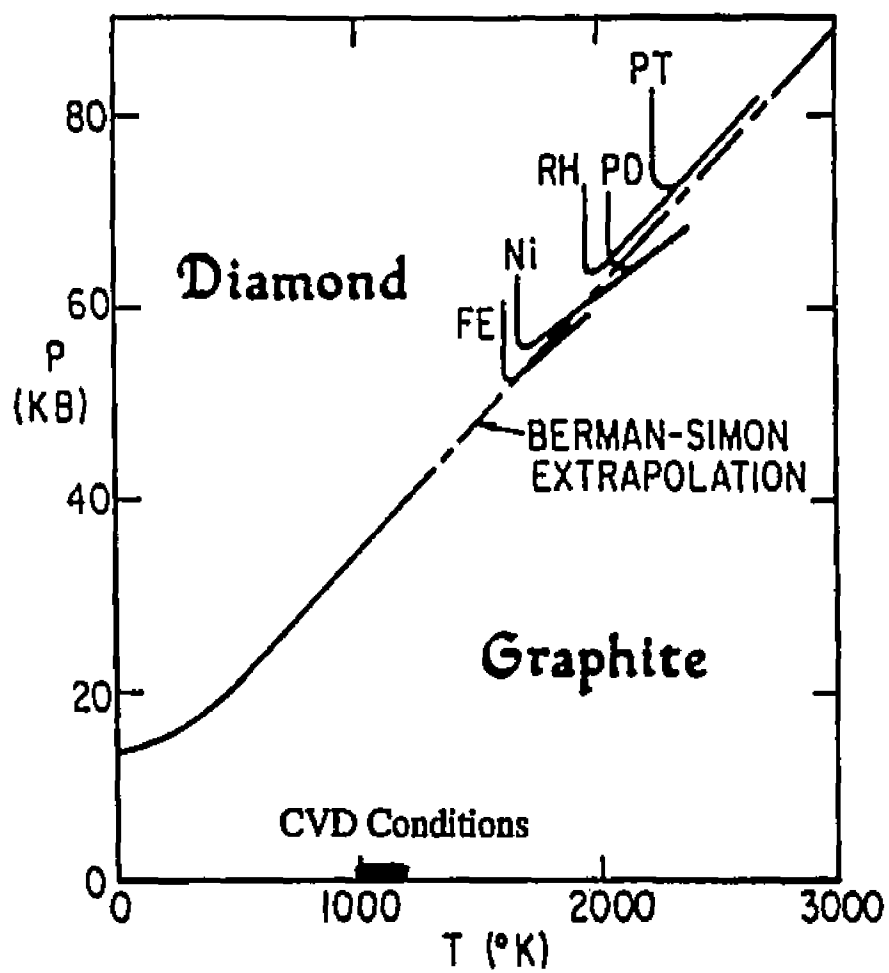
Fig. 1.2 Pressure-temperature phase diagram for elemental carbon [34].

represent diamond growth regions for different catalyst-solvent metals. The conditions under which CVD diamond is deposited is also marked in the figure. Clearly, diamond growth by HPHT technique is achieved under conditions where diamond is the thermodynamically stable phase. In contrast, vapor deposited diamond is obtained under conditions where graphite is the expected stable phase. In CVD, the vapor phase is in a high free energy state and the deposition of any form of solid carbon, diamond or graphite, has a negative free energy change and poses no thermodynamic problem. The experiment that has intrigued several researchers is that in which diamond was deposited with the simulaneous gasification of graphite [37]. The net reaction for the process being

$$C(graphite) = C(diamond) \qquad\qquad 1.1$$

Equation 1.1 has a positive free energy change and conflicts with the accepted phase diagram for carbon shown in Fig. 1.2. Thus, it becomes necessary to understand why the stable phase should be consumed and the metastable phase deposited under typical diamond deposition conditions.

Why should well-crystallized diamond form with simultaneous gasification of graphite at low pressures and relatively low temperatures where graphite is the expected stable phase? Although a unified mechanistic answer is not yet available, many of the suggested ideas assign a role to atomic hydrogen and particularly its presence in the gas phase at super-equilibrium concentrations. One argument [5,9,25] suggests that diamond growth is kinetically stable relative to graphite because graphite is more reactive to atomic hydrogen and the presence of super-equilibrium concentrations of atomic hydrogen suppresses the nucleation and growth of graphitic material. An alternative argument emphasizes the role of

atomic hydrogen in stabilizing the surfaces of diamond [6]. The heart of this hypothesis rests on the fact that diamond growth occurs at the gas-solid interface in the carbon-hydrogen system. The vapor growth process does not involve just elemental carbon, the one component which is represented in the phase diagram presented in Figure 1.2, but it also involves hydrogen. Thus, to understand the growth of diamond from the vapor phase, the relative stability of diamond and graphite surfaces, not the bulk forms, in the presence of atomic hydrogen should be examined.

1.5 Statement of Objectives

The overall objective of this study is to seek improved understanding of the role of atomic hydrogen in the hot filament assisted chemical vapor deposition of diamond. More specifically, the goals are to examine the importance of atomic hydrogen (a) in filament to substrate heat transfer and the resulting substrate temperature distribution, and (b) in determining the relative stability of diamond and graphite at the growth surface.

The formation of atomic hydrogen at the filament surface is highly endothermic. Atomic hydrogen readily recombines on solid surfaces to form molecular hydrogen and the recombination reaction is highly exothermic. Thus, atomic hydrogen acts as a carrier of heat from the filament to the growth surface and aids in substrate heating. Furthermore, the spatial distribution of atomic hydrogen plays an important role in determining the substrate temperature distribution. Understanding the factors that influence the spatial distribution of atomic hydrogen is important for modeling atomic hydrogen concentration profiles for various reactor geometries and operating conditions. Such knowledge will enable us to model the heat transfer and fluid flow in hot filament reactors and help us in understanding

the role of various process parameters and reactor geometry in determining the substrate temperature.

The role of atomic hydrogen in heat transfer in hot filament assisted chemical vapor deposition of diamond was investigated both experimentally and theoretically. The specific questions and issues addressed are: How important is atomic hydrogen recombination at the substrate surface in substrate heating? What are the roles of heat transfer by conduction, convection and radiation? What factors influence the spatial distribution of atomic hydrogen in the reactor? How do various process parameters affect the substrate temperature? How can we model heat transfer due to atomic hydrogen recombination in addition to conduction, convection, and radiation? Can the model predict the experimentally observed effect of process parameters on the substrate temperature?

The pressure-temperature phase diagram for elemental carbon, shown in Figure 1.2, indicates that vapor deposited diamond is obtained under conditions where graphite is the stable phase. This diagram is constructed for a single component, viz. carbon, using bulk free energies of formation of diamond and graphite. However, during chemical vapor deposition, diamond deposition occurs at the gas-solid interface and the growth process does not involve just elemental carbon, the one component which is represented in the phase diagram in Figure 1.2, but it also involves hydrogen. Furthermore, since growth occurs at the surface, the relative stability of diamond and graphite should be examined using surface free energies rather than bulk free energies of formation. In this study the relative stability of diamond and graphite surfaces under typical diamond deposition conditions has been examined. The specific questions and issues addressed are: How can we estimate the enthalpies and entropies of formation of various surfaces of diamond and

graphite? What role does atomic hydrogen play in influencing the relative stability of diamond and graphite? Can we rationalize the deposition of diamond under typical CVD conditions based on atomic hydrogen concentrations at the substrate surface calculated from principles of heat transfer and fluid flow?

1.6 Organization of Thesis

This thesis is divided into five chapters. Chapter 1 is the introduction; it presents a brief summary of the chemical vapor deposition of diamond with emphasis on the hot filament technique. Furthermore, the various roles attributed to atomic hydrogen in the CVD of diamond are highlighted. Chapter 2 is a review of the literature relevant to the growth of diamond films by CVD techniques and the progress made in understanding the role of atomic hydrogen, the stabilty of diamond and graphite, and the modeling of diamond growth processes. The third chapter is devoted to the description of experimental and theoretical procedures used in this study. The experimental and theoretical results are presented and discussed in the fourth chapter. Finally, chapter 5 presents a summary and conclusions of this work.

1.7 References

1. W. G. Eversole, U.S. Patent 3,030,188 (1961).

2. J. C. Angus, H. A. Hill, and W. S. Stanko, J. Appl. Phys., 39, 2915 (1968).

3. J. C. Angus, U.S. Patent 3,630,677 (1971).

4. B. V. Deryagin and D. V. Fedoseev, *Rost Almaza i Grafita iz Gazavoj Fazy*, Nauka, Moscow (1977).

5. B. V. Spitsyn, L. L. Bouilov, B. V. Deryagin, J. Cryst. Growth, 52, 219 (1981).

6. W. A. Yarbrough and R. Messier, Science, **247**, 688 (1990).

7. R. C. DeVries, Ann. Rev. Mater. Sci., **17**, 161 (1987).

8. R. Roy, Nature, **325**, 17 (1987).

9. J. C. Angus and C. C. Hayman, Science, **241**, 913 (1988).

10. K. E. Spear, J. Am. Ceram. Soc., **72(2)**, 171 (1989).

11. M. Tsuda, M. Nakajima, and S. Oikawa, J. Am. Chem. Soc., **108**, 5780 (1986).

12. M. Tsuda, M. Nakajima, and S. Oikawa, Jpn. J. Apl. Phys., **26**, L527 (1987).

13. M. Frenklach and K. E. Spear, J. Mater. Res., **3(1)**, 133 (1988).

14. D. E. Patterson, B. J. Bai, C. J. Chu, R. H. Hauge, and J. L. Margrave, in *New Diamond Science and Technology*, eds. R. Messier, J. T. Glass, J. E. Butler and R. Roy, p. 433 (MRS, Pittsburgh, PA, 1991).

15. D. E. Patterson, C. J. Chu, B. J. Bai, N. J. Komplin, R. H. Hauge, and J. L. Margrave, in *Applications of Diamond Films and Related Materials*, eds. Y. Tzeng, M. Yoshikawa, M. Murakawa, and A. Feldman, p. 569 (Elsevier Science Publishers B. V., 1991).

16. S. Matsumoto, Y. Sato, M. Kamo, and N. Setaka, Jpn. J. Appl. Phys., **21(4)**, L183 (1982).

17. S. Matsumoto, Y. Sato, M. Kamo, and N. Setaka, J. Mater. Sci., **17**, 3106 (1982).

18. K. Mitsuda, Y. Kojima, T. Yoshida, and K. Akashi, J. Mater. Sci., **22**, 1557 (1987).

19. Y. Sato, M. Kamo, and N. Setaka, in *Proceedings of the 8th International Symposium on Plasma Chemistry*, eds. K. Akashi and A. Kinbara, p. 2446, (International Union of Pure and Applied Chemistry, Oxford, England, 1987).

20. T. Kawato and K. Kondo, Jpn. J. Appl. Phys., **26(9)**, 1429 (1987).

21. Y. Hirose and Y. Terasawa, Jpn. J. Appl. Phys., **5(5)**, 565 (1986).

22. Y. Saito, K. Sato, H. Tanaka, K. Fujita, and Matsuda, J. Mater. Sci., **23(3)**, 842 (1988).

23. M. Mecray, M.S. Thesis, The Pennsylvania State University, 1991.

24. T. D. Moustakas, Solid State Ionics, **32/33**, 861 (1989).

25. D. V. Fedoseev, V. P. Varnin, and B. V. Deryagin, Russ. Chem. Rev., **53**, 435 (1985).

26. D. J. Poferl, N. C. GArdner, and J. C. Angus, J. Appl. Phys., **44**, 1428 (1973).

27. M. Frenklach, J. Appl. Phys., **65**, 5142 (1989).

28. F. G. Celii, P. E. Pehrsson, H. -t. Wang, H. H. Nelson, and J. E. Butler, *Science and Technology of New Diamond*, eds. S. Saitoh, O. Sukunaga, and M. Yoshikawa (KTK Scientific Publishers, Tokyo, Japan, 1991).

29. L. Schafer, C. P. Klages, U. Meier, and K. Kohse-Hoinghaus, Appl. Phys. Lett., **58**, 571 (1991).

30. S. J. Harris, A. M. Weiner, and T. A. Perry, Appl. Phys. Lett., **53**, 1605 (1988).

31. S. J. Harris and A. M. Weiner, J. Appl. Phys., **67**, 6520 (1990).

32. W. L. Hsu, Appl. Phys. Lett., **59**, 1427 (1991).

33. L. R. Martin, J. Appl. Phys., **70**, 5667 (1991).

34. F. P. Bundy, H. M. Strong, and R. H. Wentorf, Jr., *Chemistry and Physics of Carbon*, eds. P. L. Walker, Jr. and P. A. Thrower, 10, p. 213 (Marcel Dekker Inc., New York, 1973).

35. F. D. Rossini and R. S. Jessup, J. Res. Natl. Bur. Stds., **21**, 491 (1921).

36. R. Berman and F. Simon, Z. Elektrochem., **59**, 333 (1939).

37. H. B. Vakil, W. F. Banholzer, R. J. Kehl, and C. L.Spiro, in proceedings of ACS diamond symposium, Dallas, TX, 1989.

Chapter 2

BACKGROUND AND PREVIOUS WORK

2.1 Diamond Deposition Techniques

In the early work, diamond growth was achieved by vapor deposition of solid carbon from hydrocarbon precursors. The nucleation and growth of graphite and other non-diamond forms of carbon in this technique necessitated the alteration of a growth cycle with an etch cycle to remove the non-diamond forms of carbon. Later, Deryagin and co-workers [1] demonstrated that the use of excess hydrogen in the feed gas along with small quantities of hydrocarbons, and activating the gas prior to deposition allowed continuous deposition of diamond with little co-deposition of non-diamond carbon. They suggested the following three methods for activating the gas to generate significant concentrations of atomic hydrogen [1]:

a) catalytic, such as heated platinum for dissociating hydrogen

b) an electric discharge

c) a heated tungsten filament located close to the substrate

Based on these methods, several CVD techniques have been developed for the growth of well-crystallized diamond films. These techniques can be classified under four major headings:

a) Plasma assisted CVD [2]

b) Thermally assisted or hot filament assisted CVD [3]

c) Reactive vapor deposition [4,5]

d) Various combinations of these [6]

The diverse methods that have been used for diamond deposition show some striking similarities. First, each method employs a unique technique for the generation of reactive species, particularly atomic hydrogen. Second, most of these low pressure techniques employ substrate temperatures in the range of 800-1000 $^{\circ}$C. Third, deposits obtained from these various techniques vary from nanocrystalline to single crystal cubic diamond with little or no non-diamond carbon. These similarities have led researchers to believe that there is a common mechanism for the growth of diamond.

Among the various techniques [7], viz. dc discharge CVD, rf plasma CVD, microwave plasma CVD, hot filament CVD, electron assisted CVD, laser assisted CVD, ion beam and electron beam techniques, the hot filament assisted CVD and the microwave plasma assisted CVD are the most popular. These sub-atmospheric pressure processes yield diamond growth rates upto a few micrometers an hour. In recent years, the use of atmospheric pressure plasmas and arc discharges [8,9] has yielded diamond growth rates one to two orders of magnitude higher than the low pressure techniques. Although most of the techniques for diamond deposition depend upon a supply of atomic hydrogen, researchers at Rice University recently showed that diamond can be deposited through fluorocarbon chemistry with very little [5] or no atomic hydrogen [10]. These results have prompted researchers to recognize that diamond growth can be achieved through radically different chemistries.

2.2 Substrate Pretreatment for Nucleation

Nucleation is of prime importance in diamond film growth since the nucleation density affects the resultant morphology and its evolution. There have been several reports that diamond can be nucleated in the gas phase [11,12], but in most experiments to-date, diamond films have been grown on a solid surface including graphite [13]. However, in the absence of a surface treatment, diamond nucleation on various substrates required a rather long induction period [14]. The surface treatments used to increase the nucleation density include, polishing the diamond surface with diamond powder [15], ultrasonification of the surface in diamond powder suspensions before deposition [16] or, scratching, grit blasting or ultrasonic treatment with abrasive powders like SiC [17,18], Al_2O_3 [18] and boron nitride [14]. Although several methods of pretreatment have been tried with varying degrees of success, the most successful and popular one, seems to be, polishing the substrate surface with diamond powder before deposition.

Polishing with diamond powder is known to produce high nucleation density on a variety of substrate surfaces. Two different explanations have been proposed to explain this observation. Yarbrough et al. [19] believe that diamond, diamond-like carbon, or other carbonaceous residues from the polishing or other abrading powder adhering to or embedded in the substrate surface, supply nucleation sites for diamond growth. On the other hand, Yugo and Kimura [20] suggested that polishing results in highly disordered surface material and creates microscopic crater edges which provide high energy sites that are preferred nucleation sites for diamond.

The wide range of substrate materials used for diamond deposition can be classified into three groups: a) diamond crystals b) carbides and carbide forming materials, and c) substrates which do not form carbides. In recent years, several investigators have demonstrated that homoepitaxial diamond films can be grown on diamond substrates [21-23]. However, the rate of growth of diamond on diamond is a function of the crystallographic orientation of the substrate, with the highest rates observed on {100} surfaces, followed by {110} and {111} surfaces [11].

Diamond can be grown on non-diamond substrates, notably substrates that form stable carbides viz. Si, Mo, W and Ta, even without surface treatment as discussed earlier. However, without surface treatment, nucleation density is normally low, and a significant induction period may be required before the first evidence of diamond formation can be observed [14]. Badzian and Badzian [24] suggested that nucleation on silicon is preceded by the formation of silicon carbide. They indicated that a partial matching between the lattices of diamond and β-SiC layer formed on the Si substrate is necessary for diamond nucleation. Furthermore, they believe that diamond deposition on other carbide-forming substrates may be explained by similar matching between the diamond lattice and the respective carbide lattices [24].

2.3 Role of Process Variables

One of the challenges ahead in the field of CVD diamond growth is to understand the role of process variables on the growth rate, quality, morphology and uniformity of the films. Several researchers have performed experiments over a wide range of parameters and reported optimum conditions for diamond growth. However, there is a general lack of

consistency in the reported "optimum conditions." This can be largely attributed to the widely different reactor geometries and gas activation techniques employed by scientists from different laboratories. These differences affect the various physicochemical processes in the system, and consequently the deposition. Although the parametric studies conducted to date provide limited insight into the nature of the physical and chemical processes occurring during deposition, they provide a good starting point for achieving this goal.

2.3.1 Substrate Temperature

For the deposition of diamond films from hydrocarbon-hydrogen mixtures, there is generally a narrow range of substrate temperatures where essentially single phase diamond films are deposited at appreciable rates [25]. If the temperature is too low, a significant amount of amorphous carbon is co-deposited, whereas, if the temperature is too high, non-diamond components including microcrystalline graphite are deposited [26]. Since substrate temperature measurement is typical to a deposition system, and since it varies widely from system to system, it is rather difficult to precisely specify a common temperature window for diamond deposition. However, the most commonly encountered range is about 800 $^{\circ}$C - 1000 $^{\circ}$C. Within the optimum temperature range, there is no consistent variation of morphology with temperature. With an increase in temperature, both changes from {111} to {100} [27,28] as well as {100} to {111} faces [29,30] have been reported. Zhu et al. [27] have reported that the broad non-diamond Raman peak at about 1550 cm^{-1}, as well as the luminescence background, decrease with increase in temperature, indicating an increasing degree of structural perfection of the diamond with temperature.

2.3.2 Gas Composition

Initial experiments with pure hydrocarbon gas resulted in significant graphitic co-deposition. Diluting the hydrocarbon with hydrogen helped since it reduced the hydrocarbon dissociation [31] and reduced the concentration of the radicals important for graphitic deposition. In experiments where CH_4 is used as the hydrocarbon precursor, a gas composition of 0 - 5% CH_4 in hydrogen is common. However, the best results are obtained when the methane concentration is in the range 0.5 - 2.0%. Though methane is the most commonly used hydrocarbon precursor gas, diamond can be grown from a variety of hydrocarbon gases and organic liquids. Sato et al. [32] have grown diamond films by plasma assisted CVD using various hydrocarbons, both saturated and unsaturated, and observed that for a given C/H ratio in the input gas, the nucleation density, growth rate and growth features were essentially the same in all cases.

Addition of small amounts of oxygen to the feed gas has been found to be beneficial in accelerating the growth of diamond. Oxygen addition to the system has been tried in the form of pure O_2 [33], water vapor [34], CO [36] or oxygen bearing organic compounds [37]. It is believed that oxygen addition improves the film quality by reduction of the acetylene concentration [33], the oxidation of non-diamond carbon to CO or CO_2 [33], or increasing the atomic hydrogen concentration [37]. Furthermore, since the addition of oxygen reduces the C_2H_2 concentration and, consequently the non-diamond carbon in the films, the diamond growth rate can be increased by increases in both CH_4 flow rate and total pressure whilst retaining the film quality [33].

2.3.3 Pressure

The optimum operating pressure for diamond deposition seems to vary from system to system [27,30,38]. However, the typical range of operating pressures for vapor deposited diamond is 60 to 1.2×10^4 Pa [39]. Kawato and Kondo [33] reported that the pressure range of diamond deposition can be extended from less than 100 Torr to about 300 Torr since the addition of oxygen suppresses formation of C_2H_2, and consequently non-diamond carbon, which hinders growth of good quality diamond films at high pressures.

Matsumoto et al. [30] succeeded in depositing diamond particles at a pressure of 0.5 Torr in a HFCVD reactor, but the particles were very fine. As the pressure was increased, densely populated large particles were observed. However, at one atmosphere pressure no diamond could be deposited. Zhu et al. [27] observed that a pressure of 110 Torr was optimum for diamond deposition in their microwave plasma assisted CVD (MPCVD) reactor. Although they observed a parabolic variation of growth rate they did not observe any significant structural changes in the diamond films.

Diamond films have not been deposited at pressures close to 1 atm using the hot filament technique or glow discharges. However, the use of oxyacetylene flames and arc discharges has made the diamond growth at atmospheric pressures possible. When an oxyacetylene flame, with an oxygen to acetylene ratio close to unity, is directed towards a water cooled silicon or molybdenum substrate maintained at a temperature of 700 -1000 °C, diamond can be deposited [8,9]. These deposits are typically over small areas and exhibit significant radial variation in quality and morphology. However, uniform deposition on larger areas can be obtained at low pressures with oxygen to acetylene ratios slightly greater than unity.

2.3.4 Filament Temperature and Filament to Substrate Distance

Typical filament temperatures employed in the HFCVD of diamond range from 2000 - 2500 K [11]. Fig. 2.1 shows the calculated percent of atomic hydrogen as a function of the filament temperature at various pressures. These calculations are based on thermodynamic equilibrium between atomic and molecular hydrogen (i.e. for the reaction $1/2\ H_2 = H$). The equilibrium data for the calculations were taken from JANAF thermochemical tables [40]. It should be noted that although the percent dissociation of atomic hydrogen is highest for the lowest pressure for any given temperature, the actual equilibrium concentration of atomic hydrogen increases with increasing pressure as can be observed in Fig. 2.2. Since significant amounts of atomic hydrogen are generated only above 2000 K, a filament temperature of at least 2000 K seems to be essential for the growth of good quality diamond. In general, at low methane concentrations, the growth rate increases with increase in filament temperature. However, at high methane concentrations, high filament temperatures favor formation of graphitic carbon [30]. The filament to substrate distance is typically 1 cm. The growth rate of the film depends strongly on the distance of separation. The growth rate can be enhanced by bringing the substrate closer to the filament [30]. However, radiation heating can produce excessive substrate temperatures leading to non-uniformity and even graphitic deposits [41]. Typical lifetimes of some of the reactive species like H and CH_3 are about 1 ms [42]. The distance between the filament and substrate determines the time it takes for the species to reach the substrate surface, and hence the fraction of the species generated at the filament that safely get to the deposition site. Therefore, a high deposition rate can be expected on a substrate which is placed close to the filament.
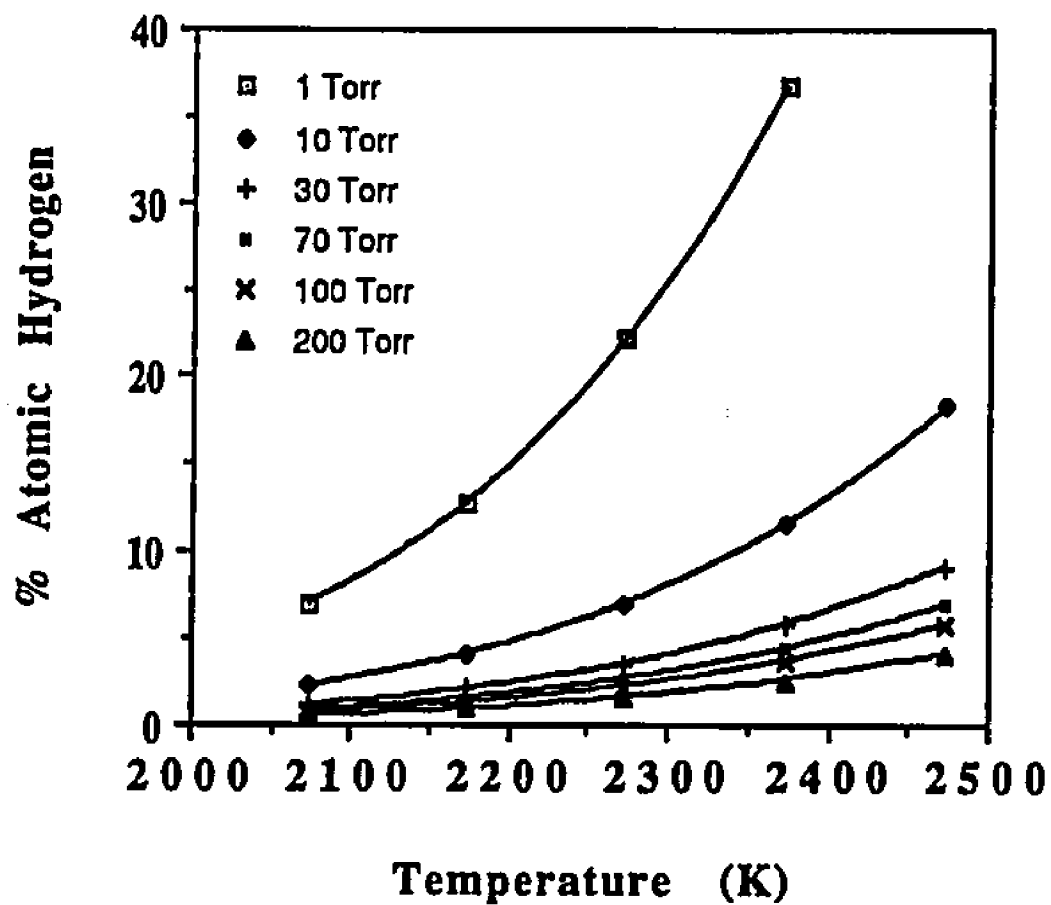
Fig. 2.1 Plot of percent atomic hydrogen vs. filament temperature for various pressures calculated from data in reference 40.
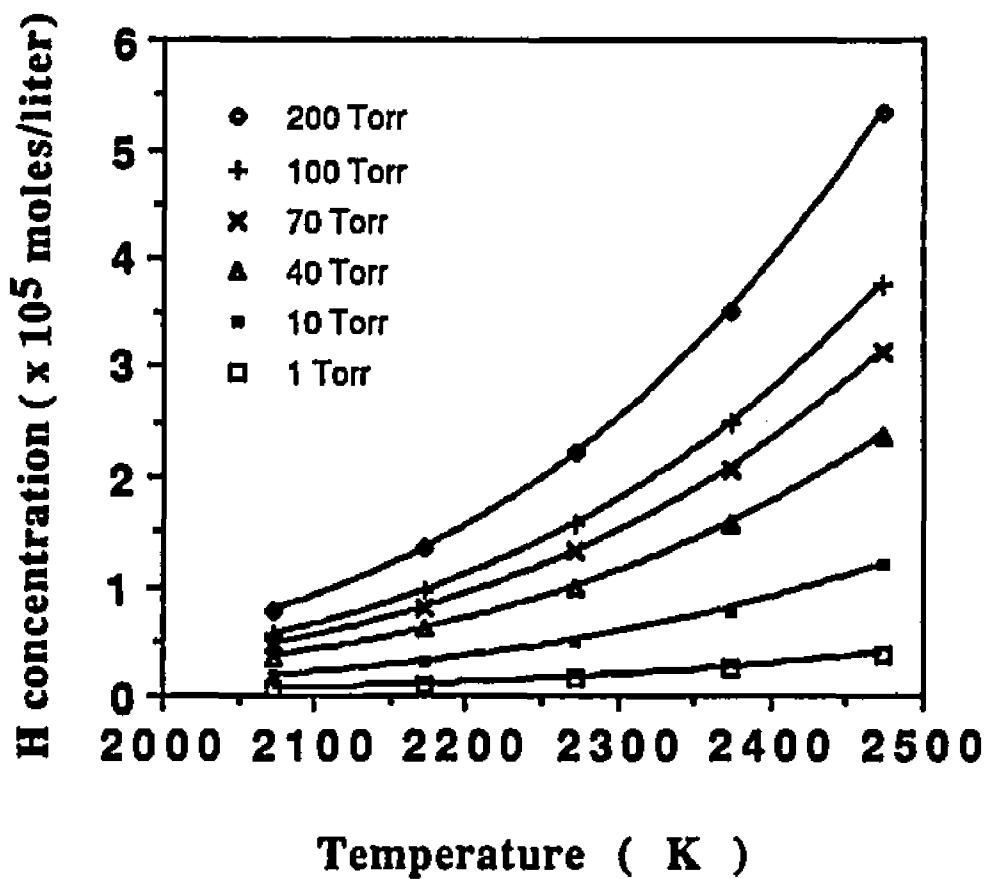
Fig. 2.2 Plot of concentration of atomic hydrogen vs. filament temperature for various pressures calculated from data in reference 40.

2.3.5 Filament Material and Geometry

The principal role of the filament is to generate significant concentrations of atomic hydrogen and various hydrocarbon species. Since significant concentrations of atomic hydrogen are generated at temperatures in excess of 2000 K, the use of refractory metal filaments is essential for diamond deposition experiments. Various refractory metal filaments, such as tungsten, tantalum and rhenium have been used for HFCVD of diamond. The use of refractory metal filaments results in incorporation of trace amounts of filament material [43] in the diamond films. Although small amounts of impurities do not significantly affect the tribological properties of these coatings, they are undesirable for optical and electronic applications. In one attempt to address this problem diamond films have been deposited using carbon rods [44], albeit at low rates.

Since the filament plays an important role in the generation of various species, particularly atomic hydrogen, important for diamond growth, understanding the role of filament material and geometry in affecting the generation of species, and consequently, the quality and growth rate of the films is of interest. Singh et al. [45] observed that there were no significant differences between diamond films deposited using tungsten, tantalum or rhenium filaments. On the other hand, Schachner [46] reported that better diamond films could be deposited when tantalum filaments were used instead of tungsten filaments. For a detailed understanding of the role of filament material in determining the quality of the diamond films, the generation of atomic hydrogen at the filament should be examined.

Jansen et al. [47] studied the efficiency of dissociation of molecular hydrogen at filaments of different diameters. They related the difference in power consumption of the filament in

hydrogen and vacuum to the extent of dissociation of molecular hydrogen to atomic hydrogen. They found that the dissociation rate per unit surface area of the filament was higher for filaments of smaller diameter. However, Schafer et al. [48] observed that the concentration of atomic hydrogen, measured using two-photon laser-induced fluorescence technique, near a 0.3 mm diameter Ta filament was less than that near a 2.0 mm diameter filament. These authors concluded that the generation of atomic hydrogen at the filament was non-equilibrium in nature.

Schafer et al [48], studied the efficiency of hydrogen dissociation using different filament materials. They found that the generation of atomic hydrogen with tantalum filaments was higher than that with iridium filaments and that the atomic hydrogen concentrations generated using a tungsten filament showed the least deviation from the equilibrium value. They also found that the addition of methane to hydrogen resulted in a decrease in the atomic hydrogen concentration. They attributed this decrease to gas phase reactions of atomic hydrogen with hydrocarbon species. However, in another paper [49], they showed that after the atomic hydrogen concentration decreased due to methane addition, changing the gas composition to pure hydrogen did not yield atomic hydrogen concentrations obtained prior to methane addition. In fact, their results showed that the atomic hydrogen concentration in pure hydrogen, after withdrawal of methane, was the same as that when methane was present. The results indicate that the nature of the filament controlled the dissociation of hydrogen and the gas phase reactions were not of significant importance. Furthermore, Goodwin and Gavillet [50] investigated the observed decrease in H atom concentration with increasing methane content in the feed gas. Their calculations indicated that the homogeneous recombination of atomic hydrogen is not fast enough to explain the

decrease in atomic hydrogen concentration. They concluded that the reduction in H atom production at the filament surface is due to hydrocarbon poisoning of the filament.

2.4 Role of Various Species in Diamond CVD

2.4.1 Atomic Hydrogen

A significant development in the science and technology of low pressure diamond synthesis occurred when Deryagin and co-workers [1] discovered that using excess hydrogen in the deposition gas and activating the gas prior to deposition resulted in significant reduction in the co-deposition of non-diamond carbon and higher growth rates. Several factors have been suggested to explain the role of hydrogen dilution. First, and probably the most popular, is the preferential etching of graphite over diamond by hydrogen atoms [51-55]. Deryagin and Fedoseev [1] observed that activated hydrogen etched graphite orders of magnitude faster than diamond. This observation led them to propose that the presence of a large concentration of atomic hydrogen at the growth surface, during CVD of diamond, is responsible for the reduction in the co-deposition of non-diamond phases. Angus et al. [51] also showed that molecular hydrogen would thermally etch graphite about 500 times faster than diamond. Setaka [56] measured etch rates of graphite, glassy carbon and diamond. He reported that the under typical activated growth conditions the etch rates of graphite, glassy carbon and diamond were 0.13, 0.11 and 0.006 mg/cm^2 hr, respectively. These data are consistent with the theory that graphite and diamond are deposited simultaneously, but since graphite is more reactive to atomic hydrogen, it is preferentially removed and the net deposit is predominantly diamond.

The second frequently discussed [53,54] effect of hydrogen is that it satisfies the dangling bonds of surface carbon atoms during growth, keeping them in sp^3 configuration and thus preventing the diamond surface from reconstructing into graphitic, sp^2 or carbynic, sp, structures. Lander and Morrison [57] were the first to show that hydrogen can stabilize a diamond surface by forming sp^3 C-H bonds with the surface carbon atoms. Fig. 2.3 shows the stacking of graphite (0001) planes and diamond (111) planes with hydrogen atoms satisfying the dangling sp^3 bonds of the carbon atoms in the top layer. In the absence of the hydrogen atoms maintaining the sp^3 character of the surface carbon atoms, it is easy to imagine the diamond (111) planes collapsing into the more stable planar graphite structure. In fact it is well known that in the absence of hydrogen the surface carbon atoms on cleaned bulk diamond crystals will reconstruct at about 900-1000 °C [58]. However, in the presence of hydrogen, the reconstruction reverses as the dangling sp^3 bonds of surface carbon atoms are satisfied by C-H bonds [57].

Atomic hydrogen is also believed to aid in the formation of various hydrocarbon species, such as CH_3 and C_2H_2, which are considered to be important for diamond growth [59-61]. Hydrogen molecules suppress the formation of polycyclic aromatic hydrocarbons in the gas phase which otherwise leads to the deposition of non-diamond carbon phases [62]. Atomic hydrogen also helps in generating new growth sites, where hydrocarbon species can be added, by abstracting hydrogen atoms bonded to surface carbon atoms [53].

Significant amount of atomic hydrogen is generated in diamond deposition reactors. The formation of atomic hydrogen from molecular hydrogen at the hot filament is highly endothermic. At low pressures typical of hot filament systems, atomic hydrogen is transported away from the filament primarily by diffusion. In the presence of a solid
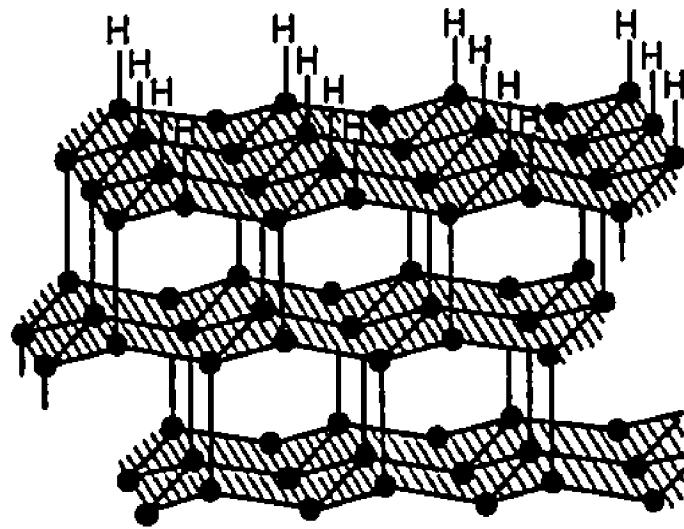
DIAMOND
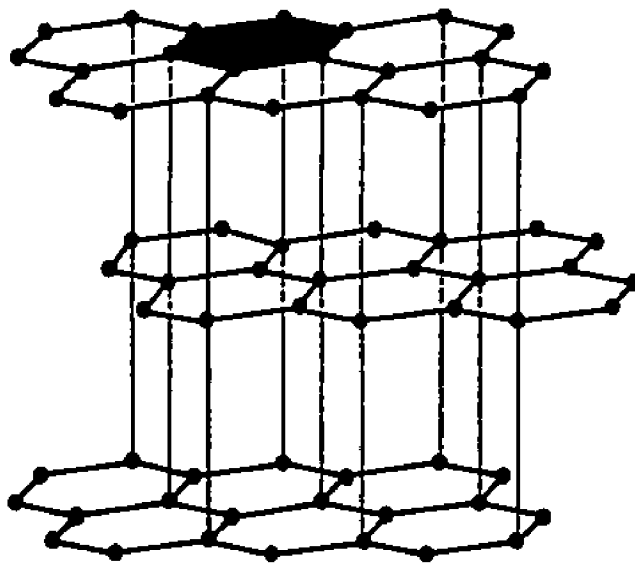
GRAPHITE

Fig. 2.3 Schematic diagrams showing similarities in the crystal structures of diamond and graphite. The hydrogen atoms bonded to the surface carbon atoms in diamond depict their role in stabilizing the diamond surface structure[39].

surface such as the substrate atomic hydrogen readily recombines to form molecular hydrogen and the recombination reaction is highly exothermic. Thus, atomic hydrogen acts as a carrier of heat from the filament to the growth surface. Although various roles have been assigned to atomic hydrogen, the importance of hydrogen assisted heat transfer in diamond deposition reactors has not been addressed.

2.4.2 Hydrocarbon Species

Although the importance of atomic hydrogen in the deposition of diamond is recognized by all in the diamond community, there is significant controversy over the nature of the hydrocarbon species important for growth. Numerous hydrocarbon species including CH_3^+ [59], CH_3 [63,64], atomic carbon [65] and C_2H_2 [61] have been suggested to be important species for the growth of diamond from the vapor phase.

Tsuda et al. [59,60,66] conducted quantum mechanical computations in order to determine the lowest energy path for a proposed mechanism of diamond growth on {111} surfaces. They initially [59] assumed that only C_1H_{1-3} ions can be the growth species in CH_4-H_2 plasmas and reported the following two step reaction sequence. In the first step, the {111} plane of the diamond surface are covered by the methyl radical group via either methylene insertion or hydrogen abstraction followed by methyl cation addition. In the second step, following the attack of a methyl cation and the loss of three H_2 molecules, three neighboring methyl groups on the {111} plane are bound together to form the diamond structure. In subsequent publications [60,66], they extended their analysis and concluded that the epitaxial growth of a diamond film is sustained, provided the surface maintains a positive charge and there is a supply of methyl radicals. This mechanism has been a

subject of several criticisms. The heat of formation for the methyl cation is much larger than that of the neutral methyl radical without much difference in the entropy. Thus, the methyl cations are expected to be in much lower concentrations than the methyl radical and are unlikely to account for the observed growth rates. In addition, in hot filament systems free electron emission occurs which can neutralize the methyl cations. In plasma assisted deposition of diamond the substrate surface is negatively, not positively charged, with respect to the plasma. These criticisms question the likelihood of the proposed mechanism.

Frenklach and Spear [61] proposed an alternative mechanism for the growth of {111} diamond surfaces, consisting basically of two alternating steps. The first step is the surface activation by H-atom removal of a surface bonded hydrogen. In the second step, this surface activated carbon radical then acts as a site for adding more carbon to the structure by reacting with acetylene. Huang, Frenklach and Maroncelli [67] tested the Frenklach and Spear mechanism using quantum chemical computation techniques and obtained results which corroborate the proposed mechanism. This mechanism also appears problematic. The first problem is that the mechanism requires a large entropy loss suggesting that acetylene addition should be slow [68]. Another difficulty is that diamond deposition has been reported in systems where acetylene generation in the amounts required seems unlikely [69].

Harris [64] proposed a reaction mechanism based upon the idea that the methyl radical is the dominant additive specie. The proposed mechanism involved addition of neutral methyl radicals to an electrically neutral diamond surface. He considered the diamond (100) surface to be made up of an ensemble of bicyclo [3.3.1] nonane (BCN) molecules. Since in BCN the orientations of the H atoms and the carbon atoms to which they are bound are

identical to those on a hydrogenated diamond (100) surface, they suggested that the growth at the hydrogenated site in BCN is similar to the growth on the diamond (100) surface. The proposed mechanism involved surface activation by hydrogen abstraction followed by methyl radical addition. Using measured concentrations of atomic hydrogen and methyl radicals near the substrate under typical hot filament assisted deposition conditions [64], they calculated the rate of addition of carbon from a methyl radical to the hydrogenated diamond (100) surface. The estimated growth rates were shown to be in good agreement with experimentally observed growth rates indicating that diamond growth can be explained by addition of methyl radicals to an electrically neutral diamond surface without requiring the presence of methyl cations or a positively charged surface.

Although theoretical models have been proposed suggesting various hydrocarbon species to be the important growth species, much of the experimental evidence to date points to methyl radical as the dominant growth specie. Martin and Hill [70] used a remote plasma technique to dissociate hydrogen and provided a methane feed downstream of the plasma. They concluded that the dominant additive specie for diamond growth is short lived and probably the methyl radical. Chu et al. [71] conducted carbon-13 studies to understand the mechanism of diamond film growth. They synthesized mixed carbon-12/carbon-13 diamond films by HFCVD, using mixtures of $^{13}CH_4$ and $^{12}CH_4$ or $^{12}C_2H_2$ in H_2. They observed that the first order Raman peak of 1332 cm^{-1} for pure carbon-12 diamond, shifted by 50 cm^{-1} to 1282 cm^{-1}, for pure carbon-13 diamond. Furthermore, for mixed isotope films, the Raman peak shift varied linearly with the mole fraction of ^{13}C. The shift in the Raman peak was used to estimate the relative incorporation of ^{13}C and ^{12}C into the films. Their results indicated that the mole fraction of ^{13}C in the films agreed closely with the mole fraction of ^{13}C inferred for the methyl radical addition but differed significantly

from that for acetylene, indicating that CH3 is the dominant growth specie. Yarbrough et al. [72] conducted experiments to examine the relative importance of various species in the HFCVD of diamond. Their experiments using local feeds of methane and acetylene at the substrate surface showed that a local methane feed considerably enhanced the growth rate and deposition uniformity while an acetylene feed showed no significant effect indicating that methyl radical is the more important deposition specie. The rationale extended for this was that since the governing reaction for the formation of CH3 in the gas phase is

$$CH_4 + H = CH_3 + H_2 \hspace{4cm} 2.1$$

a local feed of methane at the substrate surface enhances the concentration of CH_4 and hence CH_3, thereby increasing the growth rate.

2.4.3 Measurement of Species Concentrations

The exact mechanism of gas phase and surface reactions leading to the formation of well crystallized diamond is not well understood. Knowledge of these mechanisms could lead to better process control and improved material quality and characteristics. To obtain such knowledge it is necessary to determine the nature and dynamics of the species involved in the deposition process. Atomic hydrogen is believed to play an important role in the generation of hydrocarbons species, such as methyl radical and acetylene, and in the preparation of surface radical sites for the addition of carbonaceous species. Thus, understanding the generation and spatial distribution of atomic hydrogen is important for gaining insight into the gas phase and surface reaction kinetics. Similarly, knowledge of the nature and concentration of the hydrocarbon species present in the growth environment is

important for determining the species important for diamond growth. Furthermore, accurate measurement of species concentration is important for testing various proposed mechanisms for diamond growth.

Infrared diode laser absorption spectroscopy [69] was one of the first methods employed for in situ diagnostics of the filament assisted diamond growth environment. The method was used to determine the nature of the species present between the filament and the substrate during diamond growth from methane-hydrogen gas mixtures. High concentrations of CH_4 and C_2H_2 species and relatively lower densities of CH_3 and C_2H_4 species, as evidenced by the intensity of the absorption peaks, were detected. Ethane, various C_3 hydrocarbons and methylene radicals could not be detected. However, these species may have been present in concentrations below the sensitivity levels of the instrument.

Harris and coworkers used mass spectrometry to detect stable species at the diamond deposition surface [73,74]. Using a quartz sampling probe, to extract the gas present near the surface of silicon or platinum substrates, they found CH_4 and C_2H_2 to be the major species while C_2H_4 and C_2H_6 were present in lower concentrations. Using this technique they could not directly measure species like CH_3 and H which recombined in the sampling probe before reaching the mass spectrometer. However, since the primary products of recombination of CH_3 in the probe are C_2H_6 and C_2H_4, they derived CH_3 concentrations from the experimentally measured concentrations C_2H_4 and C_2H_6 species. Furthermore, they could estimate the H atom concentrations from their experimental data since reaction 2.1 is in partial equilibrium under diamond growth conditions [75]. Harris et al. [74] also calculated mole fractions CH_3 and H as a function of methane concentration in the feed gas

using a detailed chemical kinetic model. The experimentally derived mole fractions of H and CH$_3$ agreed well with predicted values, as shown in Fig. 2.4.

Celli and Butler used resonance-enhanced multiphoton ionization (REMPI) technique to detect H [76] and CH$_3$ [77] in the diamond growth environment. The REMPI signal was considered to be proportional to the concentration of these species, and was used to examine the effect of filament temperature and input gas composition on the concentration of these species. Their results, presented in Fig. 2.5, showed an increase in the H concentration with filament temperature consistent with an enhanced thermal dissociation of molecular hydrogen at higher filament temperatures. Fig. 2.5 also shows a decrease in H atom concentration with increasing methane concentration in the feed gas. They believe that the observed decrease in H atom concentration with methane addition is a result of "surface poisoning" of the filament rather than a gas phase process. Although the H atom concentration decreased with methane concentration, both CH$_3$ and C$_2$H$_2$ concentrations were found to increase [76]. Since the quality of the diamond deposited, as judged by Raman spectra, decreases with increasing methane concentration, they concluded that filament assisted diamond growth was not limited by production of CH$_3$ by H atom driven reactions, but by surface reactions such as etching of non-diamond carbon, termination of dangling bonds or surface activation by hydrogen abstraction.

Recently, two photon laser induced fluorescence (LIF) was used to determine absolute concentrations of atomic hydrogen in the vicinity of the hot filament [48,49]. Using this technique concentration profiles of atomic hydrogen upto a distance of 28 mm from the filament, with a spatial resolution of about 0.5 mm, were determined. The observed atomic hydrogen concentrations as a function of distance from the filament for different molecular
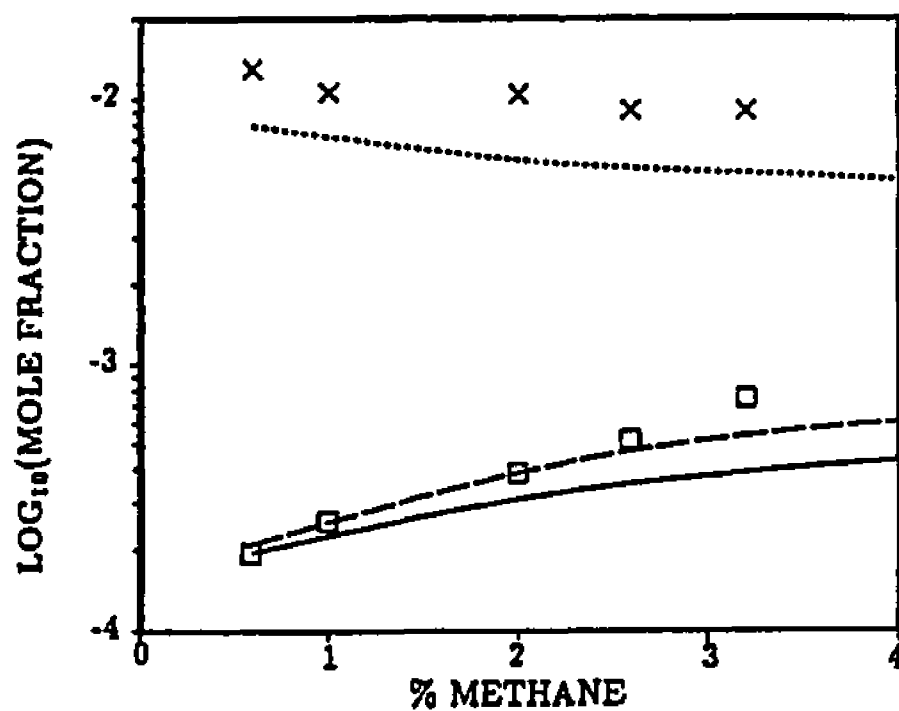
Fig. 2.4 Comparison between measured and calculated species mole fractions as a function of initial methane percentage in methane-hydrogen gas mixture. H: crosses (experiment) and dotted line (model); CH_3: squares (experiment) and solid line (model). The dashed line is the model calculation for $X_{CH_3} + X_{C_2H_4} + X_{C_2H_6}$ [74].
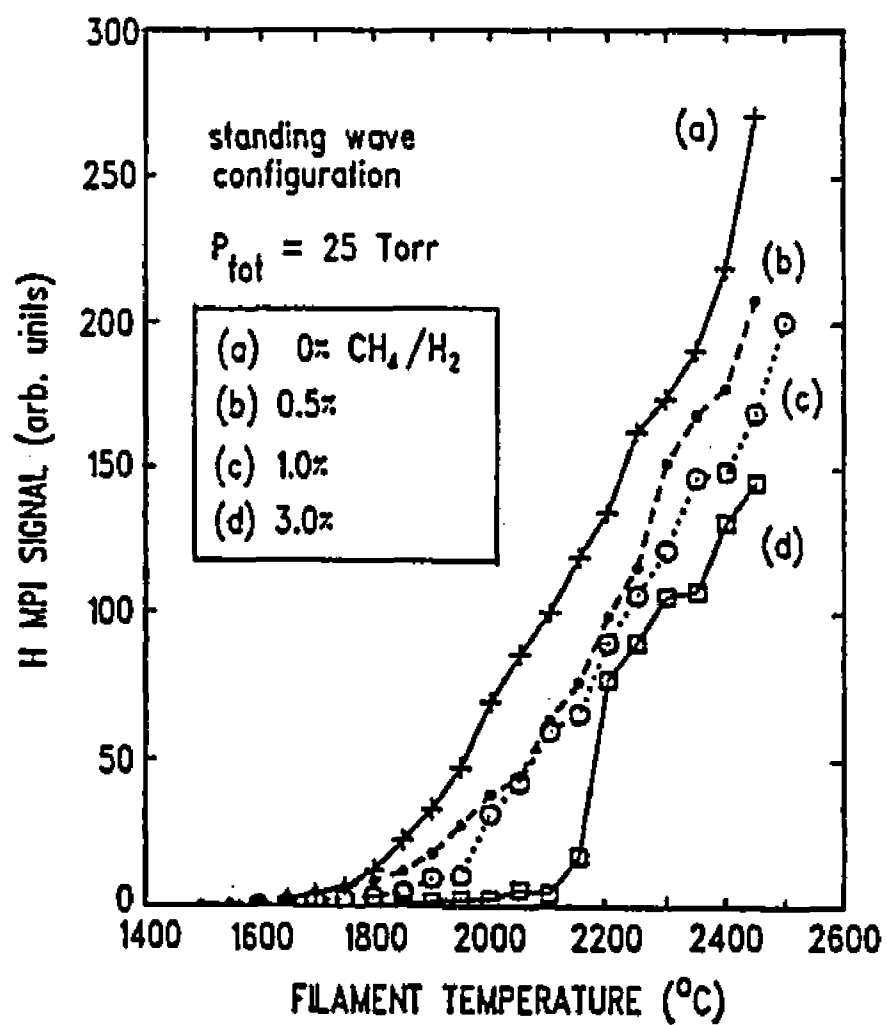
Fig. 2.5 Dependence of hydrogen atom multiphoton ionization (MPI) intensity on the filament temperature, for standing wave excitation at 364.68 nm, for various initial gas compositions [76].

hydrogen pressures and filament temperatures are presented in Figs. 2.6(a) and 2.6(b), respectively. Fig. 2.6(a) shows that the atomic hydrogen concentrations saturate at pressures in excess of 10 mbar. This is at variance with the trends of chemical equilibrium calculations, calculated using thermodynamic data from literature, which show a steady increase in atomic hydrogen concentration with pressure as shown in Fig. 2.2. Furthermore, the measured concentration at a particular pressure was less than the expected equilibrium concentration. For example, at pressures of 1.5 mbar and 100 mbar the measured concentrations were 50% and 12% of the corresponding equilibrium concentrations, respectively. Schafer et al. [48] also observed an increase in atomic hydrogen concentration with filament temperature, as shown in Fig. 2.6(b). However, they observed a stronger temperature dependence of atomic hydrogen concentration than that observed by Celii and Butler [76]. Schafer et al. [48] observed a 30% decrease in the atomic hydrogen concentration with the addition of 5% methane. Furthermore, they observed a more rapid decrease in atomic hydrogen concentration, with distance from the filament, with increasing methane concentrations, as shown in Fig. 2.7. Based on these results they suggested accelerated consumption of atomic hydrogen in the gas phase, due to reactions with hydrocarbon species, in addition to the "filament poisoning" effect suggested by Celii and Butler [76].

Martin [78] used a Linnett and Marsden type catalytic probe for measuring H atom concentrations down stream of a microwave plasma discharge, as shown in Fig 2.8(a). The probe, shown in Fig. 2.8(b), consisted of two small type-K thermocouples with alumina insulation. One thermocouple was wrapped with silver wire and the other covered with a quartz thimble for reference. The quartz thimble was held in place with a cement made of sodium silicate solution and talc. The difference in the efficacy of recombination of atomic
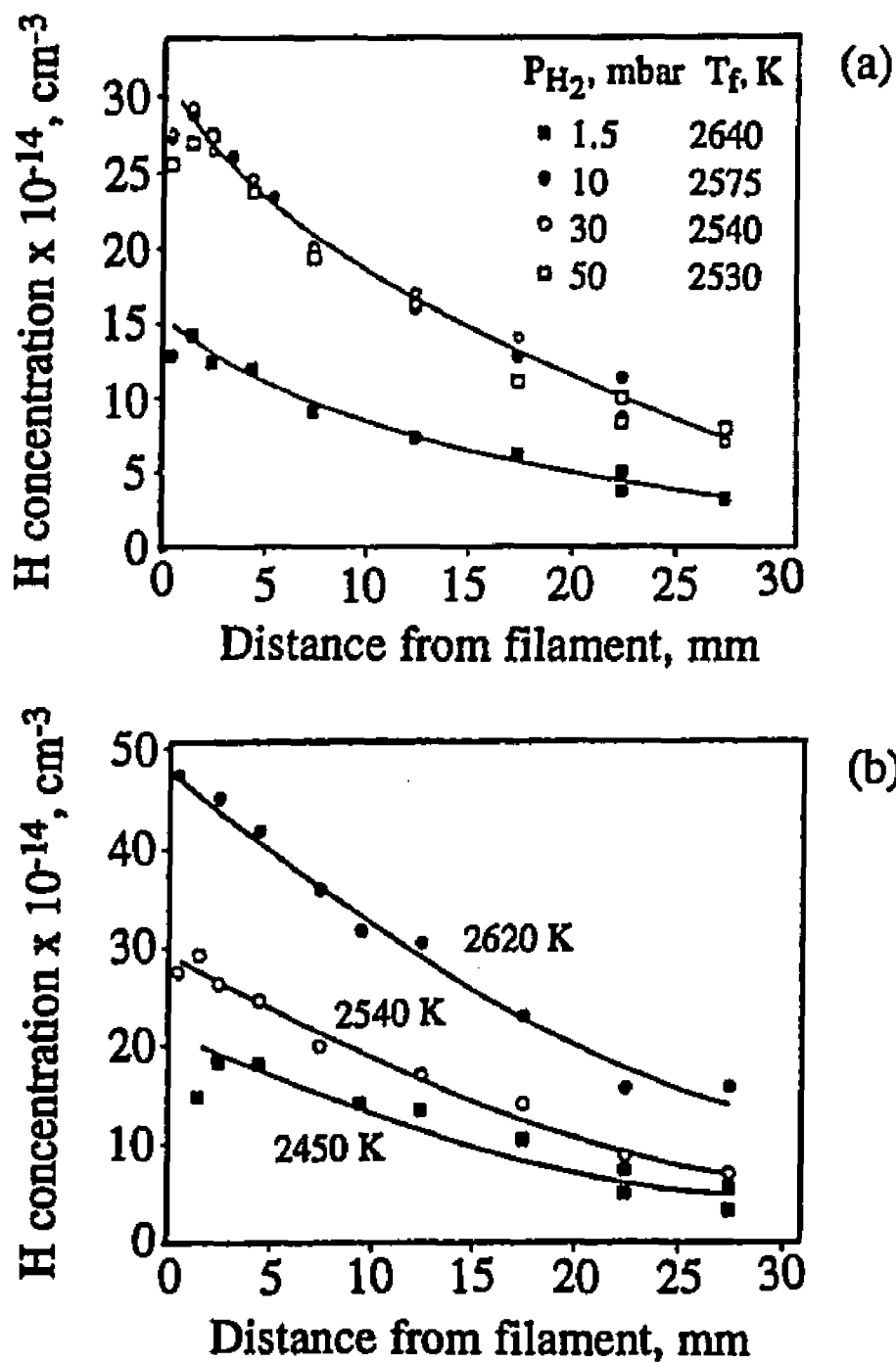
Fig. 2.6 Atomic hydrogen concentration profiles for a 2 mm tantalum filament for different (a) molecular hydrogen pressures, and (b) filament temperatures at 30 mbar molecular hydrogen pressure [48].
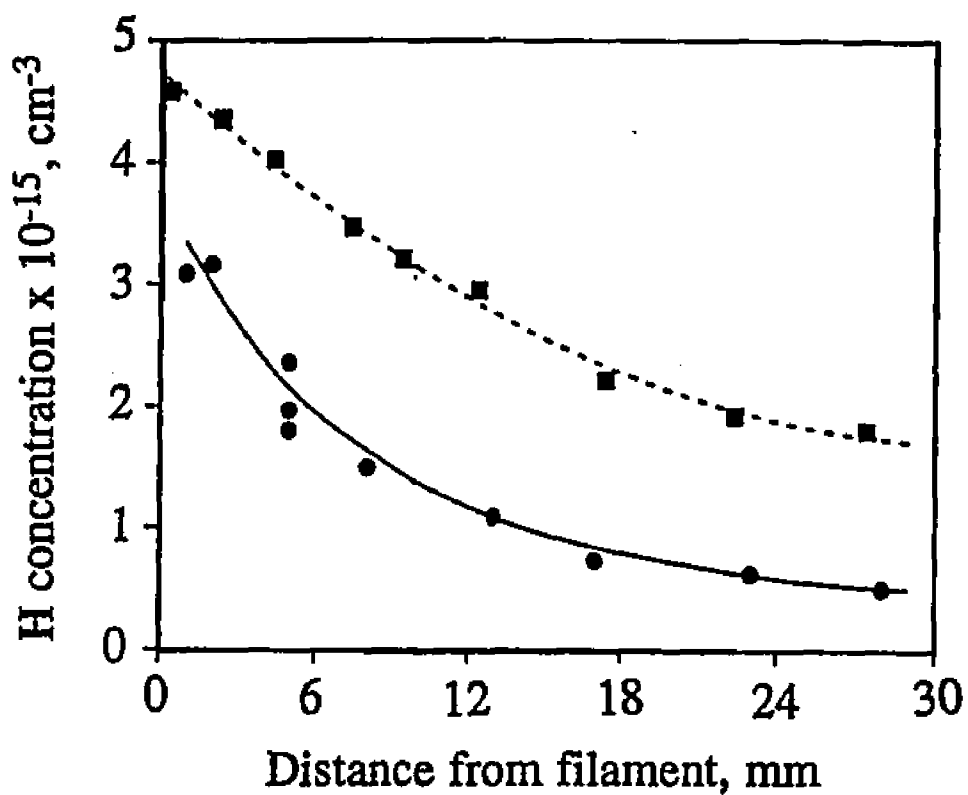
Fig. 2.7 Effect of methane addition on hydrogen atom profiles for a 2 mm tantalum wire and 30 mbar pressure. Squares represent hydrogen atom concentrations for 0% methane and 2620 K filament temperature and circles represent concentrations for 5% methane and 2700 K filament temperature [49].

Stainless Steel Tube

(a)

Injector

Tube Furnace

H probe

To M.S.
and Pump

Substrates

Microwave

Additional Boric Acid Passivation

Flow

(b)

6 mm O.D.

Quartz Thimble

SiO$_2$

Type K
Thermocouples

Silver Wire

Al$_2$O$_3$
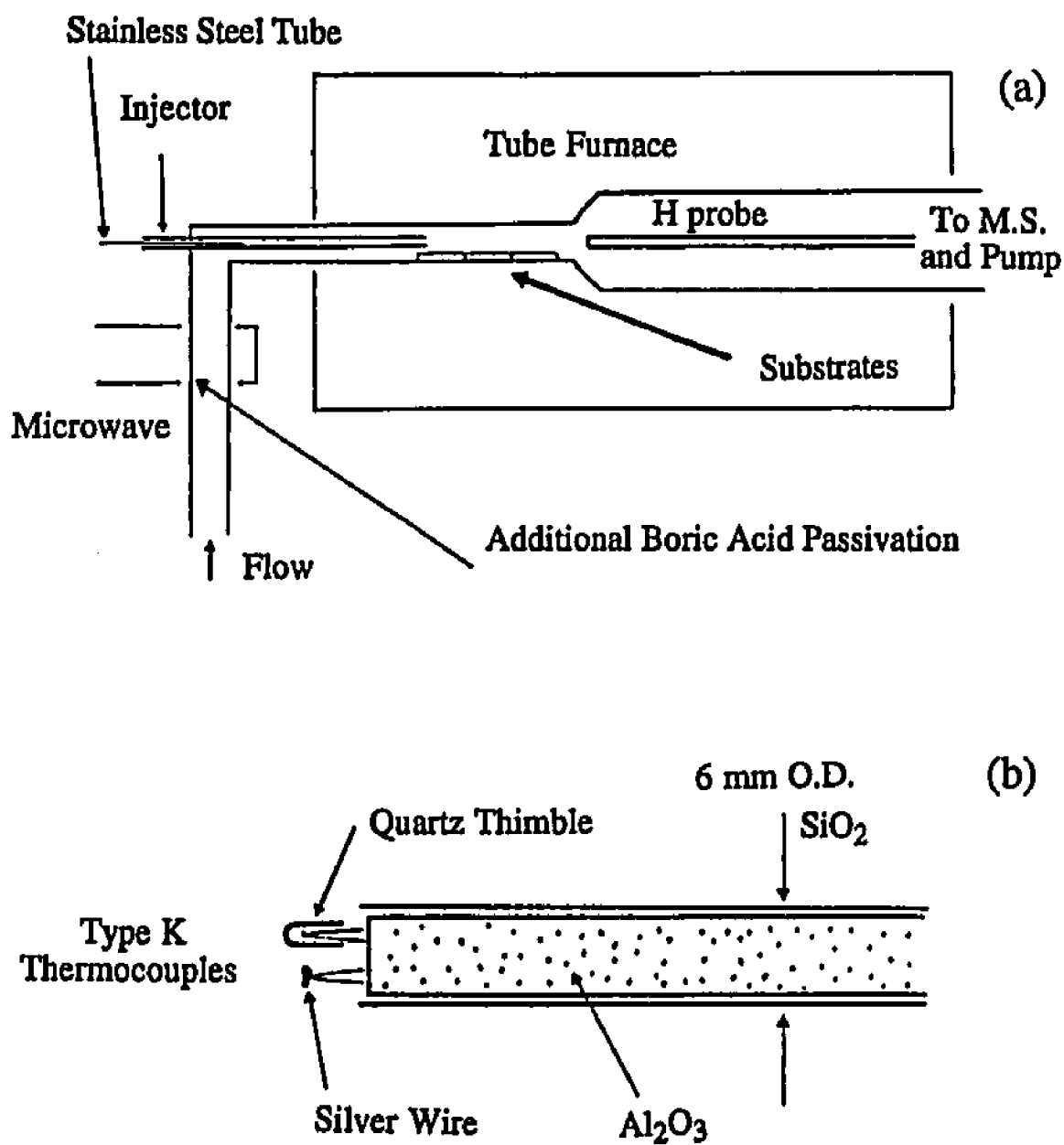
Fig. 2.8 Schematic diagram of (a) quartz flow tube and (b) hydrogen atom probe [78].

hydrogen on quartz and silver produced a temperature difference of up to 240 °C. An absolute calibration of the probe, obtained by titrating the H atoms with nitrosyl chloride [78], yielded a probe sensitivity of 36 °C per sccm of H atoms. In their experiments, they introduced methane down stream from the plasma. They observed a decrease in the temperature difference between the thermocouples with the addition of methane. An analysis of their results showed that the decrease of H atoms can not be explained on the basis of gas phase reactions between H atoms and hydrocarbon species. They concluded that methane caused a heterogeneous loss of atomic hydrogen on the substrate and reactor walls.

In this section the measurement of species concentrations primarily in filament assisted CVD has been presented. Gas phase diagnostics of other diamond depositions systems including low pressure plasmas, plasma torches, and combustion flames has been reported. Since the details of these investigations have been recently reviewed by Celii and Butler [79], they are not presented here.

2.5 Modeling of Diamond Deposition Processes

Fig. 2.9 shows a schematic diagram of a diamond CVD process. Gaseous reactants typically 1% methane in hydrogen flow into the reactor and gas phase reactions are initiated by a hot filament or a plasma. The transport of reactants and products takes place due to an interaction of free and forced convection and molecular diffusion driven by a combination of concentration and thermal gradients. Concomitantly, various chemical reactions, each with different but highly temperature sensitive kinetics occur in the gas phase at various temperatures in different locations of the reactor. Additional complexities include heat
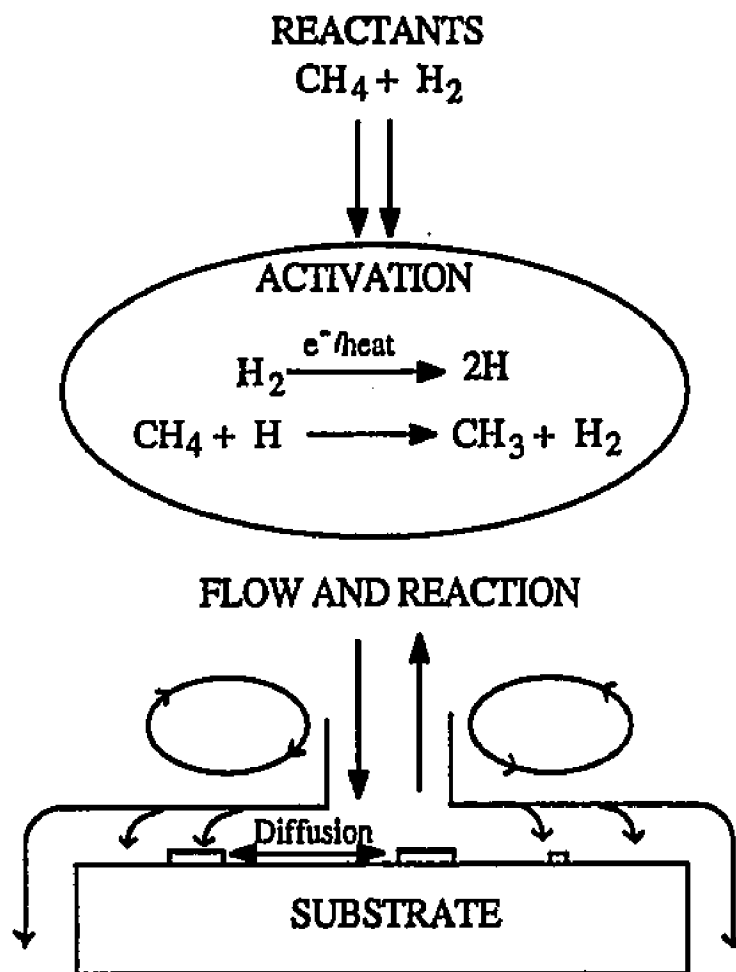
Fig. 2.9 A schematic diagram showing the principal components of diamond CVD: flow of reactants into the reactor, activation of gases by thermal or plasma techniques, reaction and transport of species to the growth surface and surface processes leading to deposition of diamond.

generation due to chemical and other effects, and the transport and interaction of ionic species and electrons with the electric field that often exists in the reactor. At the deposition surface, a sequence of deposition steps involving adsorption and other surface events such as chemical reaction, surface diffusion, lattice incorporation, and desorption take place leading to the deposition of diamond.

Although a comprehensive model taking into account various physical and chemical processes would be useful for understanding diamond growth process as a whole, concentrated efforts in specific areas can also provide significant insight into the deposition process. Gas phase chemical kinetic and transport models have provided information of the nature of the species present in the deposition environment and the dominant species transport mechanisms. Typically, only a few species in a complex mixture such as that encountered in diamond CVD systems can be detected. However, measured concentrations of these species can be used to verify models of gas phase reaction chemistry which can then be used to provide predictions for undetected species. Furthermore, surface reaction models can provide plausible schemes to describe diamond growth. In the following sections the work done in the areas of species transport and gas phase and surface chemistry are reviewed.

2.5.1 Gas Phase Chemistry and Transport

The relative importance of various mass transport mechanisms, including free and forced convection and molecular diffusion due concentration and thermal gradients, has been examined to identify the dominant species transport mechanism in diamond reactors [80,81]. The importance of natural convection can be estimated from the Grashof number,

which is a measure of the relative magnitude of buoyancy and viscous forces. Tankala [81] and Angus et al. [82] showed that an order of magnitude calculation of the Grashof number for hot filament reactors yields a value close to unity indicating that natural convection is as important as bulk convection for typical diamond deposition conditions. However, the Peclet number for mass transport, which is the ratio of convective mass transport to diffusive mass transport, is much less than one indicating that diffusion is the dominant mechanism of mass transport [80-82]. Although Peclet number calculations indicate that convection is not important in hot filament [80,81] and microwave systems [82], mass transport by convection is important in high gas velocity processes such as plasma torches and combustion flames [82].

DebRoy et al. [80] provided experimental evidence that indicates that both natural and bulk convection are unimportant in determining the quality, uniformity and growth rate of diamond films in hot filament reactors. They conducted experiments under various gas flow configurations shown in Fig 2.10(b). The flow configurations were planned such that the convective flow in the reactor either aids the transport of various species towards the sample as in configurations 1 and 2 in Fig 2.10(b), or opposes the transport as in configurations 3 and 4. Furthermore, in some cases such as in configuration 2, the flow due to natural convection aids the transport due to bulk convection and, in some other cases such as in configuration 1, opposes it. They argued that if convection were important then for configuration 3, where both free and forced convection carry the species generated at the hot filament away from the substrate, the rate of deposition should be small if not negligible, and for configuration 2, where both natural and bulk convection carry the species to the substrate the growth rate should be high. Their results showed that the quality of the diamond films, as evidenced by SEM and Raman spectra [80,81], and the
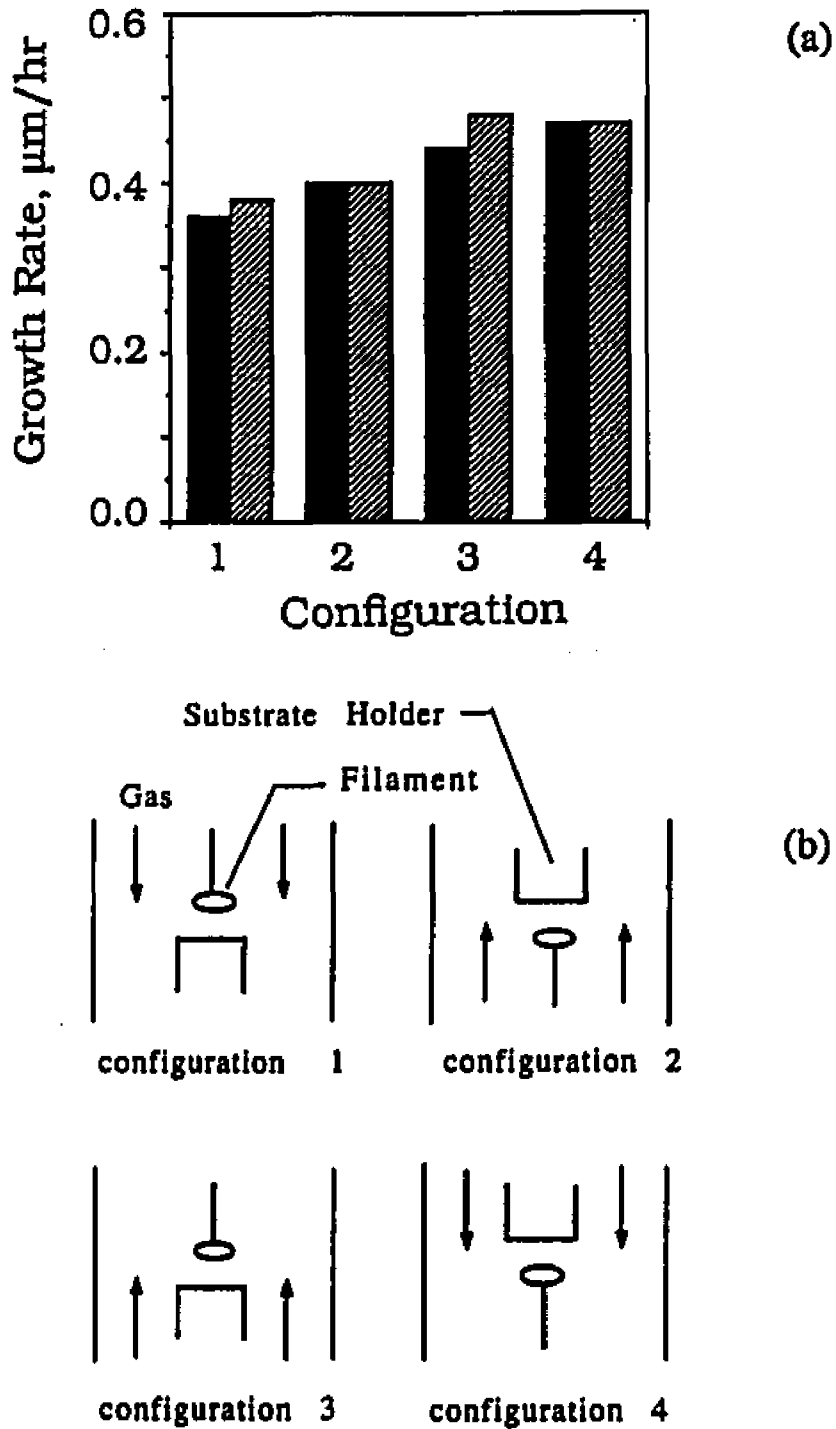
Fig. 2.10 (a) Diamond film growth rates under (b) various gas flow configurations. In each gas flow configuration the results of two experiments are presented [80].

growth rates, shown in Fig 2.10(a), of the films deposited under the widely different flow configurations were not significantly different indicating that convection is not important in the transport of species in hot filament reactors. They further used calculated temperature and species concentration gradients in the reactor to show that both ordinary and thermal diffusion are equally important in the transport of hydrocarbon species in HFCVD reactors. However, thermal diffusion is not important in the transport of atomic hydrogen [81].

The first computational analysis of gas phase chemistry during filament assisted diamond growth was provided by Harris et al. [73,74]. They used a zero-dimensional kinetic reaction model which assumed a fixed temperature profile in the reactor. The reaction rate data needed for the calculations was taken from the available hydrocarbon combustion data. They verified their calculations by comparing the predicted CH_4, C_2H_2, CH_3 and H atom concentrations with those derived from mass spectrometric measurements [73]. The authors concluded that CH_3, C_2H_2, CH_4 and C_2H_4 were the only species present in sufficient quantities to explain the observed diamond growth rates. Of these, they suggested that CH_3 and C_2H_2 are more likely to be the growth species because of their higher chemical reactivity. A similar model was used by Frenklach [83], who found that the primary role of molecular hydrogen was to suppress the formation of aromatic species, which promote the formation of non-diamond carbon. More recently, Frenklach and Wang [84] presented a diamond growth model involving gas phase and surface reaction kinetics at the diamond (111) surface. They predicted that diamond growth rates by addition of C_2H_2 was two to four orders of magnitude higher than that obtained by the addition of CH_3. This was contrary to the experimental observations of Yarbrough et al. [72], Martin and Hill [70] and Chu et al. [85].

Chauhan, Angus and Gardner [86] reported detailed kinetic data on diamond deposition on diamond seed crystals from methane and methane-hydrogen mixture without the use of a hot filament or electric discharge. In their experiments they heated the diamond seed crystals to 1438 K with high intensity infrared lamps. Harris [87] used a one dimensional chemical kinetic analysis to model the gas phase chemistry that occurred during diamond growth experiments of Chauhan, Angus and Gardner [86]. His analysis indicated that the amount of pyrolysis that occurred at 1438 K was so small that no significant amount of C_2H_2 or CH_3 was formed and the major hydrocarbon species was CH_4. Therefore, he concluded that diamond can grow from direct decomposition of CH_4 on the diamond surface.

Martin and Hill [70], in their flow tube experiments, deposited diamond films on silicon substrate down stream from a microwave discharge. A schematic diagram of their experimental set up is shown in Fig. 2.8(a). In their experiments, the microwave discharge was used only to dissociate hydrogen. Methane gas was introduced down stream from the plasma near the substrates. Harris and Martin [88], analyzed the flow tube diamond CVD experiments of Martin and Hill [70] with a chemical kinetic model. The one dimensional flow model included thermal diffusion and heterogeneous loss of H atoms. They predicted that methyl radical and methane are the only species present in sufficient concentrations to account for the observed growth rates.

Goodwin and Gavillet [50] developed a one dimensional numerical model to understand the transport and chemistry occurring during HFCVD of diamond. They obtained temperature velocity and species concentration fields for H, H_2 and various hydrocarbon species. The calculated concentrations of the stable hydrocarbon species near the substrate agreed well

with those measured by Harris et al. [73] using mass spectroscopy. From the estimated concentration profiles of various hydrocarbons they calculated upper-bound, diffusion limited growth rates for various assumed growth species. They concluded that even if the all of assumed growth specie reaching the substrate were to contribute to diamond growth, the only hydrocarbon species that can account for the experimentally measured diamond growth rates are CH_3, C_2H_2 and CH_4. The conclusion is however made on the assumption that a single hydrocarbon specie is responsible for diamond growth. They also investigated the observed decrease in H atom concentration [50] with increasing methane content in the feed gas. They concluded that since homogeneous recombination of H atoms is not fast enough, the reduced H concentration is likely due to lower H generation at the filament surface due to hydrocarbon poisoning.

One major limitation of the chemical kinetic models is that the system is approximated to a one dimensional situation. However, most real systems are two or three dimensional. In a hot filament reactor, the gas flowing in close proximity to filament experiences the high temperature of the filament and under goes significant pyrolysis. The surrounding gas is relatively cooler and experiences a lower degree of dissociation. A one dimensional model is limited in that it does not account for the mixing of species generated at various locations of the reactor. More accurate predictions of species concentration profiles in the reactor can be obtained by incorporating two or three dimensional fluid flow and heat transfer models into the chemical kinetic models.

2.5.2 Surface Chemistry

2.5.2.1 Surface Structure

Although bulk diamond is made up of only carbon, the surface of diamond is hydrogenated. Lander and Morrison [57] were the first to show that hydrogen can stabilize a diamond surface by forming sp^3 C-H bonds with the surface carbon atoms. In fact it is well known that in the absence of hydrogen the surface carbon atoms on cleaned bulk diamond crystals will reconstruct at about 900-1000 ^oC [58]. However, in the presence of hydrogen, the reconstruction reverses as the dangling sp^3 bond of surface carbon atoms are satisfied by C-H bonds [57].

Fig. 2.11 shows the (111), (110) and (100) surfaces of diamond with surface carbon atoms satisfied by C-H bonds. The dark large circles represent carbon atoms while the smaller open circles represent the surface hydrogen atoms. The (111) and (110) surfaces of diamond each require one hydrogen atom per surface carbon atom to stabilize the surface. The (100) surface, on the other hand, requires two hydrogen atoms to satisfy the two dangling bond of each surface carbon atom. The surface structures for (111) and (110) surfaces are conceivable and present no steric problem, however the structure for (100) is problematic. Using bond lengths of 1.54 A for C-C bonds and 1.10 A for C-H bonds and tetrahedral bond angles of 109.5^o, it has been shown [68] that the inter nuclear distance between the surface hydrogen atoms on the (100) surface is 0.77 A, nearly the same as that in the H_2 molecule, 0.74 A. As this is a non-bonding interaction, significant steric repulsion is expected leading to a significant deviation from the model structure shown in Fig. 2.11. Alternative model structures for the diamond (100) surface, which may be more
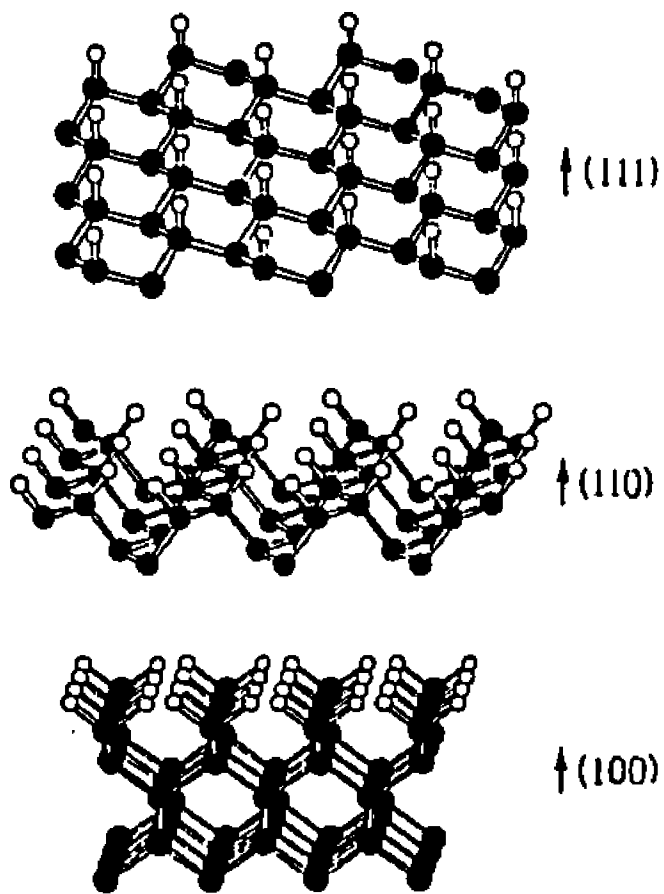
Fig. 2.11 Schematic diagrams showing diamond crystal truncated along (111), (110) and (100) planes. The dangling bonds of the surface carbon atoms are terminated by hydrogen atoms. The solid circles represent carbon atoms and the open circles represent hydrogen atoms [89].

stable, have been suggested [89,90] and are shown in Fig. 2.12. The steric problem of the dihydride diamond (100) surface, shown in Fig. 2.12 (a), can be overcome if the surface reconstructs to form a monohydride structure, as shown in Fig. 2.12(c), or form a 50:50 dihydride:monohydride structure, as shown in Fig. 2.12(b) [90].

2.5.2.2 Surface Reactions

The various reactions taking place at the growth surface leading to the formation of diamond can be classified as (a) surface activation, (b) carbon addition, and (c) carbon incorporation. Atomic hydrogen plays an important role in the formation of surface active sites. A surface activated site is required for the addition of carbon in the form of hydrocarbon species. The following reactions represent the surface activation and hydrocarbon addition [68]:

$$C_{(s)}H + H = C_{(s)}^* + H_2 \qquad\qquad 2.2$$

$$C_{(s)}^* + H = C_{(s)}H \qquad\qquad 2.3$$

$$C_{(s)}^* + CH_3 = C_{(s)}CH_3 \qquad\qquad 2.4$$
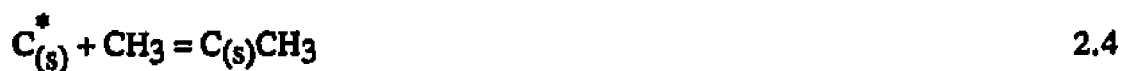
where, $C_{(s)}$ is a carbon atom at the surface of diamond, $C_{(s)}^*$ is a surface active site and $C_{(s)}H$ is a H bonded surface carbon atom. Reaction 2.2 represents activation of a surface site by hydrogen abstraction. The surface activated site can recombine with atomic hydrogen resulting in deactivation, or at elevated temperatures the reverse of reaction 2.3

(a)

(b)

(c)
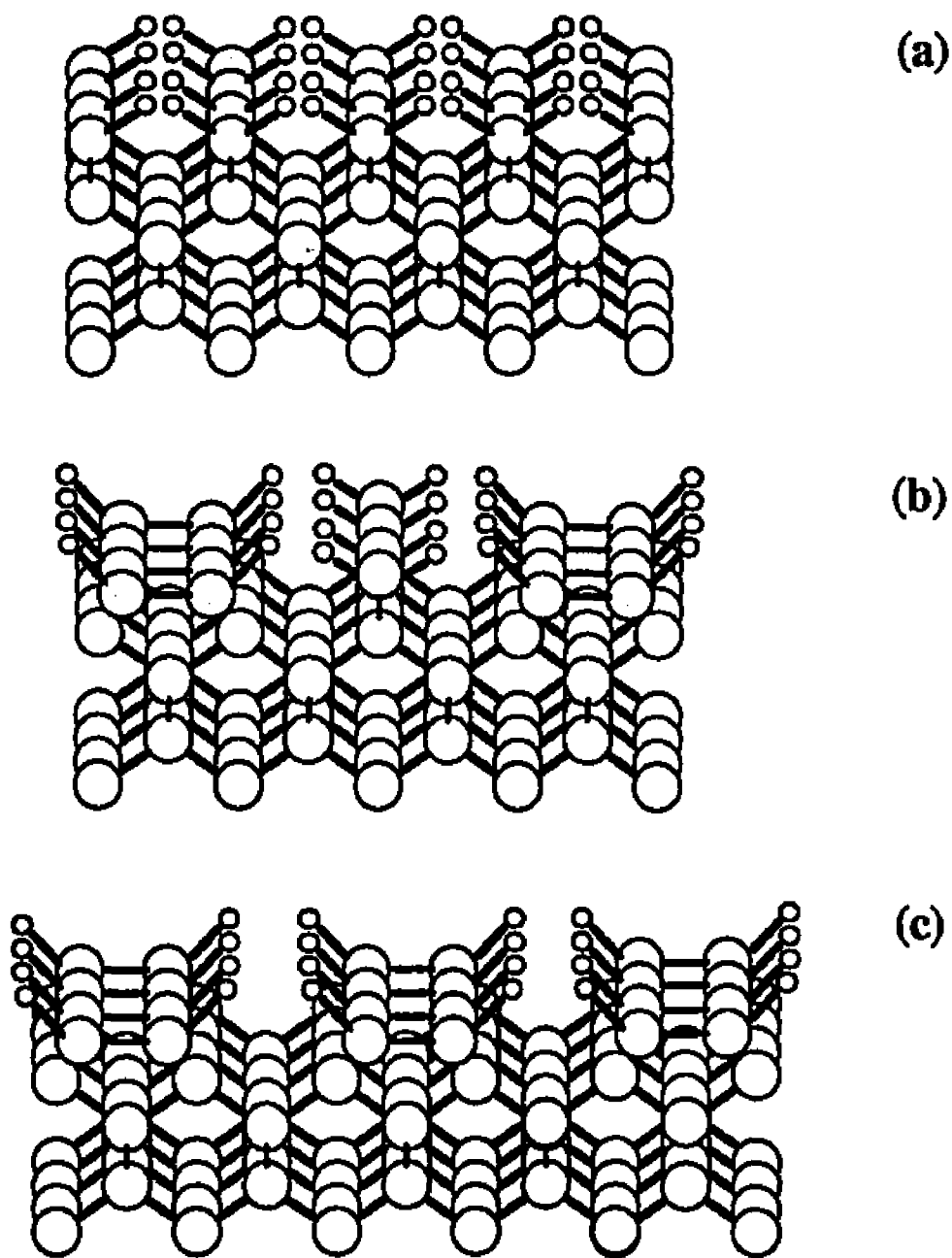
Fig. 2.12 Schematic diagrams of various possible surface structures of hydrogen terminated diamond (100) surface. (a) Dihydride, (b) 50:50 dihydride:monohydride and (c) monohydride structures. The large circles represent carbon atoms and the small circles represent hydrogen atoms.

can lead to surface activation. Reaction 2.4 represents the addition of a hydrocarbon species to an activated site.

A close examination of reactions 2.2 and 2.3 shows that a dominant process occurring at the surface is the recombination of atomic hydrogen to form molecular hydrogen.

$$H + H = H_2 \qquad \Delta H^0{}_{1200\,K} = -52 \text{ kcal/mole of H} \qquad\qquad 2.5$$

This is a highly exothermic reaction and can result in significant substrate heating. Furthermore, a spatial variation in the atomic hydrogen flux at the growth surface can result in substrate temperature non-uniformity. Since the kinetics of various surface reactions are temperature sensitive, a non-uniform temperature distribution on the growth surface can result in the deposition of non-uniform films.

Upon addition of a hydrocarbon to the surface, the newly added carbon has one bond to the lattice. For the added carbon to be incorporated, additional bonds should be formed with the diamond lattice. Since the newly added carbon atom is in the form of a hydrocarbon species and the hydrocarbon is hydrogenated, incorporation of the carbon atom involves removal of the hydrogen atoms. The removal of hydrogen atoms bonded to the added hydrocarbon is facilitated by atomic hydrogen through hydrogen abstraction reactions. The following set of reactions represent removal of hydrogen atoms from the added hydrocarbon and incorporation of the added carbon [68]:

$$C_{(s)}CH3 + H = C_{(s)}CH_2 + H_2 \qquad\qquad 2.6$$

$$C_{(s)}CH3 = C_{(s)}CH_2 + H \qquad\qquad 2.7$$

$$C_{(s)}CH_2 + C_{(s)}CH_2 = C_{(s)}CH_2CH_2C_{(s)} \qquad\qquad 2.8$$

$$C_{(s)}CH_2 + C(s) = C_{(s)}CH_2C_{(s)} \qquad\qquad 2.9$$
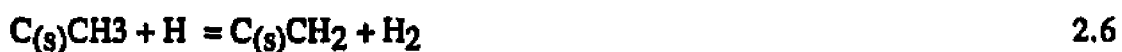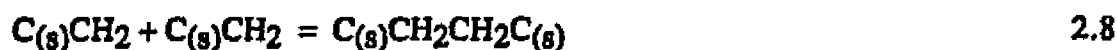
Using these basic steps diamond growth on diamond (111) surface [61,62], diamond (110) surface [68], unreconstructed diamond (100) surface [64], and (2 X 1) reconstructed diamond (100) surface [91], have been proposed.

2.6 Diamond vs. Graphite

Figure 1.2 shows that diamond growth at low pressures and relatively low temperatures, encountered in CVD techniques, occurs under conditions where graphite is the expected stable phase. The growth of diamond instead of graphite or some other form of graphitic carbon under these conditions has intrigued several researchers. Numerous theories have been suggested to account for the metastable growth of diamond. Many of these ideas assign a role to the presence of super-equilibrium concentrations of atomic hydrogen in the gas phase. One of the early theories proposed that atomic hydrogen etches graphite more readily than diamond and diamond growth is possible because the nucleation and growth of graphitic material is suppressed. More recent theories include, pseudomorphic stabilization of diamond relative to graphite by surfaces [92], defect induced stabilization of diamond [93], and role of atomic hydrogen in stabilizing diamond surfaces [94].

One of the most popular theories on the growth of diamond instead of graphitic carbon under low pressure conditions is based on kinetic arguments. Atomic hydrogen is known to gasify graphitic carbon orders of magnitude faster than diamond [51,56]. From this point of view, it is thought that diamond growth is kinetically more stable because the nucleation and growth of graphitic material is suppressed. Sommer and Smith [95] incorporated the enhanced etching of graphitic carbon by atomic hydrogen into their thermodynamic quasi-equilibrium model and predicted that there is a region in the C-H phase diagram where diamond is the only stable solid phase. Fig. 2.13 shows the predicted phase diagram for a total pressure of 36 Torr. The lines represent the phase boundaries between the region where solid carbon exists and the region where no condensed phases exist for graphite, g, and diamond, d. The region between the lines d and g represents the region where diamond is the only stable solid phase. They compared the model predictions with the experimental results of Matsumoto et al. [30]. The squares in the figure represent the experimental conditions of Matsumoto et al. where well crystallized diamond was obtained, while the open and filled circles correspond to poorly defined particles and large particles covered with graphitic deposits, respectively. These results are in good agreement with the predicted phase diagram, since the conditions leading to well-crystallized diamond fall in the region where diamond is the only stable phase. The line marked d(760) is the phase boundary for diamond at atmospheric pressure. Since the data points now lie in the etching region, the model also explains the absence of diamond growth above atmospheric pressures.

Bar-Yam and Moustakas [93] proposed that the stabilization of diamond relative to graphite is brought about by the presence of vacancies near the growth surface during low pressure diamond growth. They showed that although the free energies of formation of bulk
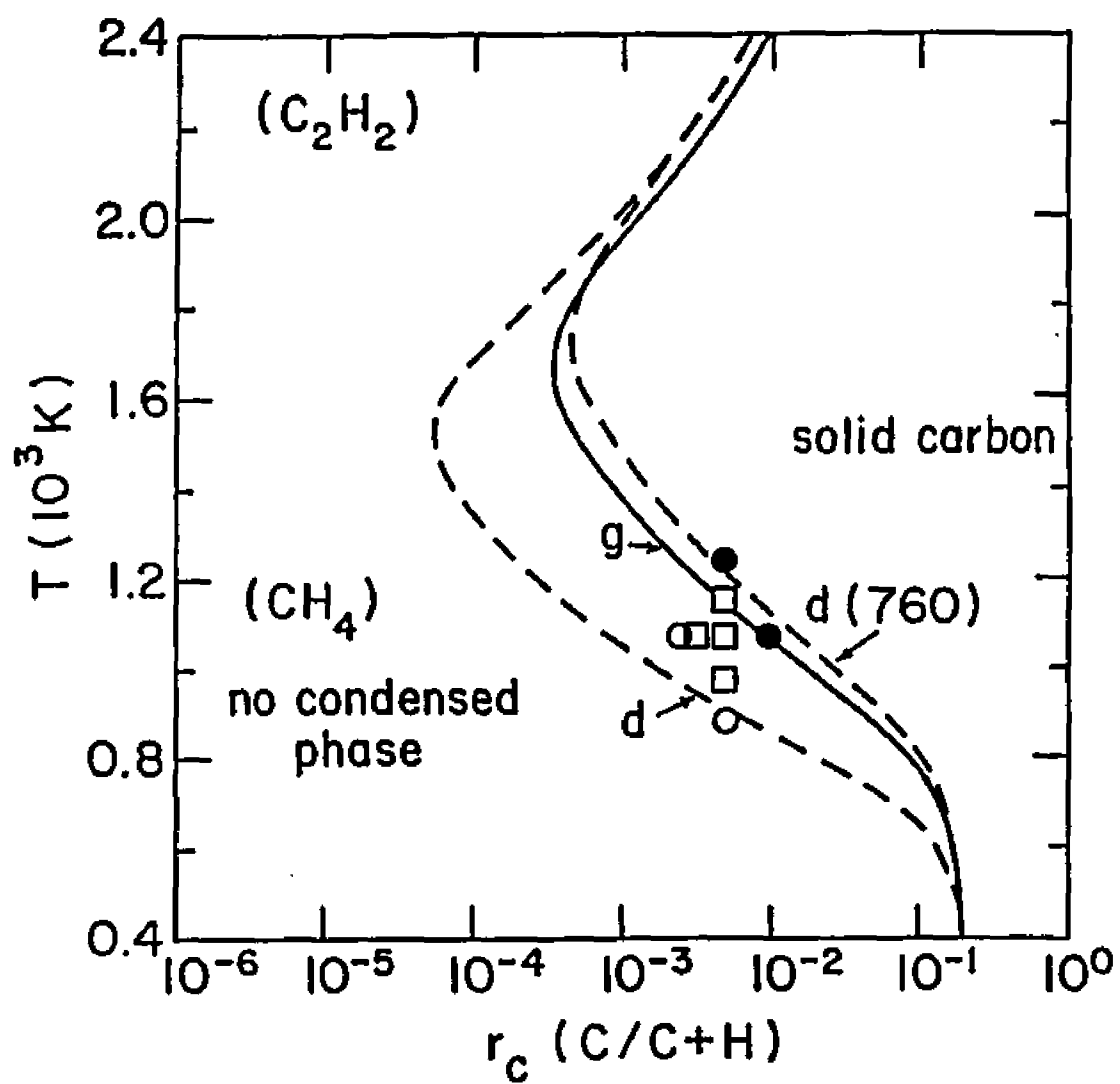
Fig. 2.13 Predicted phase diagram for carbon-hydrogen system at 36 Torr [95].

diamond is higher than that of graphite, including the free energy of formation of vacancies, formed at the growth surface during diamond growth, can change the relative stability of diamond and graphite. They argued that since the enthalpy of formation of vacancy in graphite is higher than the enthalpy of formation of a vacancy in diamond, the presence of a small concentration of vacancies can lead to a lower total free energy of formation for the diamond structure compared to the graphite structure. That is,

$$F_b(dia) + n_{dia} F_d(dia) < F_b(gr) + n_{gr} F_d(gr) \qquad 2.10$$

where, $F_b(dia)$ and $F_b(gr)$ are the free energies of formation of bulk diamond and graphite respectively, $F_d(dia)$ and $F_d(gr)$ are the free energies of formation of vacancies in diamond and graphite respectively, and n_{dia} and n_{gr} are concentrations of vacancies in diamond and graphite respectively. An important implication of this theory is that if the presence of vacancies is necessary for stabilizing diamond growth, the formation of highly defect free diamond films for electronic and optical applications is very difficult, if not impossible. Two main difficulties are associated with this theory of defect induced stabilization of diamond. First, the theory requires the assumption of surface states which have not been experimentally observed. Second, the presence of vacancies near the surface increases the free energy, and the diamond surface has been observed to reconstruct to lower its free energy [58].

Machlin [92], suggested that the growth of diamond relative to graphite is controlled by the nature of the substrate and the diamond structure is pseudomorphically stabilized by the underlying structure. They argued that in thin film deposition the contribution of substrate-film interface energies to the total free energy can not be neglected. The stability of diamond

relative to graphite should not be examined based only on their bulk free energies. Rather, the total free energies, i.e. the sum of the bulk free energy and the substrate-film interface energy, for substrate-diamond and substrate-graphite systems should be examined. They showed that for suitable substrates the contribution of interface energies were significant and the diamond structure yields a lower free energy, for the substrate-film system, than the graphite structure. Machlin's theory does not incorporate the important role of atomic hydrogen in the deposition of diamond and suggests that, in the presence of a suitable substrate that pseudomorphically stabilizes diamond, continuous growth of diamond should be possible. This theory explains the initial growth of diamond on diamond seed crystals in the experiments of Chauhan et. al. [86], where diamond was deposited from methane gas without any gas phase activation. According to Machlin's theory Chauhan et. al. [86] should have observed continuous growth of diamond. However, in their experiments they observed that after an initial growth of diamond there was nucleation and growth of graphitic material.

Another approach emphasizes the role of surfaces in the diamond CVD process. In this theory, atomic hydrogen, instead of serving as a reagent to etch graphite, is thought to stabilize the diamond surface and prevent it from reconstructing [58,96]. This approach argues that since diamond growth occurs at the surface and not in the bulk, the stability of diamond relative to graphite should be examined by comparing their surface free energies of formation rather than the bulk free energies of formation. Yarbrough [94] estimated the enthalpies of formation of the principal surfaces of diamond, graphite and lonsdaleite. A comparison of the data indicated that the hydrogenated surface of diamond had a lower enthalpy of formation than the hydrogenated surfaces of graphite or lonsdaleite. He assumed that the surface entropies are the same as the bulk entropies per mole of carbon for

the respective phases. Using these estimates and a free energy minimization routine, SOLGASMIX, he determined the proportion of various surfaces that led to the lowest free energy of the system composed of the solid surface, atomic and molecular hydrogen. Fig. 2.14 shows the variation of the predicted phases with atomic hydrogen partial pressure. He observed that for a substrate temperature of 950 °C, as the atomic hydrogen partial pressure increased, the proportion of diamond surface relative to graphite and lonsdaleite increased. Thus, he argued that diamond growth occurs not necessarily because of any kinetic competition between diamond and graphitic carbon but because, under the conditions of growth, the diamond surface is thermodynamically more stable than the graphite surfaces.

2.7 Summary

Significant progress has been made in understanding diamond deposition by various chemical vapor deposition techniques. Both experimental and modeling efforts have provided detailed insight into various important physical and chemical processes occurring during diamond deposition. Several researchers have examined the importance of various hydrogen and hydrocarbon species in the growth process. Although there is some controversy over the nature of the hydrocarbon species important for diamond deposition, the importance of atomic hydrogen is widely recognized. Various roles have been assigned to atomic hydrogen. These include selective etching of graphitic deposits, stabilization of sp^3 bonds necessary for the formation of diamond, generation of surface reactive sites by hydrogen abstraction and generation of hydrocarbon species important for diamond growth.
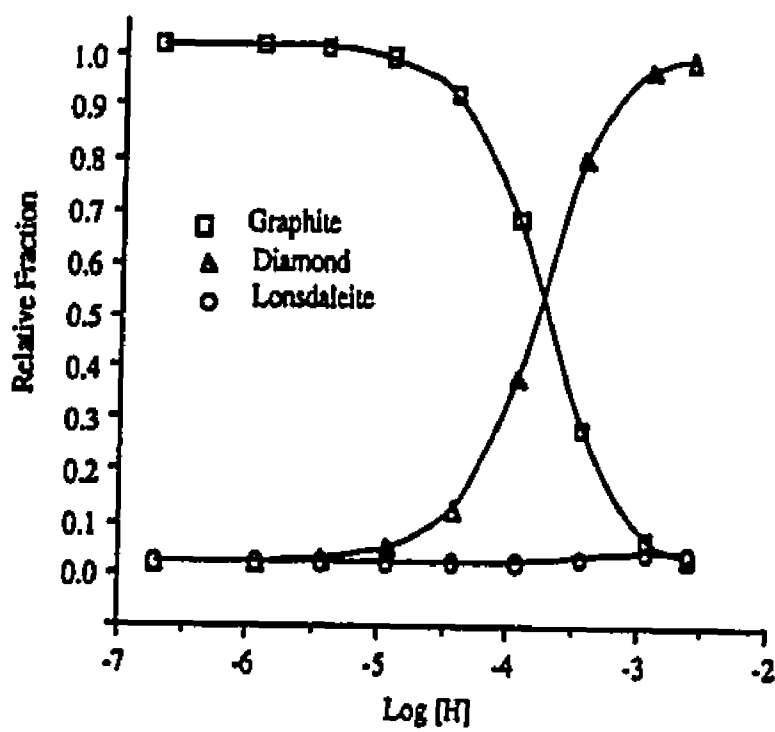
Fig. 2.14 Variation of predicted phase with atomic hydrogen partial pressure at a substrate temperature of 950 °C [94].

The formation of atomic hydrogen at the filament is highly endothermic. On the other hand, atomic hydrogen readily recombines on solid surfaces to form molecular hydrogen and the recombination reaction is highly exothermic. Thus, atomic hydrogen can act as a carrier of heat from the filament to the growth surface. Furthermore, the spatial variation of atomic hydrogen at the substrate surface can result in spatial variation of substrate temperature, and consequently, non-uniform film quality and thickness. Atomic hydrogen concentrations have been measured by several techniques. Much of the previous work was undertaken to develop a better understanding of the gas phase chemistry, gas-surface reactions and the growth mechanism. However, the role of atomic hydrogen in affecting the substrate temperature has not been investigated. Furthermore, there is significant controversy over the factors that influence the spatial distribution of atomic hydrogen in the reactor.

Various process parameters affect the quality, morphology and growth rate of the diamond films. Changes in process parameters can significantly influence the spatial distribution of nutrient species at the growth surface, and hence, the growth rate and quality. The process parameters can also influence the generation and transport of atomic hydrogen resulting in a spatial distribution of atomic hydrogen at the substrate, and hence, deposition of non-uniform films. Thus, the effect of process parameters on the substrate temperature needs to be examined. Furthermore, a fluid flow and heat transfer model that accounts for substrate heating due to atomic hydrogen recombination in addition to conduction, convection and radiation will be useful for reactor design and scale-up.

The bulk free energies of diamond and graphite can not explain t diamond growth with simultaneous gasification of graphite at low pressures and relatively low temperatures, encountered in CVD techniques, where graphite is the expected stable phase. Several

theories have been proposed to account for the metastable growth of diamond. However, a unified mechanistic answer is not yet available. One approach emphasizes the role of surfaces in the CVD of diamond. The structure and composition of diamond and graphite surfaces are significantly different from that of the bulk. Furthermore, diamond growth occurs at the gas-solid interface in the presence of atomic hydrogen. Thus, the stability of diamond and graphite surfaces, rather than their bulk forms, and the influence of atomic hydrogen concentration on their relative stability should be examined.

2.7 References

1. B. V. Deryagin and D. V. Fedoseev, *Rost Almaza i Grafita iz Gazavoj Fazy*, Nauka, Moscow (1977).

2. N.Fujimori, T. Imai and A. Doi, Vacuum, 36, 1 (1986); Y. Saito, K. Sato, H. Tanaka, K. Fujita, S. Matuda, J. Mater. Sci., 23, 842 (1988).

3. B. Singh, Y. Arie, A. W. Levine, O. R. Mesker, Appl. Phy. Lett. 52, 451 (1988); T. Kawato and K. Kondo, Jpn. J. Appl. Phys., 26, 1429 (1987);

4. Y. Hirose and N. Kondo, paper presented at the Japan Society of Applied Physics Meeting, 29th March 1988 Tokyo, Japan; L. M. Hanssen, W. A. Physics Meeting, 29th March 1988 Tokyo, Japan; L. M. Hanssen, W. A. Carrington, J. E. Butler, K. A. Snail, Mat.Sci. Lett., 7, 289 (1988).

5. D. E. Patterson, B. J. Bai, C. J. Chu, R. H. Hauge and J. L. Margrave, in *New Diamond Science and Technology*, eds. R. Messier, J. T. Glass, J. E. Butler and R. Roy, p. 433 (MRS, Pittsburgh, PA, 1991).

6. N. Fujimori, A. Ikegaya, T. Imai, K. Fukushima, N. Ohta, in *Proceedings of the First International Symposium on Diamond and Diamond-Like Films*, eds. J.P. Dismukes et al., (The Electrochemical Society, Pennington, NJ, 1989).

7. A. R. Badzian, P. K. Bachmann, T. Hartnett, T. Badzian and R. Messier, Materials Research Society Meeting, XV, p. 63 (1987).

8. Y. Matsui, A. Yuuki, M. Sahara and Y. Hirose, Jpn. J. Appl. Phys., 28(9), 1718 (1989).

9. L. M. Hanssen, W. A. Carrington and J. E. Butler and K. A. Snail, Mater. Lett., 7, 289 (1988).

10. D. E. Patterson, C. J. Chu, B. J. Bai, N. J. Komplin, R. H. Hauge and J. L. Margrave, in *Applications of Diamond Films and Related Materials*, eds. Y. Tzeng, M. Yoshikawa, M. Murakawa, and A. Feldman, p. 569 (Elsevier Science Publishers B. V., 1991).

11. J. C. Angus and C. C. Hayman, Science, **241**, 913 (1988).

12. S. Mitura, J. Cryst. Growth, **80**, 417 (1987).

13. A. R. Badzian, T. Badzian, R. Roy, R. Messier and K. E. Spear, Mat. Res. Bull., **23**, 531 (1988).

14. P. K. Bachmann, W. Drawl, D. S. Knight, R. Weimer and R. Messier, in *Diamond and Diamond-Like Materials Synthesis*, Extended Abstracts, MRS, Pittsburgh, PA. 1988.

15. K. Kobashi, K. Nishimura, Y. Kawate and T. Horuchi, Phys. Rev. B, **38**, 4067 (1988).

16. K. Hirabayashi, K. Ikoma, Y. Taniguchi and N. I. Kurihara, in *Proceedings of the First International Conference on the New Diamond Science and Technology*, Program and Abstracts, JNDF, Tokyo, 1988.

17. Y. Mitsuda, Y. Kojima, T. Yoshida and K.Akashi, J.Mater. Sci., **22**, 1557 (1987).

18. Y. Mitsuda, T. Yoshida and K. Akashi, ISPC/Tokyo 1987, in*Eight International Symposium on Plasma Chemistry*, Symposium Proceedings, eds., K. Akashi and A. Kinbara, 2469 (1987).

19. W. A. Yarbrough, A. Kumar and R. Roy, paper presented at the Fall Meeting, MRS, Boston, MA., 1989.

20. S. Yugo and T. Kimura, in *Proceedings of the First Int. Conf. on the New Diamond Science and Technology*, Program and Abstracts, JNDF, Tokyo, 1988.

21. B. V. Derjaguin, B. V. Spitsyn, A. E. Goridetsky, A. P. Zakharov, L. L. Bouilov and A.E. Sleksenko, J. Cryst. Growth, **31**, 44 (1975).

22. M. Kamo, Y. Sato, S. Matsumoto and N. Setaka, J. Cryst. Growth, **62**, 64 (1983).

23. M. W. Gies, D. D. Rathman, J. J. Zayhowski, D. L. Smythe, D. K. Smith and G. A. Ditmer, in Diamond and Diamond-Like Materials Synthesis, Eds., G.H. Johnson, A.R. Badzian and M.W. Gies, MRS, Pittsburgh, PA., 1988.

24. A. R. Badzian and T. Badzian, Surface and Coatings Technol., **36**, 283 (1988).

25. A. R. Badzian and R. C. DeVries, Mat. Res. Bull., **23**, 385 (1988).

26. W. Zhu, C. A. Randall, A. R. Badzian and R. Messier, J. Vac. Sci. Technol., A7, 2315 (1989).

27. W. Zhu, R. Messier and A. R. Badzian, in *Proceedings of the First International Symposium on Diamond and Diamond Like Films*, eds., J.P. Dismukes et al, (The Electrochemical Society, Pennington, NJ, 1989).

28. K. A. Bulonkov, A. F. Bolianin, A. E. Aleksenko and B. V. Spitsyn, in *Proceedings USSR Conference on Crystal Growth*, Cahkadzor, Armenian SSR, 1985.

29. B. V. Spitsyn and L. L. Bouilov, in Diamond and Diamond-Like Materials Synthesis, Extended Abstracts, eds., G.H. Johnson, A.R. Badzian and M.W. Gies, (MRS, Pittsburgh, PA., 1988).

30. S. Matsumoto, Y. Sato, M. Tsutsumi and N.Setaka, J. Mater. Sci., **17**, 3106, (1982).

31. B.V. Derjaguin and D.V. Fedoseev, *Growth of Diamond and Graphite from Gas Phase*, Nauka, Moscow, 1977.

32. Y. Sato, M. Kamo and N. Setaka, in*Proceedings of the 8th International Symposium on Plasma Chemistry*, p. 2446, Tokyo, Japan.

33. T. Kawato and K. Kondo, Jpn. J. Appl. Phys., **26**(9), 1429 (1987).

34. Y. Saito, K. Sato, H. Tanaka, K. Fujita, and S. Matsuda, J. Mat. Sci., **23**(3), 842 (1988).

35. J. A. Mucha, D. L. Flamm, and D. E. Ibbotson, paper presented at SDIO/IST-ONR Diamond Technology Initiative Symposium, Crystal City, VA., 1988.

36. Y. Hirose and Y. Terasawa, Jpn. J. Appl. Phys., **5**(5), 565 (1986).

37. A. Inspektor, Y. Liou, T. McKenna, and R. Messier, Surf. and Coat. Technol., **39/40**, 211 (1989).

38. Y. Saito, S. Matsuda and S, Nogita, J. Mater. Sci. Lett., **5**, 565 (1986).

39. K. E. Spear, J. Am. Ceram. Soc., **72** (2), 171 (1989).

40. JANAF Thermochemical Tables, Vol. 14, 3rd ed., American Institute of Physics, New York, 1985.

41. K. Suzuki, A. Sawabe, H. Yasuda and T. Inuzuka, Appl. Phys. Lett., **50**, 728 (1987).

42. L. E. Kline, W. D. Partlow, and W. E. Bies, J. Appl. Phys., **65**, 70 (1989).

43. F. Jansen, M. A. Machonkin and D. E. Kuhman, J. Vac. Sci. Technol., A5, 3785 (1990).

44. M. Mecray, M.S. Thesis, The Pennsylvania State university, 1991.

45. B. Singh, Y. Arie, A. W. Levine and O. R. Mesker, Appl. Phys. Lett., 52(6), 451 (1988).

46. H. Schachner, Swedish Patent SE 8403429-7, 1984.

47. F. Jansen, I. Chen and M. A. Machonkin, J. Appl. Phys., 66, 5749 (1989).

48. L. Schafer, C. -P. Klages, U. Meier and K. Kohse-Hoinghaus, Appl. Phys. Lett., 58(6), 571 (1991).

49. U. Meier, K. Kohse-Hoinghaus, L. Schafer and C.-P. Klages, Applied Optics, 29(33), 4993 (1990).

50. D. G. Goodwin and G. G. Gavillet, J. Appl. Phys., 68, 6393 (1990).

51. J. C. Angus, H. A. Hill, W. S. Stanko, J. Appl. Phys., 39, 2915 (1968).

52. B. V. Spitsyn, L. L. Bouilov, B. V. Deryagin, J. Cryst. Growth, 52, 219 (1981).

53. J. C. Angus and C. C. Hayman, Science, 241, 913 (1988).

54. D. V. Fedoseev, V. P. Varnin, and B. V. Deryagin, Russ. Chem. Rev., 53, 435 (1985).

55. D. J. Poferl, N. C. Gardner, and J. C. Angus, J. Appl. Phys., 44, 1428 (1973).

56. N. Setaka, in Chemical Vapor Deposition, *Proceedings of the 10th International Conference on Chemical Vapor Deposition*, eds. G. W. Cullen and J. Blocher Jr., p. 1156, (The Electrchemical Society, Pennington, NJ, 1987).

57. J. J. Lander and J. Morrison, Surf. Sci., 4, 241 (1966).

58. B. B. Pate, Surf. Sci., 165, 83 (1986).

59. M. Tsuda, M. Nakajima and S. Oikawa, J. Am. Chem. Soc., 108, 5780 (1986).

60. M. Tsuda, M. Nakajima and S. Oikawa, Jpn. J. Apl. Phys., 26, L527 (1987).

61. M. Frenklach and K. E. Spear, J. Mater. Res., 3(1), 133 (1988).

62. M. Frenklach, J. Appl. Phys., 65, 5142 (1989).

63. R. Mania, L. Stobierski and R. Pampuch, Cryst. Res. Tech., 16, 785 (1981).

64. S. J. Harris, Appl. Phys. Lett., 56(23), 2298 (1990).

65. K. Suzuki, A. Sawabe and T. Inuzuka, Appl. Phys. Lett., 53(19), 1818 (1988).

66. M. Tsuda, M. Nakajima and S. Oikawa, in *Proceedings of the 8th Intenational Symposium on Plasma Chemistry*, Vol. 1, Tokyo, Japan, eds., K. Akashi and A. Kinbara, International Union of Pure and Applied Chemistry, Oxford, England, 1987.

67. D. Huang, M. Frenklach and M. Maroncelli, J. Phys. Chem., **92**, 6378 (1988).

68 W. A. Yarbrough, Diamond Optics IV, Ed. S. Holly and A. Feldman, SPIE Proc. **1534**, 99 (1991).

69. F. G. Celii, P. E. Pehrsson, H.-t. Wang and J. E. Butler, Appl. Phys. Lett., **52(24)**, 2043 (1988).

70. L. R. Martin and M. W. Hill, Appl. Phys. Lett., **55(21)**, 2248 (1989).

71. C. J. Chu, B. J. Bai, M. P. D'Evelyn, R. H. Hague and J. L. Margrave, in Diamond, Silicon Carbide and Related Wide Bandgap Semiconductors, Eds., J.T. Glass, R. Messier and N. Fujimori, Mater. Res. Soc. Proc., **162**, Pittsburgh, PA, 1990.

72. W.A. Yarbrough, K. Tankala, and T. DebRoy, J. Mater. Res., 7(2), 379 (1992).

73. S. J. Harris, A. M. Weiner and T. A. Perry, Appl. Phys. Lett., **53(17)**, 1605 (1988).

74. S. J. Harris and A. M. Weiner, J. Appl. Phys., **67**, 6520 (1990).

75. J. H. Miller and P. M. Taylor, Combust. Sci. Tech., **52**, 139 (1987).

76. F. G. Celii and J. E. Butler, Appl. Phys. Lett., **54(11)**, 1031 (1989).

77. F. G. Celii and J. E. Butler, in *New Diamond Sciemce and Technology*, eds. R. Messier, J. T. Glass, J. E. Butler and R. Roy, p. 201 (MRS, Pittsburgh, PA, 1991).

78. L. R. Martin, J. Appl. Phys., **70(10)**, 5667 (1991).

79. F. G. Celii and J. E. Butler, Annu. Rev. Phys. Chem., **42**, 643 (1991).

80. T. DebRoy, K. Tankala, W. A. Yarbrough and R. Messier, J. Appl. Phys., **68(5)**, 2424 (1990).

81. K. Tankala, M.S. Thesis, The Pennsylvania State University, 1991.

82. J. C. Angus, A. Argoitia, R. Gat and Z. Li, Phil. Trans. R. Soc. Lond., **A342**, 195 (1993).

83. M. Frenklach, J. Appl. Phys., **65**, 5142 (1989).

84. M. Frenklach and H. Wang, Phys. Rev., **B43**, 1520 (1991).

85. C. J. Chu, M. P. D'Evelyn, R. H. Hauge and J. L. Margrave, J. Mater.Res., **5**, 2405 (1990).

86. S. P. Chauhan, J.C. Angus and N.C. Gardner, J. Appl. Phys., **47(11)**, 4746 (1976).

87. S. J. Harris, J. Appl. Phys., **65(8)**, 3044 (1989).

88. S. J. Harris and L. R. Martin, J. Mater. Res., **5**, 2313 (1990).

89. J. E. Butler and R. L. Woodin, Phil. Trans. R. Soc. Lond., **A342**, 209 (1993).

90. Y. L. Yang and M. P. D'Evelyn, J. Am. Chem. Soc., **114**, 2796 (1992).

91. B. J. Garrison, E. J. Dawnkaski, D. Srivastava and D. W. Brenner, Science, **255**, 835 (1992).

92. E.S. Machlin, J. Mater. Res., **3(5)**, 958 (1988).

93. Y. Bar-Yam and T. D. Moustakas, Nature, **342**, 786 (1989).

94. W. A. Yarbrough, MRS Symp. Proc., **162**, 75 (1990).

95. M. Sommer, K. Mui, and F.W. Smith, Final Program and abstracts, Third Annual SDIO/IST Diamond Symposium, Crystal city, VA., 1988.

96. S. V. Pepper, J. Vac. Sci. Technol., **20**, 213 (1982).

Chapter 3

PROCEDURES

3.1 Description of HFCVD Reactors

3.1.1 Tubular Reactor

To understand the role of atomic hydrogen in heat transfer, experiments were conducted to measure the temperature and atomic hydrogen concentration profiles in a specially designed hot filament reactor. Fig. 3.1 is a schematic diagram of the experimental set-up. The reactor consisted of a quartz tube, 40 cm long and 5 cm in diameter, along with two four-way stainless steel crosses on either end. The flow control system consisted of two 0-500 sccm mass flow controllers and an MKS 247C four channel power supply and read out device. Two gas cylinders, a 99.995% pure hydrogen cylinder and a 5% methane-hydrogen cylinder, were connected to the two mass flow controllers. The total gas flow rate and the methane concentration in the feed gas could be controlled by choosing appropriate flow rates of the individual gases. The gases, fed through mass flow controllers, were mixed prior to their entry into the system. The system was pumped down to the required pressure by a roughing pump. The system pressure is controlled down stream by a Baratron pressure gauge, which is connected to an electrically operated throttle valve, which in turn controls the pumping speed. To achieve two dimensional symmetry, an inductively heated tantalum ring filament, 18 mm in diameter, was positioned inside the quartz reaction tube. The tantalum filament is inductively heated to the required temperature with a 450 kHz, 10 kW radio frequency generator. The temperature of the filament was measured with a two
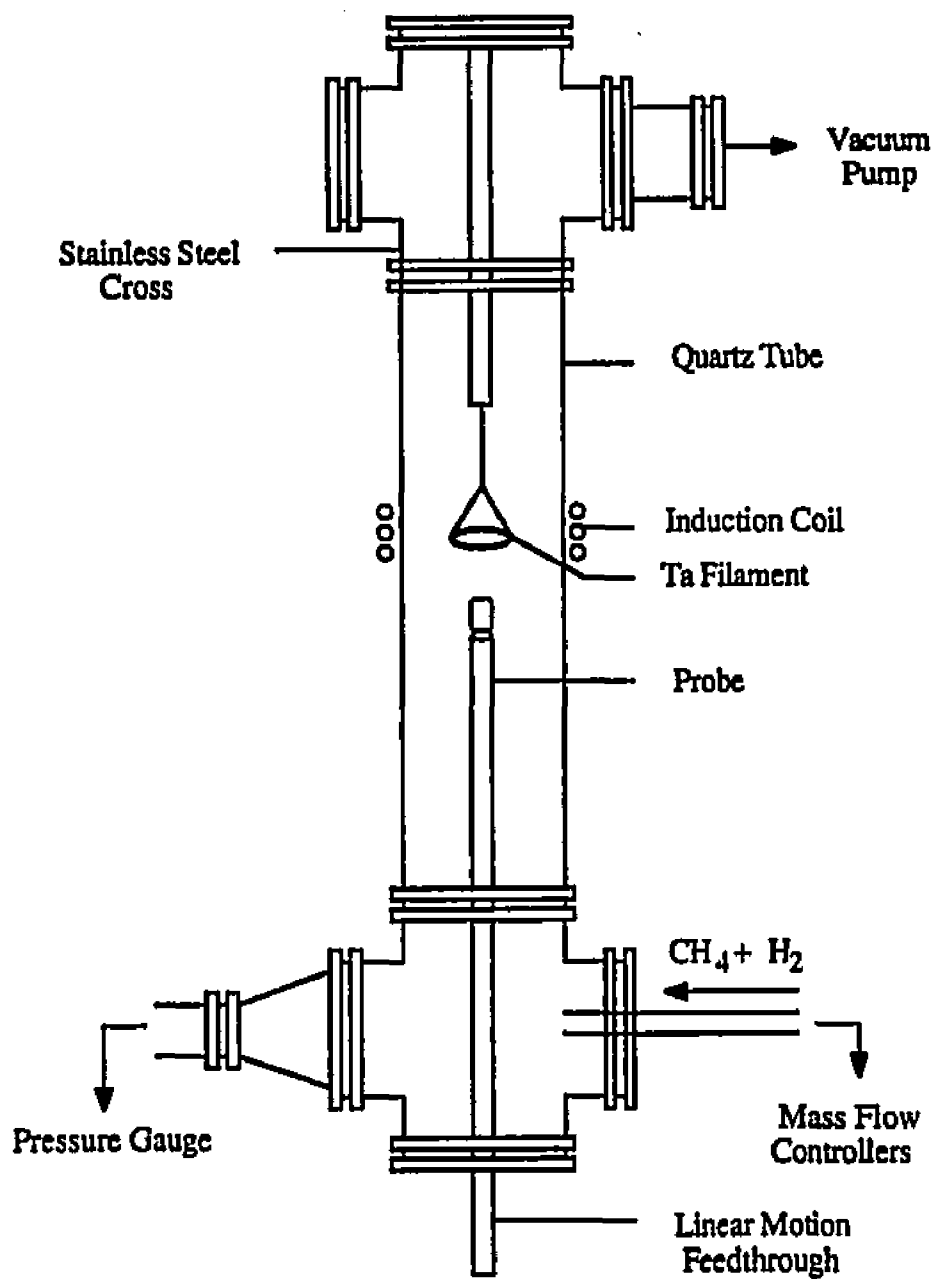
Fig. 3.1 Schematic diagram of the tubular hot filament reactor used for examining the role of atomic hydrogen in heat transfer.

color optical pyrometer. A specially designed hydrogen atom probe was positioned along the axis of the reactor. The distance between the tip of the probe and the filament could be adjusted with a linear motion feed through. The design of the probe is discussed in detail in a later section.

3.1.2 Bell Jar Reactor

A typical bell jar type hot filament reactor was used for examining the role of various process parameters in affecting atomic hydrogen generation rate at the filament and the substrate temperature. A schematic diagram of the bell jar system is presented in Fig. 3.2. The bell jar system consisted of a Pyrex bell jar 45 cm in diameter and 45 cm in height. The bell jar rested on a stainless steel base plate 50 cm in diameter. The base plate had several vacuum ports for gas inlet and outlet manifolds, pressure measurement and electrical and thermocouple feedthroughs. The gas flow and pressure control system for the bell jar system was essentially the same as that for the tubular hot filament reactor. Tantalum or tungsten filaments, 0.25 mm in diameter, were used in the bell jar system. The filaments were heated resistively and the power required to heat the filament to the desired temperature was determined from the applied voltage and the current flowing through the filaments. The filament temperature was measured with a two color optical pyrometer. Typically two filaments placed 6 mm apart were used. The filaments rested on water cooled stainless steel electrodes and were spring loaded to accommodate thermal expansion. This helped in maintaining a constant filament to substrate distance through out the duration of the experiment. The substrate, a 2.5 cm diameter silicon wafer, was placed 6 to 7 mm from the filaments and rested on two alumina rods. A type K, chromel-alumel, thermocouple
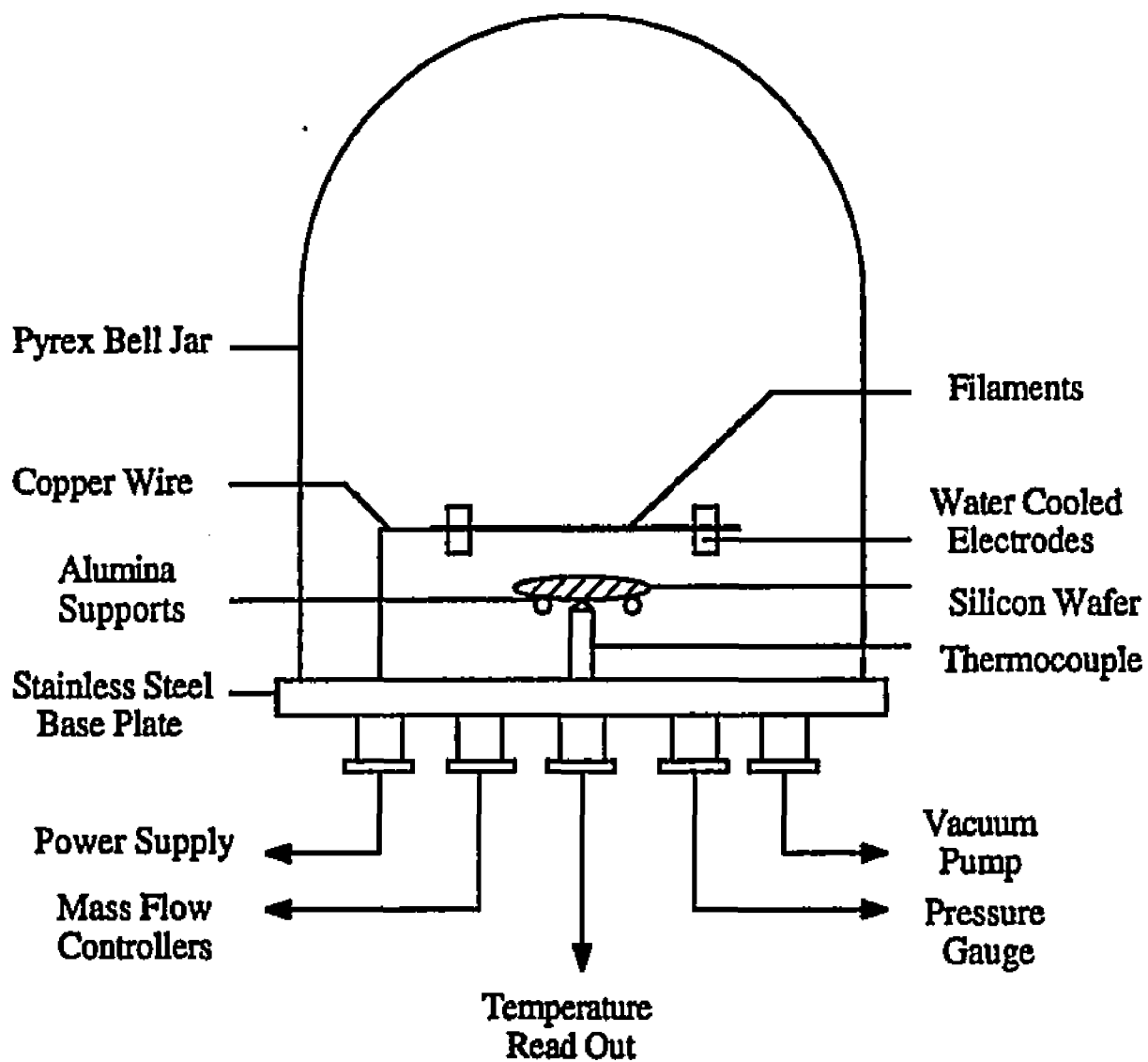
Fig. 3.2 Schematic diagram of bell jar type hot filament reactor used for determining the effect of process parameters on the substrate temperature.

was placed in contact with the back side of the silicon wafer and was used to measure the substrate temperature.

3.2 Design of the Hydrogen Probe

A thermocouple probe was designed to examine the importance of atomic hydrogen in filament to substrate heat transfer and to measure the atomic hydrogen concentration profiles in the reactor. Initially the hydrogen atom probe was constructed with two thermocouples, as shown in Fig. 3.3(a). The tip of one thermocouple was covered with a quartz thimble while the other thermocouple tip was wrapped with a silver wire. The quartz thimble was passivated by rinsing it with ethanol saturated with boric acid and drying [1]. The passivation was designed to minimize hydrogen atom recombination on the quartz thimble. Furthermore, the silver wire provided a catalytic surface for hydrogen atom recombination. The difference between the temperatures of the two thermocouples should then be a measure of the heat generated by atomic hydrogen recombination and consequently a measure of the local concentration of hydrogen atoms.

Preliminary experiments were conducted for a filament temperature of 2473 K, a reactor pressure of 30 Torr and a gas flow rate of 200 sccm to examine the sensitivity of the two thermocouple probe. Temperature measurements were made in hydrogen and helium. Results of several careful experiments indicated that the temperatures were significantly different in hydrogen and helium environments. However, the temperature difference indicated by the two thermocouples in hydrogen was not significantly different from that observed in helium. A careful study of Martin's paper [2] indicated that there are several important reasons why the two thermocouple probe, which worked well for his flow tube

Silver wire

Quartz Thimble

(cemented with of sodium
silicate + hydrous
magnesium silicate)

Alumina Sheath

Quartz Tube

Type K Thermocouples

(a)   (b)
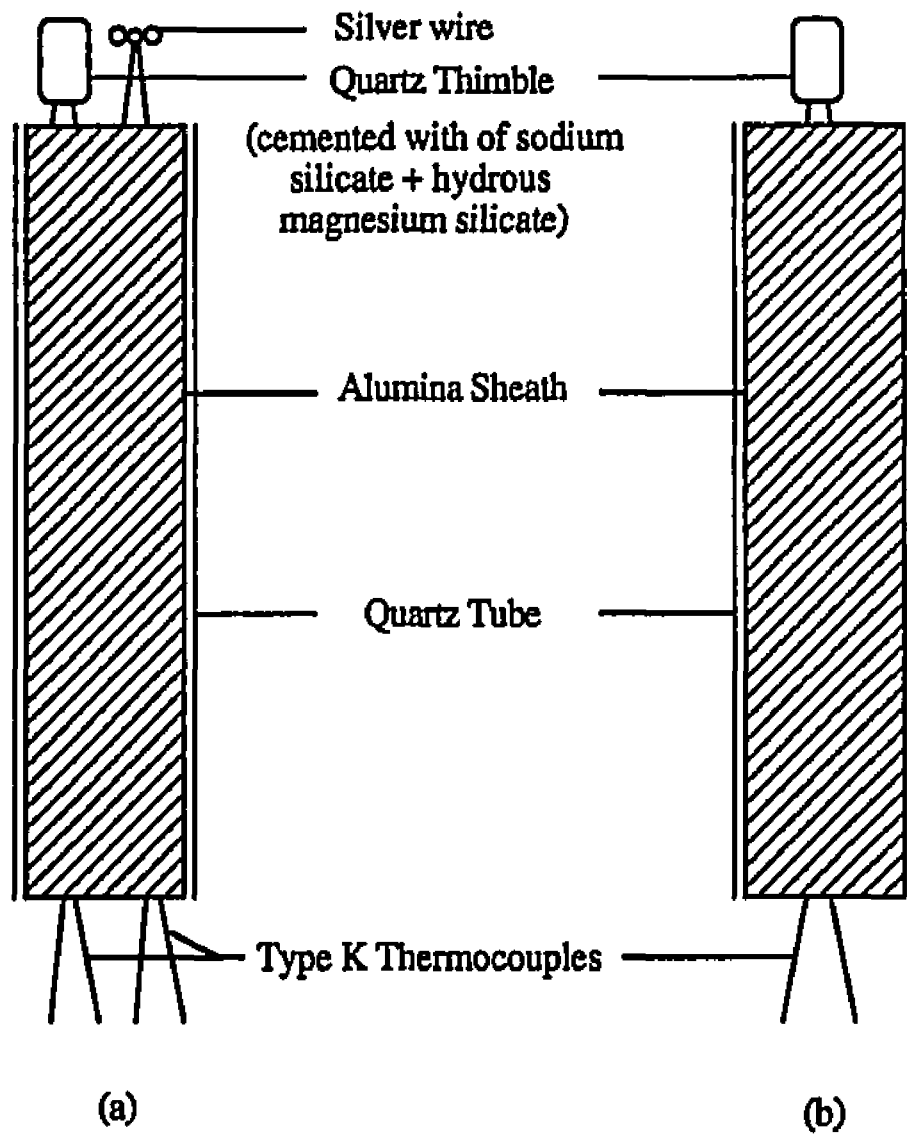
Fig. 3.3 Schematic diagram of (a) single-gas-two-thermocouple probe, and (b) two-gas-single-thermocouple probe used for detecting hydrogen atoms.

experiments, is ineffective for our experiments. First, Martin indicated in his paper that the two thermocouple "probe responds to the hydrogen atom flux through the tube rather than to atomic hydrogen concentration" and that "the temperature difference is linear in atomic hydrogen flux." In Martin's experiments very high gas velocities had to be maintained to achieve a high flux of atomic hydrogen. In our system, the gas velocities used were representative of those typical of hot filament systems which are about two orders of magnitude lower than those used by Martin in his flow tube experiments. At low gas velocities typical of hot filament systems, the flux of atomic hydrogen is much lower and is not sufficient to generate significant differences in the temperatures of the two thermocouples. Second, in Martin's experiments, the thermocouple probe was not located in the direct line of sight of a hot filament heated to 2473 K as in our case. In the presence of a radiation source, the difference between the temperatures of the two thermocouples is diminished thus reducing the sensitivity of the two thermocouple probe. Third, the gas temperatures near the probe in our system are much higher than those encountered in Martin's system. Martin observed that "when the temperature of the flow tube is raised from room temperature to 600 °C, the H-atom signal falls to 0.5 of the room temperature value." Thus, in the presence of an additional heat source such as the convective heat transfer from the gas to the thermocouple, the sensitivity of the two thermocouple probe is severely diminished. In summary the single-gas-two-thermocouple probe is not as accurate as the two-gas-single-thermocouple probe for our experimental conditions.

In all subsequent experiments, a single thermocouple probe consisting of a type K thermocouple was used. The tip of the thermocouple was covered with a quartz thimble as shown in Fig. 3.3(b), however, no boric acid passivation was used. The temperatures of the single thermocouple probe were recorded in pure helium and in hydrogen containing

gases. The temperature recorded in helium was taken as a suitable reference for heat transfer due to convection, conduction and radiation from the filament. The temperatures measured in hydrogen, on the other hand, were representative of the heat generated by the recombination of atomic hydrogen at the tip of the thermocouple in addition to the contributions of conduction, convection and radiation. Since helium is monatomic and no heat of recombination is involved and the rate of heat transfer due to conduction, convection and radiation are roughly equal in hydrogen and helium, switching hydrogen with helium provided a credible means of measurement of the reaction heat. Thus, from the temperatures recorded in helium and hydrogen, the recombination heat and hence the atomic hydrogen concentration can be derived.

3.3 Experimental Procedures

3.3.1 Role of Atomic Hydrogen in Heat Transfer

In the hot filament assisted chemical vapor deposition of diamond, the mechanism of heat transfer is unique. In addition to conduction, convection and radiation, filament to substrate heat transfer takes place by dissociation of molecular hydrogen at or near the filament and recombination of atomic hydrogen at the substrate surface. Experiments were conducted in the tubular hot filament reactor to evaluate the importance of atomic hydrogen recombination at the substrate surface in substrate heating. Probe temperatures were recorded in helium and hydrogen atmospheres for a filament temperature of 2473 K, a reactor pressure of 30 Torr, and a gas flow rate of 200 sccm. As discussed earlier the difference in the temperatures of the probe in hydrogen and helium atmospheres was a

measure of the recombination heat, and was used to determine the importance of hydrogen assisted heat transfer in hot filament reactors.

Since the recombination of atomic hydrogen at the substrate surface is potentially important in substrate heating, the flux of atomic hydrogen at the substrate surface, and hence, the spatial distribution of atomic hydrogen in the reactor is important for determining the substrate temperature. Thus, the factors that influence the spatial distribution of atomic hydrogen in the reactor are of interest. Apart from homogeneous reactions in the gas phase, convective and diffusive mixing of atomic hydrogen with the other species in the gas phase are responsible for the establishment of the atomic hydrogen concentration profile in the reactor. In order to examine the relative importance of homogeneous chemical reactions and mixing of atomic hydrogen with other species in determining the concentration profile of atomic hydrogen, computed values of atomic hydrogen concentration profiles were compared with experimentally determined values.

In order to determine the temperature and atomic hydrogen concentration profiles in the reactor, probe temperatures were recorded, in helium and hydrogen atmospheres, at various locations along the axis of the reactor for a filament temperature of 2473 K, reactor pressure of 30 Torr and a gas flow rate of 200 sccm. The temperatures recorded in helium and hydrogen were used to determine the local concentration of atomic hydrogen along the axis of the reactor. Since typical diamond deposition experiments are conducted with dilute mixtures of methane in hydrogen, the effect of addition of small quantities of methane on the substrate temperature and the spatial distribution of atomic hydrogen was examined. Probe temperatures, in helium and 1% methane-hydrogen mixture, were recorded at various locations along the axis of the reactor and the measured values were used to

determine the atomic hydrogen concentration profile for a filament temperature of 2473 K, reactor pressure of 30 Torr and a gas flow rate of 200 sccm.

3.3.2 Effect of Process Parameters on Substrate Temperature

In order to examine the influence of process parameters such as filament temperature, pressure and gas flow rate on the atomic hydrogen generation rate and the substrate temperature, experiments were conducted in the bell jar type hot filament reactor. Two filaments of tantalum or tungsten, 0.25 mm in diameter and 6 mm apart, were heated resistively to the desired temperature. The temperature of a silicon wafer placed 7 mm from the filaments was monitored with a type K thermocouple placed in contact with the back side of the wafer. Measurements were made in helium and hydrogen containing gases.

A standard protocol was followed for carrying out the experiments to limit any extraneous parameters from affecting the temperature measurements, or at least keep them common for all experiments. After loading the filaments and the substrate the system was pumped down to the minimum attainable pressure. The system was pumped down for an additional half an hour to reduce the moisture present in the system. The exhaust valve was then closed and the pump shut off to check the system for leaks. A leak rate of less than 0.1 Torr per hour was considered acceptable. The system was then filled with hydrogen, or helium if temperature measurements were to be made in helium, and subsequently evacuated to flush the system of any remnant, undesirable gases. This process was repeated three times.

To examine the effect of filament temperature, gas flow rate and pressure, substrate temperature measurements were made in pure hydrogen. Each parameter was varied while

keeping all other conditions constant. Substrate temperature and the power required to heat the filament was recorded in each case. Furthermore, the power required to heat the filament in helium under corresponding identical conditions was recorded. The difference in the power required to heat the filament in hydrogen and helium was used to calculate the atomic hydrogen generation rate. Experiments were repeated to check for reproducibility of the measurements.

3.4 Modeling of Heat Transfer and Fluid Flow in the HFCVD Reactors

3.4.1 Tubular Reactor

The heat transfer and fluid flow phenomena in the cylindrical HFCVD reactor are represented by equations of the following form for the conservation of momentum, enthalpy and concentration [3] of hydrogen atoms.

$$\frac{\partial}{\partial x_j}(\rho\, u_j\, \phi) = \frac{\partial}{\partial x_j}\left(\Gamma \frac{\partial \phi}{\partial x_j}\right) + S \qquad\qquad 3.1$$

where ρ is the density, u_j is the component of velocity in the j direction, ϕ is the dependent variable which can represent velocity components, temperature or concentration of hydrogen atoms, S is the volumetric source term, and Γ is the diffusion coefficient which is given an appropriate meaning depending on the variable considered. The details of the specific equations in cylindrical coordinates are described in standard textbooks [3,4] and are not presented here.

The calculations were performed for a two-dimensional, steady, laminar flow case considering spatial variation of density, viscosity, thermal conductivity, diffusion coefficient and specific heat. The data used for the calculations are presented in Table 3.1. The input to the model included the size and shape of the reactor and its contents, the thermophysical properties, the rate of supply, and the composition of the input gas mixture and the heating conditions. The velocity, temperature and atomic hydrogen concentration fields were obtained from the calculations. The boundary conditions included prescription of the input parabolic velocity distribution at the top of the reactor based on the total gas flow rate. The temperature of the inlet gas stream was prescribed to be the room temperature. At the axis of the reactor, the velocity, temperature and hydrogen atom concentration gradients were taken to be zero on the basis of the symmetry consideration. At the reactor wall, the velocities were assumed to be zero on the basis of the no-slip condition, the temperature was prescribed to be the room temperature and the hydrogen atom concentration was taken to be negligible. At the exit end, the velocity, temperature and atomic hydrogen concentration fields were assumed to be fully developed. The equations were represented in a finite difference form and solved iteratively on a line-by-line basis. The details of the solution procedure are described elsewhere [3,5]. A non-uniform grid spacing was used for obtaining maximum advantage in the resolution of variables. The adaptation routine, used in conjunction with a general purpose computer program to solve equations of conservation of mass, momentum, and enthalpy, for predicting the temperature and atomic hydrogen concentration fields in the reactor is presented in Appendix A.

Table 3.1 Data used for calculation of velocity, temperature and atomic hydrogen concentration fields in tubular hot filament reactor. The values of density, thermal conductivity, specific heat and viscosity are for pure hydrogen.

Property	Symbol	Value
Pressure, Torr	P	30
Filament temperature, K	T_f	2473
Gas flow rate, sccm	Q	200
Density, gm/cm^3	ρ	2P/(760 RT)
Thermal conductivity, cal/(cm s K)	k	$0.8 \times 10^{-4} + 0.86 \times 10^{-6}\, T$
Specific heat, cal/(gm K)	C_p	$3.34 + 3.4 \times 10^{-4}\, T$
Viscosity, poise	μ	$2.434 \times 10^{-6}\, T^{0.636}$
Diffusion coefficient, cm^2/s	D_{H/H_2}	$1346 \left(\dfrac{T}{1672}\right)^{1.5} \left(\dfrac{30}{P}\right)$

3.4.2 Bell Jar Reactor

The heat transfer and fluid flow in the bell jar type HFCVD reactor was modeled to examine the influence of various process parameters and reactor geometry on the substrate temperature distribution. The heat transfer and fluid flow phenomena in the HFCVD reactor can be represented by equations, of the form presented in equation 3.1, for the conservation of momentum, enthalpy and concentration [3,4] of hydrogen atoms. The contributions of radiation and chemical heating effects were incorporated into the calculations by defining appropriate source terms and are discussed in subsequent sections.

Fig. 3.4 shows a schematic diagram of the computational domain representing the essential features of the bell jar reactor. The domain represents a vertical half-section of the bell jar reactor bound by the axis of the reactor on the left and the reactor wall on the right. Since the system is symmetric about a plane passing through the axis of the reactor, only half a section of the reactor was considered to minimize the computational task. The calculations were performed for a two-dimensional, steady state, laminar flow case considering spatial variation of density, viscosity, thermal conductivity, specific heat and diffusion coefficient. The data used for the calculations are presented in Table 3.2. The input to the model included the size and shape of the reactor and its contents, the thermophysical properties, the rate of supply and the composition of the inlet gas mixture, and the heating conditions. The temperature at the filament locations was specified by prescribing the gas temperature to be the filament temperature. The velocity, temperature and atomic hydrogen concentration fields were obtained from the heat transfer and fluid flow calculations. The boundary conditions included prescription of the input velocity distribution at the top of the reactor based on the total gas flow rate. The temperature of the inlet gas stream was

Gas In

Axis of
Symmetry

Reactor
Wall

Filament

Silicon Wafer

Gas Out
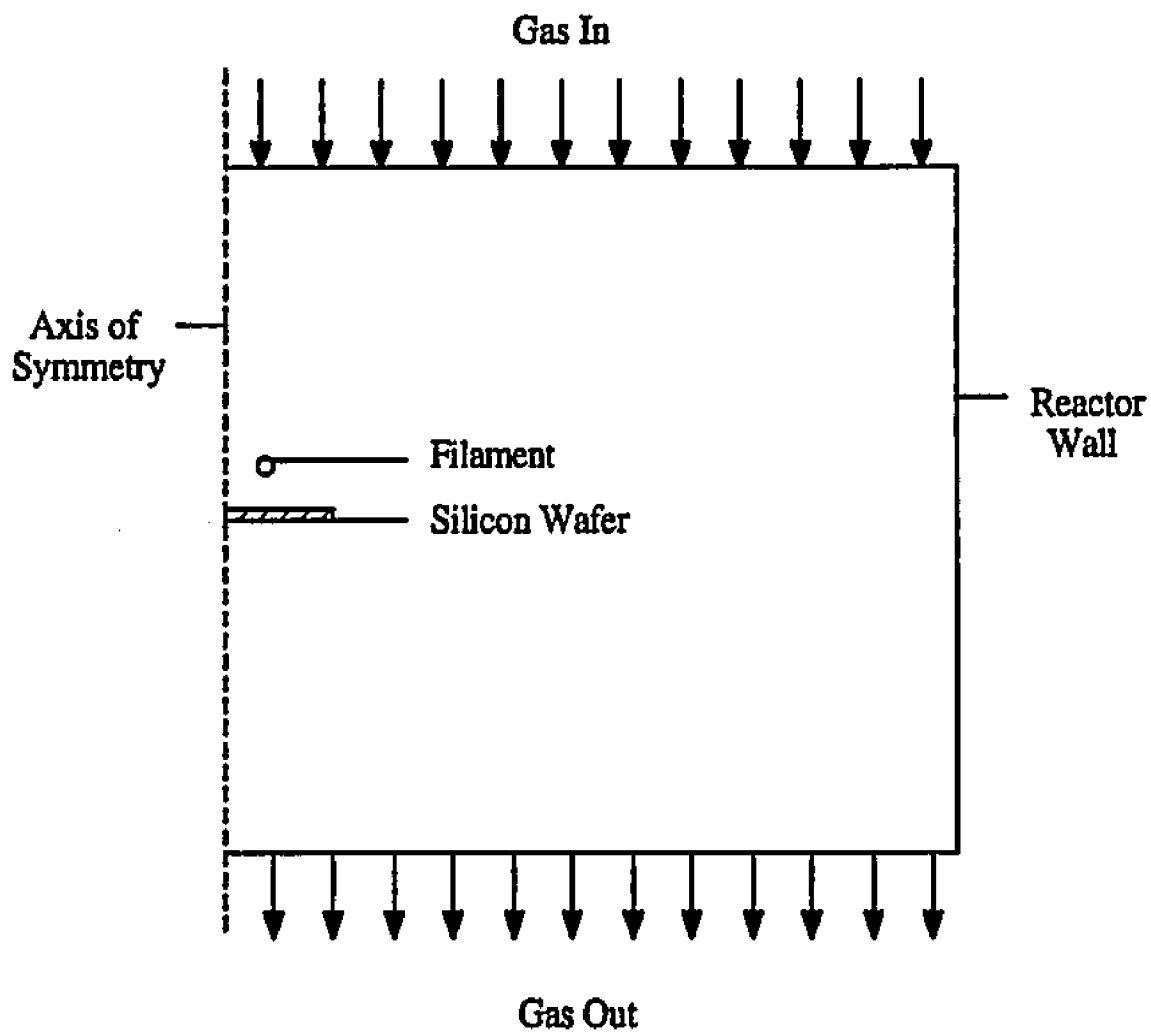
Fig. 3.4 Schematic diagram of computational domain chosen for calculation of velocity, temperature and atomic hydrogen concentration fields.

Table 3.2 Data used for calculation of velocity, temperature and atomic hydrogen concentration fields in bell jar type hot filament reactor.

Property	Symbol	Value
Pressure, Torr	P	10 - 70
Filament temperature, K	T_f	2100 - 2500
Gas flow rate, sccm	Q	100 - 600
Density, gm/cm^3 Hydrogen Silicon	ρ_{H_2} ρ_{Si}	$2P/(760\ RT)$ 2.33
Thermal conductivity, cal/(cm s K) Hydrogen Silicon	k_{H_2} k_{Si}	$1.47 \times 10^{-4} + 0.39 \times 10^{-6}\ T$ 0.06
Specific heat, cal/(gm K) Hydrogen Silicon	C_{p,H_2} $C_{p,Si}$	$3.67 + 3.74 \times 10^{-4}\ T$ 0.27
Viscosity of hydrogen, poise	μ_{H_2}	$2.434 \times 10^{-6}\ T^{0.636}$
Diffusion coefficient, cm^2/s	D_{H/H_2}	$1346 \left(\dfrac{T}{1672}\right)^{1.5} \left(\dfrac{30}{P}\right)$

prescribed to be the room temperature. At the axis of the reactor, the velocity, temperature and hydrogen atom concentration gradients were taken to be zero on the basis of the symmetry consideration. At the walls of the reactor and at all solid surfaces the velocities were assumed to be zero on the basis of the no-slip condition. At the reactor walls, the temperature was prescribed to be the room temperature and the hydrogen atom concentration was taken to be negligible. At the exit end, the velocity, temperature and atomic hydrogen concentration fields were assumed to be fully developed. The equations were represented in a finite difference form and solved iteratively [3,5] on a line-by-line basis. A non-uniform grid spacing was used for obtaining maximum advantage in the resolution of variables. The adaptation routine, used in conjunction with a general purpose computer program to solve equations of conservation of mass, momentum, and enthalpy, for predicting the substrate temperatures is presented in Appendix B.

3.4.2.1 Radiation Heat

Consider for the sake of simplicity a hot filament reactor using a single filament placed along the diameter of the substrate and at a distance "c" from it. Figs. 3.5(a) and 3.5(b) show the top and side views of the arrangement. The amount of radiation from the filament intercepted by an element "1" of the substrate shown shaded in Fig. 3.5(a) is given by [6]:

$$Q_{21} = \sigma \varepsilon A_2 F_{21} T_f^4 \qquad\qquad 3.2$$

where, σ is the Stefan-Boltzmann constant, ε is the emissivity of the filament, A_i is the area of element i, T_f is the temperature of the filament and F_{21} is the view factor. The view factor can be calculated from the geometry and is given by [6]:
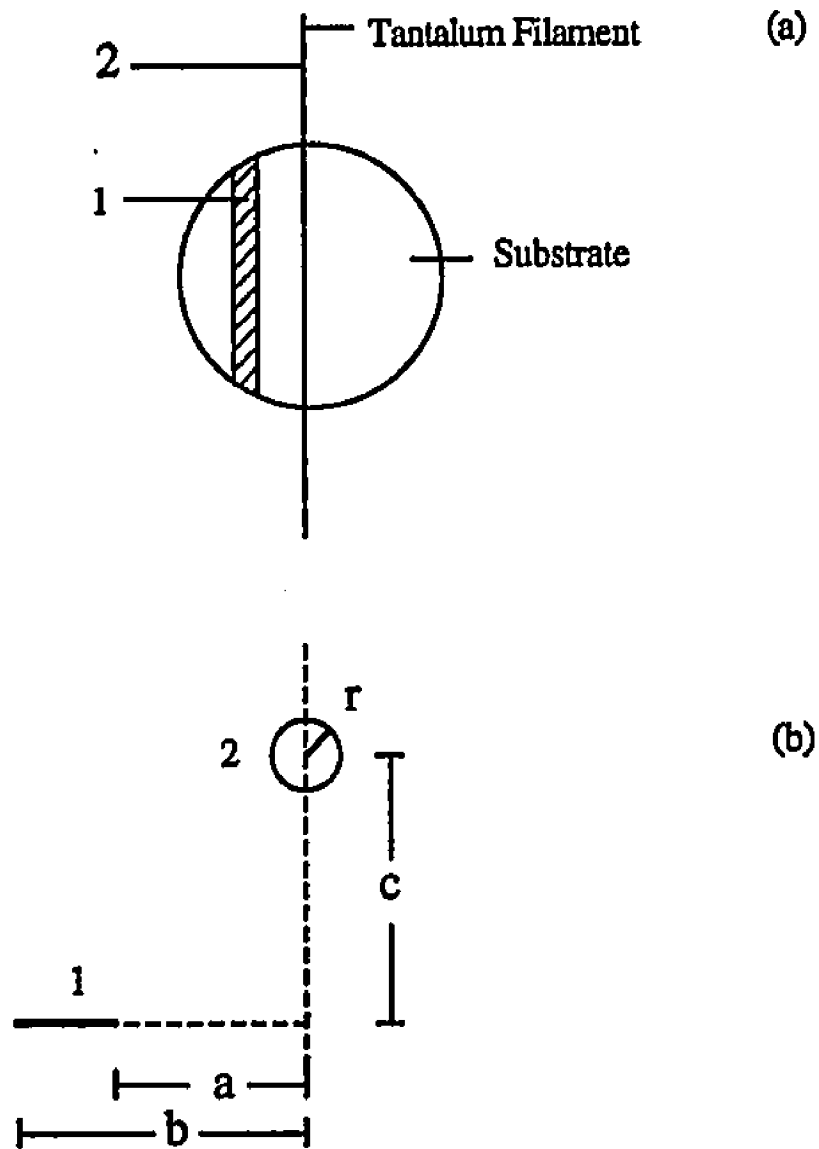
Fig. 3.5 Schematic diagram of (a) top view, and (b) side view of the filament and substrate arrangement used for calculation of the radiation view factor.

$$F_{21} = \frac{A_1}{A_2} \frac{r}{b-a} \left[\tan^{-1}(b/c) - \tan^{-1}(a/c) \right] \qquad 3.3$$

3.4.2.2 Chemical Heat

The rate of heat input to the substrate due to recombination of atomic hydrogen at its surface can be calculated from the flux of atomic hydrogen at the substrate surface. The flux of atomic hydrogen, J_H, is given by [4]

$$J_H = - D_{H/H_2} \frac{\partial C_H}{\partial z} \qquad 3.4$$

where D_{H/H_2} is the diffusion coefficient of H in H_2 and $\frac{\partial C_H}{\partial z}$ is the spatial gradient of atomic hydrogen at the substrate surface. If ΔH is the recombination heat per mole of atomic hydrogen consumed in the reaction

$$H + H = H_2 \qquad \Delta H_{1200 \, K} = -52 \, kcal/mole \, of \, H \qquad 3.5$$
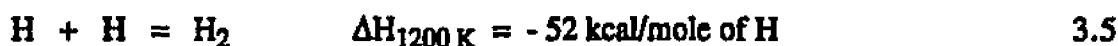
then, the rate of heat input, Q_H, to an element of the substrate of area A is given by

$$Q_H = A \Delta H J_H \qquad 3.6$$

3.5 Estimation of Enthalpies and Entropies of Formation of Surfaces

In order to examine the relative stability of diamond and graphite surfaces, we need the enthalpies and entropies of formation of various diamond and graphite surfaces.

Unfortunately, experimental data of the enthalpies and entropies of formation of various principal surfaces of diamond and graphite are not available, and therefore, have to be estimated. Extensive work has shown that the thermodynamic properties of most hydrocarbon species can be accurately estimated using principles of group additivity [7,8] and bond energy contributions [9]. Principles of group additivity have been used to estimate the thermodynamic properties of diamond, graphite and lonsdaleite surfaces [10-12]. In this study, enthalpies and entropies of diamond and graphite surfaces have been estimated using Laidler parameters [9] for bond energy contributions.

3.5.1 Estimates from Principles of Group Additivity

The formation reactions for each of the principal surfaces of diamond graphite and lonsdaleite were written as reactions between atomic hydrogen and graphite (0001) surface. For example, the formation reaction for diamond (111) surface was written as [10]:

$$C_2[\text{graphite }(0001)] + H^0 = C_2H[\text{diamond }(111)] \qquad 3.7$$

where H^0 represents atomic hydrogen in the ground state. The formation reactions for all the principal surfaces of diamond, graphite and lonsdaleite are presented in Table 3.3.

Enthalpies of formation of various surfaces were estimated by first choosing a unit mesh of the surface of interest such that integral translation of it along its axes would generate the surface to any desired extent. A mole of surface is then defined as Avogadro's number of such unit meshes [10]. A functional group formula is written for the unit mesh representative of each surface and its enthalpy of formation is estimated by adding together

Table 3.3 Formation reactions for diamond, graphite and lonsdaleite surfaces.

Surface	Formation Reaction
graphite(0001)	C_2 [graphite (0001)] = C_2 [graphite(0001)]
graphite(11$\bar{2}$0)	$4C_2$[graphite (0001)] + $4H^o$ = C_8H_4[graphite(11$\bar{2}$0)]
graphite(10$\bar{1}$0)	$2C_2$[graphite (0001)] + $2H^o$ = C_4H_2[graphite(10$\bar{1}$0)]
diamond(111)	C_2[graphite (0001)] + H^o = C_2H[diamond(111)]
diamond(110)	C_2[graphite (0001)] + $2H^o$ = C_2H_2[diamond(110)]
diamond(100)	C_2[graphite (0001)] + $2H^o$ = C_2H_2[diamond(100)]
lonsdaleite(0001)	C_2[graphite (0001)] + H^o = C_2H[lonsdaleite(0001)]
lonsdaleite(10$\bar{1}$0)	$2C_2$[graphite (0001)] + $2H^o$ = C_4H_2[lonsdaleite(10$\bar{1}$0)]
lonsdaleite(11$\bar{2}$0)	$2C_2$[graphite (0001)] + $4H^o$ = C_4H_4[lonsdaleite(11$\bar{2}$0)]

the contribution from each of the functional groups needed to describe the unit mesh. In the estimation of the enthalpies of formation of various surfaces, graphite (0001) has been taken as the reference state and assigned a zero enthalpy of formation. Fig. 3.6 shows the structures of graphite (0001) and diamond (111) surfaces and illustrates the method of estimation. The unit mesh chosen for both these surfaces is a rhombus with minor angles of 60° and major angles of 120°. The unit mesh for graphite (0001) and diamond (111) surfaces measure 0.226 nm and 0.252 nm on a side, respectively. The unit mesh for graphite (0001) consists of two $C_B(C_B)_3$ groups, i.e., two resonance stabilized sp^2 carbon atoms each connected to three other resonance stabilized sp^2 carbon atoms. The diamond (111) unit mesh consists of a $CH(C)_3$ group, i.e., an sp^3 carbon atom bonded to three other sp^3 carbon atoms and a hydrogen atom, and a $C(C)_4$ group, i.e., an sp^3 carbon atom bonded to four other sp^3 carbon atoms. Using the published estimates [7,8], this gives -1.48 + 0.5 or - 0.98 kcal/mol as the hydrogenated diamond (111) surface at 298 K. The details of the estimation procedure for the other principal surfaces of diamond, graphite and lonsdaleite are described in a recent paper [10] and are not presented here. However, for quick reference the choice of unit mesh, the functional group formulas and the estimated enthalpies of formation for the various surfaces of interest are presented in Table 3.4. Although the enthalpies of formation can be estimated using group additivity principles, a similar approach is not readily available for estimating absolute or even relative entropies for the different surfaces. For the sake of calculation, the bulk entropy per mole of carbon was assigned to each respective surface [10]. The surface entropy data used for the calculations are also presented in Table 3.4.

(a)

C Atom at
Surface

Unit Mesh

(b)

H Atom

C Atom at
Surface

Unit Mesh

C Atom 0.051 nm
Below Surface
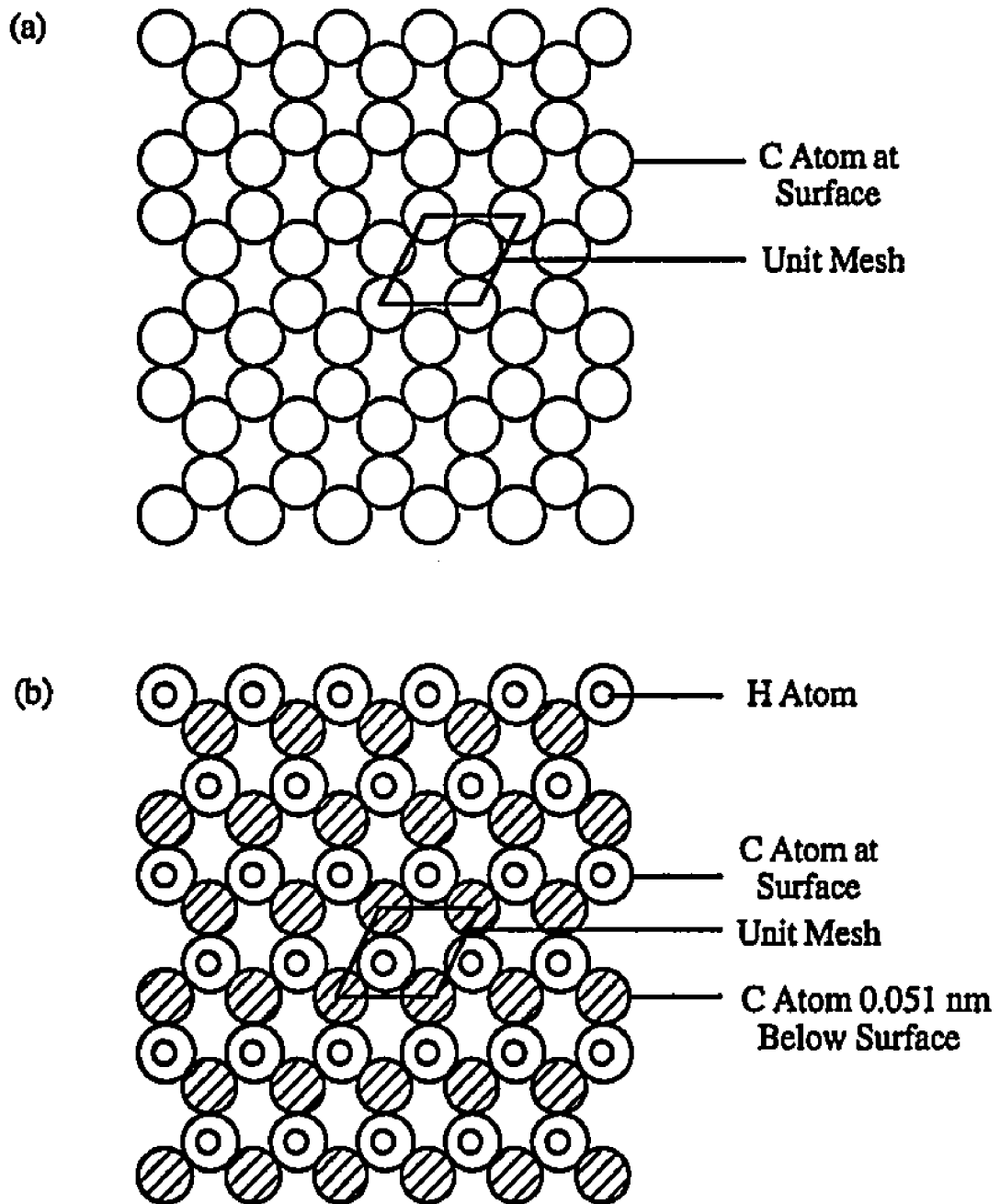
Fig. 3.6 Top view of (a) graphite (0001) surface and (b) diamond (111) surface.In diamond (111) surface, the hydrogen atoms are bonded to the surface carbon atoms with the C-H bond perpendicular to the plane of the surface.

Table 3.4 Enthalpies and entropies of formation for principal surfaces of diamond, graphite and lonsdaleite.

Surface	Unit cell (length=nm)	Functional Group	ΔH_f (kcal/mol)	S^o_{298} (kcal/mol K)
G(0001)*	rhombus 0.226, 60°	$2\,C_B(C_B)_3$	0.0	2.744
G(11$\bar{2}$0)	rectangle 0.671 x 0.530	$4\,C_BH(C_B)_2$ $4\,C_B(C_B)_3$	+ 13.2	10.976
G(10$\bar{1}$0)	rectangle 0.671 x 0.246	$2\,C_BH(C_B)_2$ $2\,C_B(C_B)_3$	+ 6.6	5.488
D(111)	rhombus 0.252, 60°	$1\,CH(C)_3$ $1\,C(C)_4$	- 0.98	1.132
D(110)	rectangle 0.252 x 0.357	$2\,CH(C)_3$	- 2.96	1.132
D(100)	square 0.252	$1\,CH_2(C)_2$ $1\,C(C)_4$	- 1.92	1.132
L(10$\bar{1}$0)	rectangle 0.252 x 0.412	$2\,CH(C)_3$ $1\,C(C)_4$	+ 4.94	2.264
L(11$\bar{2}$0)	rectangle 0.437 x 0.412	$4\,CH(C)_3$	- 2.47	2.264

* Chosen as reference state

3.5.2 Estimates from Bond Energy Contributions

3.5.2.1 Enthalpies of Formation

In order to estimate the enthalpies of formation of various principal surfaces of diamond and graphite, the bonding configuration of the surface carbon for each of the surfaces was determined. The bonding configurations of surface carbon atoms on various surfaces of diamond and graphite are presented in Table 3.5. The heat of atomization of a mole of such carbon atoms, representative of a surface, was calculated from the energy required to break various bonds and atomize the surface carbon atom. The values of bond energies used in this study are those suggested by Laidler, and are referred to as Laidler parameters. The Laidler parameters have been used to accurately estimate experimentally observed heats of formation of a variety of hydrocarbon species [9]. A list of the Laidler parameters used in this study is presented in Table 3.6. The heat of formation of the surface of interest was then calculated from the heat of atomization of a mole of surface carbon atoms and the heats of atomization of graphite and molecular hydrogen as illustrated in the following example.

A carbon atom at the surface of a hydrogenated diamond (111) surface makes three bonds with carbon atoms in the diamond lattice and one bond with a hydrogen atom. Thus, the heat of atomization of a carbon atom on diamond (111) is given by

$$\Delta H_a \text{ [diamond (111)]} = \frac{3}{2} E(C\text{-}C) + E(C\text{-}H)_t \qquad 3.8$$

where $E(C\text{-}C)$ is the carbon-carbon bond energy in diamond and $E(C\text{-}H)_t$ is the bond energy for a hydrogen atom bonded to a tertiary carbon atom. Using values tabulated in

Table 3.5 Bonding configurations of surface carbon atoms on various principal surfaces of diamond and graphite.

Surface	Bonding Configuration*
diamond (111)	$\begin{matrix} & H \\ & | \\ \diagup & \overset{|}{C} & \diagdown \end{matrix}$
diamond (110)	$\begin{matrix} & H \\ & | \\ \diagup & \overset{|}{C} & \diagdown \end{matrix}$
diamond (100)	$\begin{matrix} H & & H \\ & \diagdown C \diagup & \\ \diagup & & \diagdown \end{matrix}$
graphite (0001)	$\begin{matrix} \diagdown & & \\ & \diagup C & - \\ \diagup & \vdots & \end{matrix}$
graphite (10$\bar{1}$0)	$\begin{matrix} & \vdots & \\ - & C & \diagup \\ & \vdots & \diagdown H \end{matrix}$
graphite (11$\bar{2}$0)	$\begin{matrix} & | & \diagup (C{-}H) \\ - & C & \\ & \vdots & \diagdown H \end{matrix}$

* ——— covalent bond

    - - - - van der Waal bond

Table 3.6 Values of Laidler parameters used in the estimation of enthalpies and entropies of formation of diamond and graphite surfaces [9].

Bond Type	Bond Energy, kcal/mole
$E(C-C)$	85.48
$E(C-H)_S$	97.27
$E(C-H)_t$	96.53
$E(^H_{>}C-C<^H)$	119.17
$E(>C-H)$	100.53
$E(^H_{>}C-C<)$	114.30
$E(>C-C<)$	112.80

Table 3.6 the heat of atomization of surface carbon atoms on diamond (111) is calculated to be 224.75 kcal/mole. i.e.,

$$CH \text{ [diamond (111)]} = C + H \qquad \Delta H_a = 224.75 \text{ kcal/mole} \qquad 3.9$$

Furthermore, from the data in JANAF tables [13] we have

$$C(\text{graphite}) = C(g) \qquad \Delta H_a = 171.29 \text{ kcal/mole} \qquad 3.10$$

$$\frac{1}{2} H_2(g) = H(g) \qquad \Delta H_a = 52.103 \text{ kcal/mole} \qquad 3.11$$

From reactions 3.9 through 3.11 we get

$$C(\text{graphite}) + \frac{1}{2} H_2 = CH \text{ [diamond (111)]} \qquad \Delta H_f^0 = -1.357 \text{ kcal/mole} \qquad 3.12$$
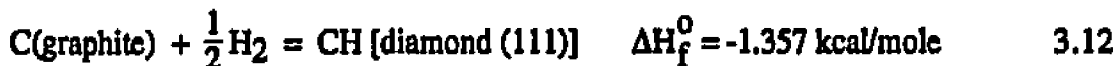
where ΔH_f^0 is the heat of formation of diamond (111) surface at 298 K. The enthalpies of formation of the other principal surfaces can be calculated by a similar procedure. The details of the calculations are presented in Appendix C.

Calculation of the enthalpies of formation of various graphite surfaces requires knowledge of the energy of C-C bonds between sp^2 hybridized carbon atoms in the basal planes of graphite as well as the energy of the van der Waal bonds between carbon atoms in adjacent basal planes. Although Laidler provides data for the covalent bonds between sp^2 hybridized carbon atoms, no value has been suggested for the van der Waal bonds. The

heat of atomization of graphite calculated by accounting only for the covalent bonds is 169.2 kcal/mole. However, the heat of atomization of graphite reported in JANAF tables [13] is 171.29 kcal/mole. The difference in the two values, 2.09 kcal/mole, can be ascribed to the van der Waal bonds in the graphite structure. Since there are 0.5 moles of van der Waal bonds for every mole of carbon atoms the bond energy per mole of van der Waal bonds, $E_{v.b}$, is 4.18 kcal. The heat of atomization of a mole of carbon atoms on the surface of graphite (0001), for example, can be calculated as follows:

$$\Delta H_a \text{ [graphite (0001)]} = \frac{3}{2} E(>C-C<) + \frac{1}{4} E_{v.b} \qquad 3.13$$

From the data in Table 3.6 and using $E_{v.b} = 4.18$ kcal/mole, we get

$$C\text{[graphite (0001)]} = C(g) \qquad \Delta H_a = 170.245 \text{ kcal/mole} \qquad 3.14$$

From equations 3.10 and 3.14 we get

$$C\text{(graphite)} = C\text{[graphite (0001)]} \qquad \Delta H_f^0 = -1.045 \text{ kcal/mole} \qquad 3.15$$

where ΔH_f^0 is the enthalpy of formation of graphite (0001) surface. The details of the calculations of the enthalpies of formation for the other surfaces of graphite are presented in Appendix C.

3.5.2.2 Entropies of Formation

Although bond enthalpy values are available for the calculation of enthalpies of formation of diamond and graphite surfaces, bond entropy data for the calculation of entropies of formation are not available. It is well known that the vibrational entropy of a crystal is inversely proportional to the vibrational frequency of the atoms in crystal [14]. Furthermore, the vibrational frequency of the atoms is directly proportional to the bond strength. Thus, as a first approximation we can write

$$S^o_{298} = \frac{K}{\text{Bond Energy}} \qquad \qquad 3.16$$

where K is a proportionality constant. The value of K for C-C bonds in diamond, K_D, and in graphite, K_G, can be calculated from the absolute entropies for diamond and graphite, respectively. The entropy per mole of diamond is 0.585 cal/mole-K [15]. In diamond, there are 2N bonds per mole of carbon atoms, where N is the Avogadro's number. Hence, the entropy per mole of carbon-carbon bonds in diamond, $S^o_{298}(\text{C-C})$, is 0.2965 cal/mole-K. Thus,

$$K_D = S^o_{298} \times E(\text{C-C}) = 0.2965 \times 85480 = 25003 \text{ cal}^2/\text{mole}^2 \text{ K} \qquad 3.17$$

The entropy per mole of graphite is 1.372 cal/mole-K [15]. In graphite we have 3/2 moles of C-C bonds and 1/2 moles of van der Waal bonds per mole of carbon. Thus,

$$S^o_{298}(\text{graphite}) = \frac{3}{2} S^o_{\text{C-C}} + \frac{1}{2} S^o_{v.b} = 1.372 \qquad 3.18$$

Assuming K_G to be constant for C-C bonds and van der Waal bonds we have from equation 3.16

$$\frac{S^o_{C-C}}{S^o_{v.b}} = \frac{E_{v.b}}{E(>C-C<)} = \frac{4.18}{112.8} = 0.037 \qquad\qquad 3.19$$

From equations 3.18 and 3.19 we get $S^o_{C-C} = 0.09$ cal/mole-K, $S^o_{v.b} = 2.47$ cal/mole-K

and $K_G = 10322$ cal^2/mole^2 K. Using the values of K_D and K_G, the entropies of various surfaces of diamond and graphite were calculated. The entropy of hydrogenated diamond (111) surface, assuming that K for E(C-H)$_t$ is same as K_D, is given by

$$S^o_{298}[\text{diamond (111)}] = \frac{3}{2}\frac{K_D}{E(C-C)} + \frac{K_D}{E(C-H)_t} = 0.698 \text{ cal/mole-K} \qquad\qquad 3.20$$

Similarly, the entropy of graphite (0001) is given by

$$S^o_{298}[\text{graphite (0001)}] = \frac{3}{2}\frac{K_G}{E(>C-C<)} + \frac{1}{4}\frac{K_G}{E_{v.b}} = 0.755 \text{ cal/mole-K} \qquad\qquad 3.21$$

The entropies of various surfaces of diamond and graphite can be estimated by a similar procedure. The enthalpies and entropies of formation of various surfaces calculated using the above procedure are tabulated in Table 3.7.

Table 3.7 Enthalpies and entropies of formation of various principal surfaces of diamond and graphite estimated using bond energy contributions.

Formation reaction	ΔH_f^o (kcal/mole)	ΔS_f^o (cal/mole K)
$C(gr) + \frac{1}{2} H_2 = CH[diamond(111)]$	- 1.357	- 16.29
$C(gr) + \frac{1}{2} H_2 = CH[diamond(110)]$	- 1.357	- 16.29
$C(gr) + H_2 = CH_2[diamond(110)]$	- 4.524	- 31.8
$C(gr) = C[graphite(0001)]$	+ 1.045	- 0.617
$C(gr) + \frac{1}{2} H_2 = CH[graphite(10\bar{1}0)]$	+ 6.473	- 15.561
$C(gr) + \frac{1}{2} H_2 = CH[graphite(11\bar{2}0)]$	+ 4.038	- 15.563

3.6 References

1. L. R. Martin and M. W. Hill, in New Diamond Science and Technology, eds. R. Messier, J. T. Glass, J. E. Butler, and R. Roy (MRS, Pittsburgh, PA, 1991).

2. L. R. Martin, J. Appl. Phys., **70**, 5667 (1991).

3. S. V. Patankar, *Numerical Heat Transfer and Fluid Flow* (McGraw-Hill, New York, NY, 1980).

4. R. B. Bird, W. E. Stewart, and E. N. Lightfoot, *Transport Phenomena* (Wiley, New York, NY, 1960).

5. S. V. Patankar, Reference Manual for MicroCompact version 1.1, Innovative Research Inc., MN, 1988.

6. E. M. Sparrow and R. D. Cess, *Radiation Heat Transfer* (Brooks/Cole Publishing Company, Belmont, CA, 1970).

7. S. W. Benson, *Thermochemical Kinetics* (Wiley, New York, NY, 1968).

8. S. W. Benson and J. H. Buss, J. Chem. Phys., **29**, 546 (1958).

9. J. D. Cox and G. Pilcher, *Thermochemistry of Organic and Organometallic Compounds* (Academic Press, New York, NY, 1970).

10. W. A. Yarbrough, MRS Symp. Proc., **162**, 75 (1990).

11. W. A. Yarbrough, J. Elect. Mater., **43**, 133 (1990).

12. W. A. Yarbrough, J. Am. Ceram. Soc., **75**(12), 3179 (1992).

13. JANAF Thermochemical Tables, vol. 14, 3rd ed., (American Institute of Physics, New York, NY, 1985).

14. R. A. Swalin, *Thermodynamics of Solids* (Wiley, New York, NY, 1967).

15. E. S. Domalski, W. H. Evans, and E. D. Hearing, *Heat Capacities and Entropies of Organic Compounds in the Condensed Phase*, J. Phys. Chem. Ref. Data, vol 13, Suppl. 1, 1984.

Chapter 4

RESULTS AND DISCUSSION

4.1 Heat Transfer in Hot Filament Reactors

Experiments were conducted in the tubular hot filament reactor to examine the importance of the recombination of atomic hydrogen at the growth surface in substrate heating. Fig. 4.1 shows the variation of probe temperature with distance along the axis of the reactor, in ultra high purity helium, hydrogen and a mixture of 1% methane in hydrogen. The error in the temperature measurement was small, with the reproducibility being within $\pm$ 10 $^{\circ}$C. In each case, the temperature decreased rapidly with distance from the filament. At any monitoring location, the temperature in helium was significantly lower than that measured in either pure hydrogen or in 1% CH_4-H_2 mixture. Furthermore, when methane was present in the feed gas, the temperature was somewhat lower than that observed in pure hydrogen. Several interesting questions arise from the perusal of the data. Why are the temperatures so different in helium and hydrogen? What are the roles of conduction, convection and radiation in heat transfer? How important is atomic hydrogen recombination, at the substrate surface, in substrate heating? Can the local concentration of atomic hydrogen be derived from the data? Why does the addition of small quantities of methane affect the temperature?

4.1.1 Conduction, Convection and Radiation

The temperature and velocity fields, computed for typical diamond deposition conditions, were used to examine the relative importance of heat transfer by conduction and convection
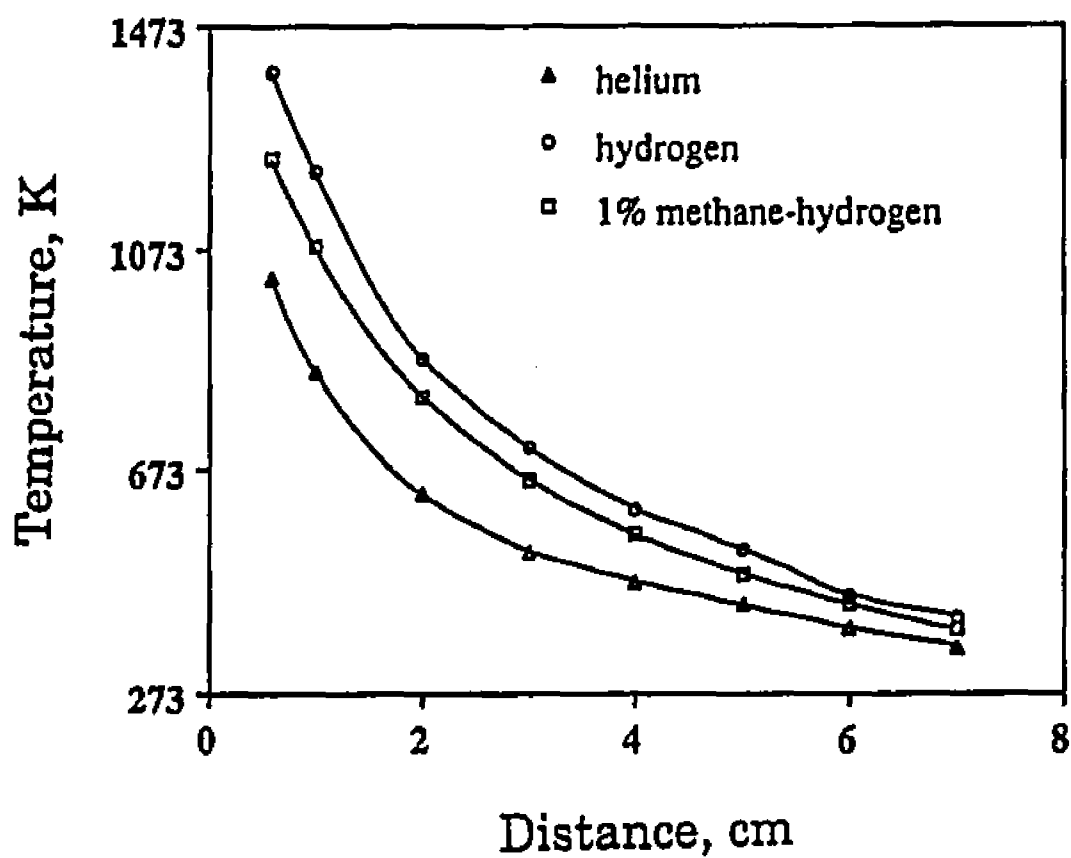
Fig. 4.1 Probe temperatures recorded in helium, hydrogen, and 1% CH_4-H_2 environments for a filament temperature of 2473 K, reactor pressure of 30 Torr, and a gas flow rate of 200 sccm.

in the gas phase. From the temperature field, shown in Fig. 4.2, it is clear that the temperature profiles are roughly symmetrical about the filament. However, a careful examination shows that the profiles are slightly compressed upstream from the filament while the profiles downstream are relatively spread out. This indicates that the gas flow has an insignificant influence on the temperature distribution and that conduction is the primary factor in establishing the temperature field. The ratio of the convective heat transport to conductive heat transport, the Peclet number for heat transfer, is given by $puLC_p/k$, where L is a characteristic length for the system, u is the average velocity, and ρ, C_p and k are the density, specific heat and the thermal conductivity of the gas respectively. Under the conditions of this investigation, the Peclet number for heat transfer is of the order of 0.05. The computed temperature field in Fig. 4.2 is consistent with the low value of the Peclet number and indicates that conduction, and not convection, is the dominant mechanism of heat transfer in the gas phase.

Experiments were conducted to verify the computed temperature profiles. The gas temperatures were derived from the measured thermocouple temperatures by a standard procedure [1]. The gas temperatures are derived from the thermocouple temperatures in helium by writing an energy balance at the thermocouple tip for steady state conditions. At the thermocouple tip the radiation heat loss from the thermocouple to the surroundings equals the heat gained by convection from the gas and radiation from the filament. The gas temperature is then given by

$$T_g = T_t + \frac{1}{h_c}\left(\epsilon_t \, \sigma \, v_{wt} \, T_t^4 - \epsilon_f \, \sigma \, v_{tf} \, T_f^4\right)$$

4.1
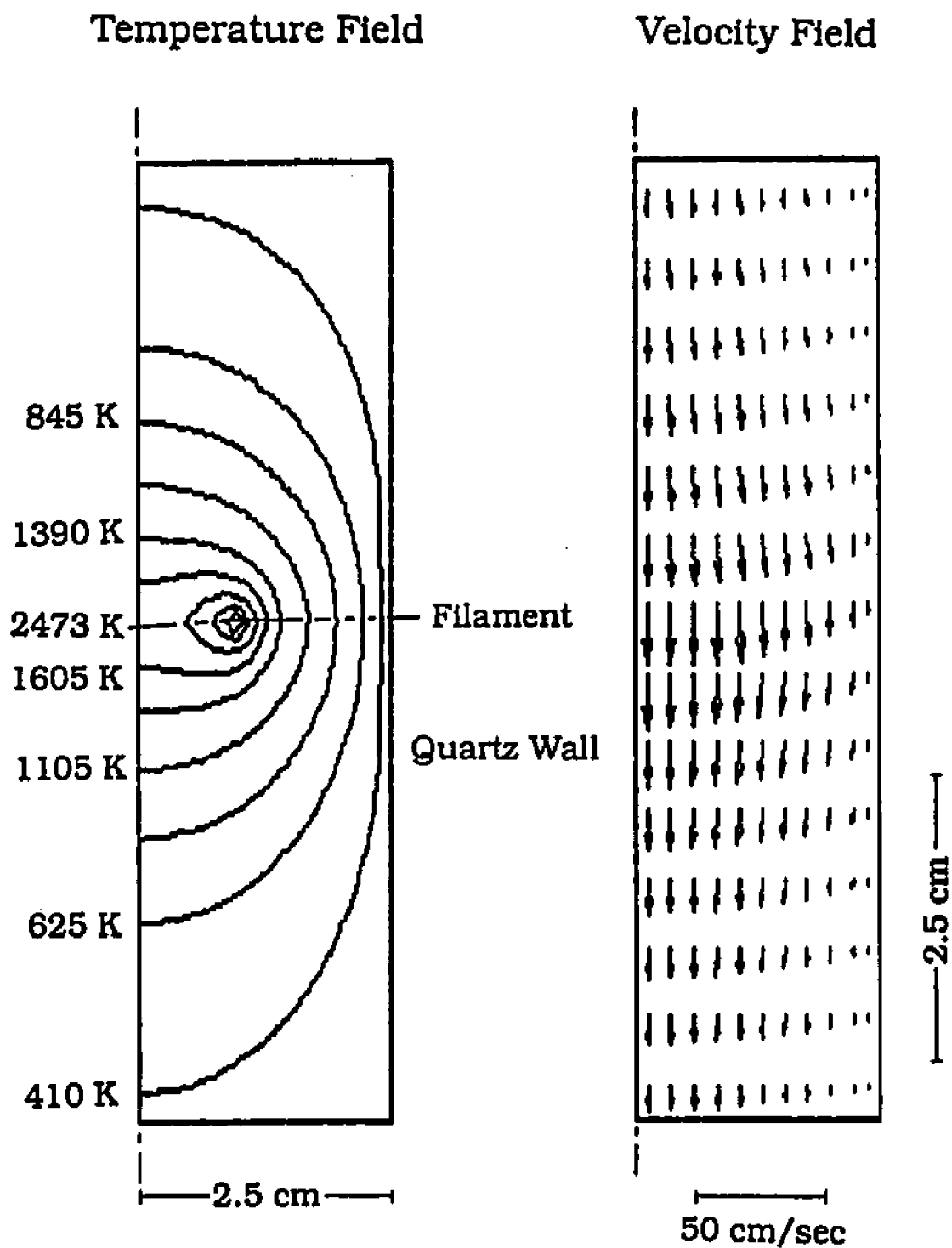
Fig. 4.2 Temperature and velocity fields computed for typical diamond deposition conditions of 2473 K filament temperature, 30 Torr reactor pressure, and 200 sccm gas flow rate.

where T_g is the gas temperature, T_t is the temperature recorded by the thermocouple, T_f is the temperature of the filament, h_c is the convective heat transfer coefficient, ε_f and ε_t are the emissivities of the filament and thermocouple respectively, σ is the Stefan-Boltzmann constant, v_{tf} and v_{wt} are the view factors. In order to avoid correction of the thermocouple temperature for heating due to chemical reactions at the thermocouple tip, temperature measurements were made in helium. Fig. 4.3 shows a comparison of the calculated temperatures indicated by the solid line with the experimentally determined values represented by the open circles. It is observed that the computed values are in fairly good agreement with the experimental observations. Thus, the model predictions of the temperature distribution in the reactor are reliable.

The relative importance of heat transfer by conduction, convection and radiation can also be examined from the experimental results of Mecray [2]. In his experiments Mecray heated tantalum filaments to 2350 °C in a typical bell jar reactor. Silicon substrates were placed on narrow alumina supports such that the distance between the filaments and the substrate was about 8 to 9 mm. The substrate temperature was measured at its back side with a single wavelength disappearing filament optical pyrometer. The power required to heat the filament to 2350 °C and the extent of substrate heating in vacuum, helium and hydrogen was determined. Fig. 4.4 shows the power consumption of a tantalum filament heated to 2350 °C in vacuum, and ultra high purity helium and hydrogen in the bell jar reactor. The corresponding substrate temperatures measured using the optical pyrometer are also presented. The results indicate that the power requirements were almost equal in vacuum and helium environments. Furthermore, the difference in the substrate temperatures was insignificant.
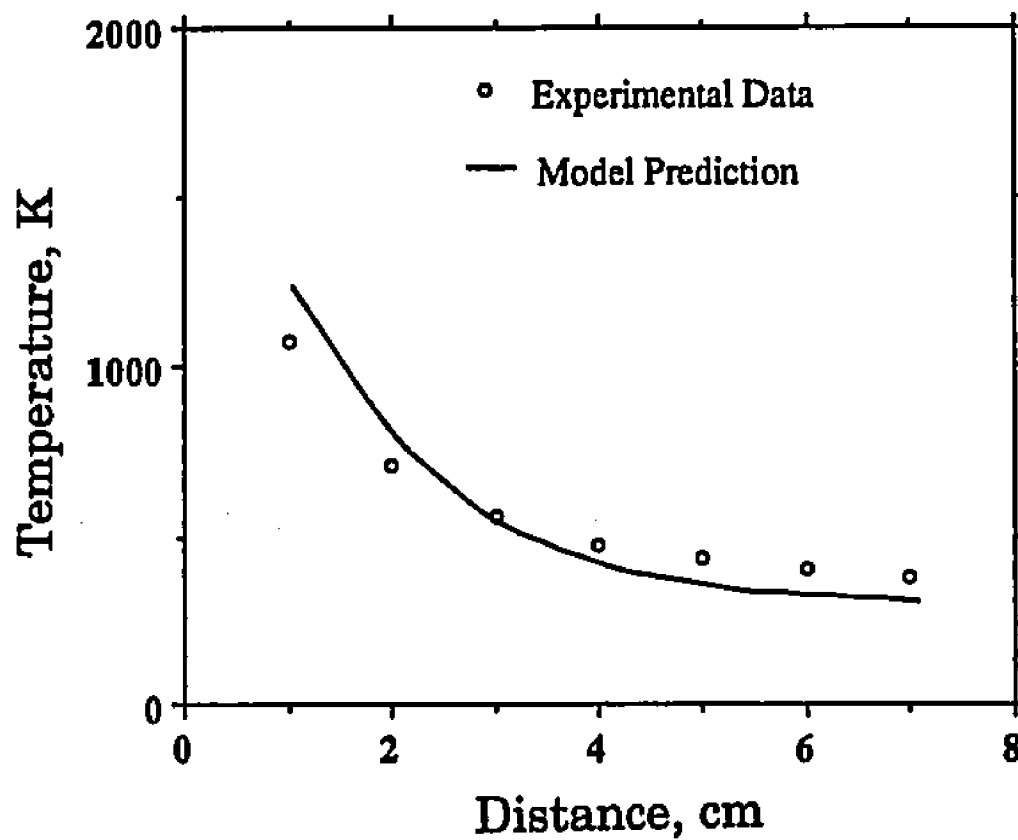
Fig. 4.3 Comparison of experimentally determined gas temperatures with numerically computed values.
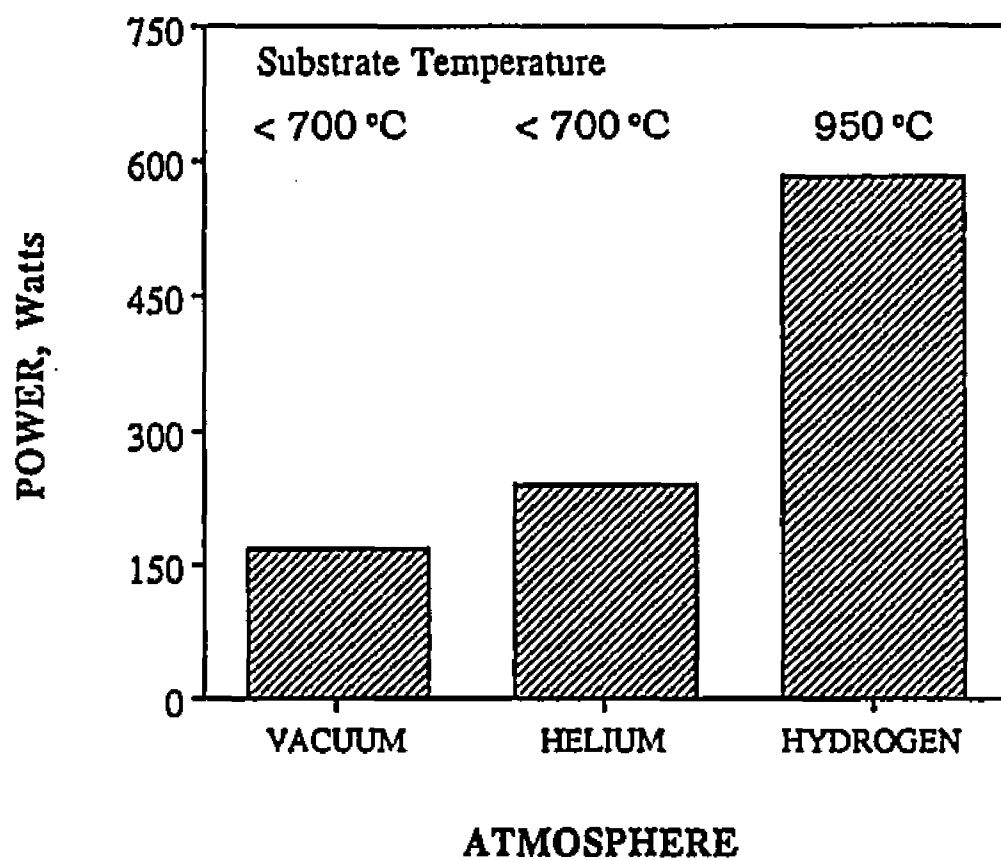
Fig. 4.4 Power consumption in maintaining tantalum filaments at 2350 °C, and substrate temperatures in various environments [2].

At steady state, the power consumption by the filament is equal to the combined effects of heat loss by convection, conduction and radiation, and the energy absorption by the endothermic reactions at the filament surface. Since there are no conduction and convection heat losses in vacuum, the power consumed to heat the filament to a given temperature is equal to radiative heat loss from the filament. The power consumption in helium is indicative of the heat losses due to conduction and convection in addition to radiation. The small increase in the power requirement when helium is introduced in the vacuum chamber indicates that conductive and convective heat losses from the filament are small compared to the radiative heat loss under typical hot filament assisted diamond deposition conditions. The substrate temperature in vacuum was less than the minimum detectable, about 700 °C, and did not appear to increase when the filament was heated in helium instead of vacuum. These results indicate that conductive and convective heat transfer to the substrate are negligible compared to radiative heat transfer.

4.1.2 Substrate Heating due to Atomic Hydrogen Recombination

The temperatures measured by the thermocouple in hydrogen were significantly different from the temperatures recorded in helium under identical conditions of filament temperature, reactor pressure and gas flow rate as can be observed from Fig. 4.1. Results of independent experiments, presented in Fig. 4.4, also indicate that the substrate temperature in hydrogen is at least 250 °C higher than that in helium. Since the rate of heat transfer by conduction, convection and radiation is roughly equal in helium and hydrogen, the above evidence suggests an additional mechanism of heat transport in hydrogen environment. A significant quantity of atomic hydrogen is generated at or near a filament heated in excess of 2000 °C at low pressures. The observation, in Fig. 4.4, that the power

required to heat the filament to a desired temperature in hydrogen was higher than that in helium is consistent with endothermic dissociation of hydrogen. Higher filament power requirements in hydrogen were also reported by Jansen [3]. Atomic hydrogen is transported away from the filament primarily by convection and diffusion. In the presence of a solid surface, such as the tip of a thermocouple, atomic hydrogen readily recombines to form molecular hydrogen.

$$H + H = H_2 \qquad \Delta H^o_{1200\ K} = -104\ kcal/mole\ of\ H_2 \qquad\qquad 4.2$$
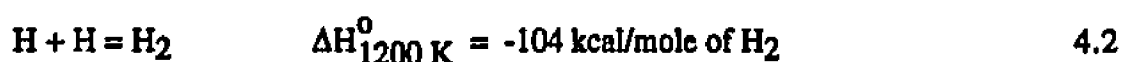
The recombination reaction is highly exothermic and the energy released heats the substrate. Thus, the endothermic generation of atomic hydrogen at or near the filament and its subsequent transport to the growth surface, where it recombines to form molecular hydrogen, serves as an additional mechanism of heat transport to the substrate. Fig. 4.1 clearly shows that in hydrogen the thermocouple temperatures are higher than the corresponding values in helium by about 400 °C when the thermocouple is placed about a centimeter away from the filament. Thus, in typical hot filament systems where the substrate is placed about 5 to 10 mm away from the filament, the recombination heat plays a major role in substrate heating.

Mecray's measurements [2] of substrate temperatures and the power required to heat carbon filaments in vacuum, helium and hydrogen atmospheres can be used to confirm that the enhanced heating of the substrate in hydrogen was primarily due to atomic hydrogen recombination. If the atomic hydrogen generation rate at the filament is diminished, the flux and hence the recombination rate of atomic hydrogen at the substrate will also be diminished. Thus, if a change in the atomic hydrogen generation rate brings about a

corresponding change in the substrate temperature, the observed effect can be attributed to atomic hydrogen recombination. The presence of carbon at the filament surface suppresses the generation of atomic hydrogen at the filament [4,5]. Carbon filaments were heated to 2350 °C at 30 Torr and a gas flow rate of 200 sccm. The power consumed by the filament in different atmospheres and the corresponding substrate temperatures are presented in Fig. 4.5. Once again, it is observed from the measurements of filament power consumption and substrate temperature in vacuum and helium that heat transfer by convection and conduction are negligible compared to radiative heat transfer. When a carbon filament was used, the power requirement in hydrogen was only slightly higher than that in helium. This suggests that a relatively small amount of atomic hydrogen is generated at the surface of the carbon filament. Furthermore, the substrate temperature in hydrogen was not very different from that in helium. Thus, atomic hydrogen plays a major role in heating the substrate only when present in substantial amounts. When carbon filaments are used and the concentration of atomic hydrogen is low, substrate heating occurs primarily by radiation. Diamond deposition has been achieved using carbon elements, albeit at relatively low growth rates. The details of diamond growth using carbon filaments are available elsewhere [2].

4.2 Factors Influencing Spatial Distribution of Atomic Hydrogen

Since the recombination of atomic hydrogen is of significant importance in substrate heating, the spatial variation of atomic hydrogen flux at the substrate surface and therefore, the distribution of the atomic hydrogen concentration in the gas phase is important for establishing the substrate temperature distribution. Furthermore, the factors responsible for the establishment of the concentration profile in the reactor are also of interest. Apart from homogeneous reactions in the gas phase, convective and diffusive mixing of atomic
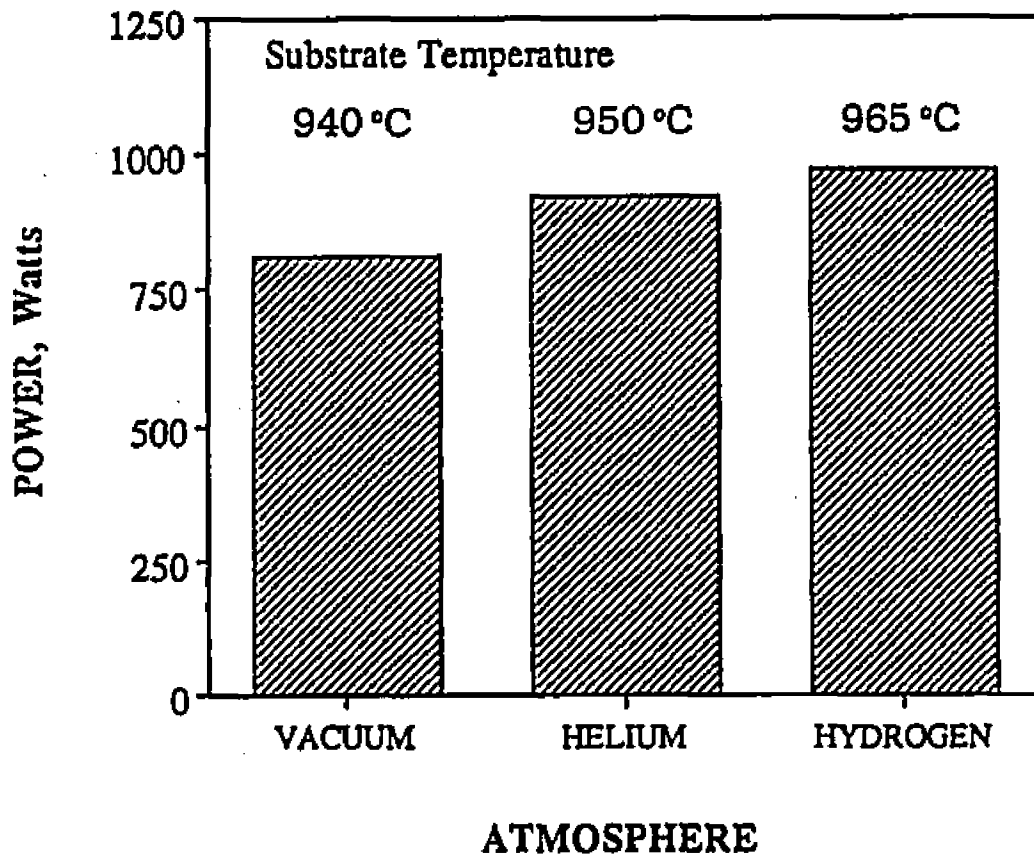
Fig. 4.5 Power consumption in maintaining carbon filaments at 2350 °C, and substrate temperatures in various environments [2].

hydrogen with the other species in the gas phase are responsible for the establishment of the species concentration fields. The relative importance of convection, diffusion and homogeneous chemical reactions in determining the atomic hydrogen concentration profile need to be examined.

The importance of convection in the transport of atomic hydrogen in the hot filament reactor can be examined from the velocity field presented in Fig. 4.2. In the vicinity of the filament, the velocities were of the order of 25 cm/sec. At these velocities, it takes approximately 40 ms for the species such as CH_3, C_2H_2 and H to travel from the filament to a substrate placed one centimeter away. Since the time constants for the loss of some of these species are of the order of a millisecond, the species cannot be transported to the growth surface by convective mass transport. The relative importance of mass transport by convection and diffusion can be examined with the help of a dimensionless number, the Peclet number for mass transfer, Pe. The Peclet number is defined as the ratio of convective mass transfer to diffusive mass transfer and is given by uL/D, where u is the average velocity, L is a characteristic length and D is the diffusion coefficient. An order-of-magnitude calculation of the Peclet number for the system yields a value of 0.08 indicating that diffusion, and not convection, is the dominant mechanism of mass transport. Therefore, the two main factors in the establishment of the atomic hydrogen concentrations in the gas phase are homogeneous chemical reactions of atomic hydrogen and its diffusive mixing with other gases.

In order to examine the relative importance of these two processes in determining the concentration profile of atomic hydrogen, computed values of atomic hydrogen concentration profiles were compared with experimentally determined values. The local

concentrations of atomic hydrogen in the reactor were obtained by solving the equations of conservation of energy for the probe in helium and hydrogen environments. At steady state, the probe energy balance can be expressed as

$$Q_{rad} + Q_{conv} + Q_{chem} + Q_{cond} = \frac{d}{dt}(m\,c_p T) = 0 \qquad\qquad 4.3$$

where Q_{rad}, Q_{conv}, Q_{cond}, and Q_{chem} are the net heat gains due to radiation, convection, conduction and chemical reactions respectively, and m, c_p and T are mass, specific heat and temperature of the thermocouple tip, respectively. The contributions of radiation, conduction and convection were calculated from the thermocouple temperatures in hydrogen and helium. In helium there is no contribution due to chemical reactions. In contrast, the hydrogen atoms are strongly adsorbed at the tip of the thermocouple. Assuming an Eley-Rideal mechanism [6] for the recombination of hydrogen atoms, Q_{chem} can be expressed as:

$$Q_{chem} = - k_f C_H A\,\Delta H^o \qquad\qquad 4.4$$

where k_f is the forward reaction rate constant for the recombination of atomic hydrogen, C_H is the concentration of hydrogen atoms, A is the area of the thermocouple tip and ΔH^o is the enthalpy of recombination of hydrogen atoms. An order-of-magnitude calculation indicated that the heat lost by conduction through the thermocouple wires was negligible compared to the heat gained by convection and radiation. Therefore, the conduction heat transfer through the thermocouple wires was ignored in the analysis. Thus, the energy balance for the probe in hydrogen and helium can be expressed by equations 4.5 and 4.6 respectively.

$$A_f \, v \, \varepsilon_f \, \sigma \, T_f^4 - \varepsilon_{th} \, \sigma \, A \, T_{H_2}^4 + h_c \, A \, (T_g - T_{H_2}) - k_f C_H \, A \, \Delta H^o = 0 \qquad 4.5$$

$$A_f \, v \, \varepsilon_f \, \sigma \, T_f^4 - \varepsilon_{th} \, \sigma \, A \, T_{He}^4 + h_c \, A \, (T_g - T_{He}) = 0 \qquad 4.6$$

where A_f is the area of the filament, T_{H_2} and T_{He} are the probe temperatures in hydrogen and helium respectively, T_f is the filament temperature, T_g is the gas temperature, h_c is the heat transfer coefficient, ε_{th} and ε_f are the emissivities of the probe and the filament respectively, σ is the Stefan-Boltzmann constant and v is the view factor. The following expression for the concentration of atomic hydrogen was derived by subtracting equation 4.6 from 4.5.

$$C_H = -\frac{T_{H_2}-T_{He}}{k_f \Delta H^o}\left[h_c + \varepsilon_{th}\sigma(T_{H_2}^2 + T_{He}^2)\,(T_{H_2} + T_{He})\right] \qquad 4.7$$

$$= f(T_{H_2}, T_{He}, h_c, \varepsilon_{th})/(k_f \Delta H^o) \qquad 4.8$$

Fig. 4.6 shows the computed concentration profiles of hydrogen atoms in a typical hot filament reactor. The contour values, shown in the figure, represent the local concentrations of atomic hydrogen as fractions of its concentration at the filament. It is observed that in the absence of a substrate, the contours are nearly symmetrical about the filament indicating the importance of diffusive transport of atomic hydrogen. In the calculation of the atomic hydrogen concentrations, homogeneous chemical reactions were assumed to be of negligible importance. If chemical reactions of atomic hydrogen were of significant importance and diffusive mixing was not the only important factor for the establishment of
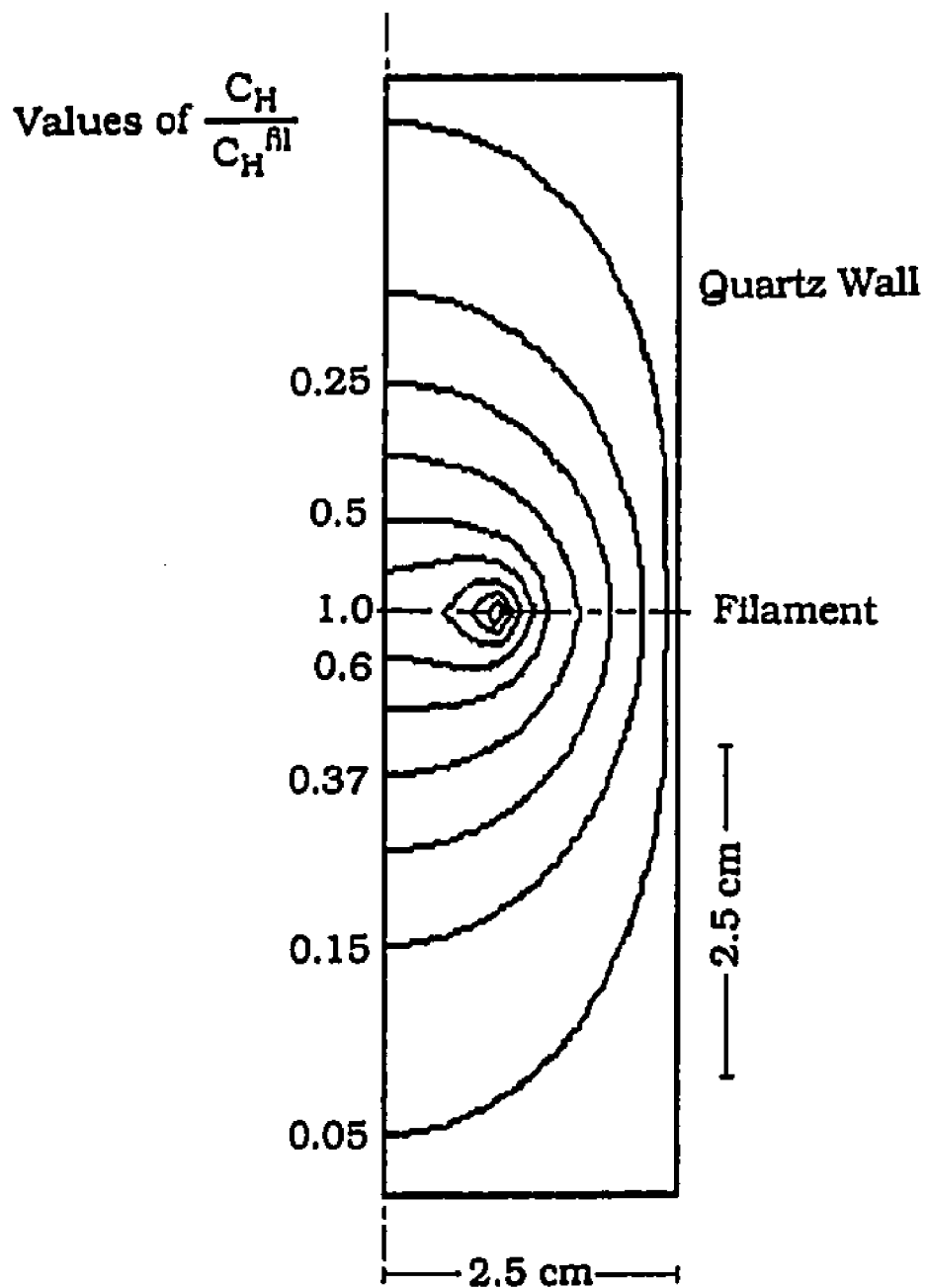
Fig. 4.6 Computed atomic hydrogen concentration field for a filament temperature of 2473 K, reactor pressure of 30 Torr, and a gas flow rate of 200 sccm.

the concentration profile, the computed concentration profile would have been substantially different from the experimentally determined profile. Fig. 4.7 shows a comparison of the experimental and the computed concentration profiles. It is observed that the computed concentration profile is in good agreement with experimental observations. Under conditions typical of the HFCVD of diamond, homogeneous chemical reactions do not play a significant role in determining the concentration profile of atomic hydrogen. The diffusive mixing of atomic hydrogen with other gases is the dominant factor in the establishment of the atomic hydrogen concentration profiles.

The addition of small amounts of methane to hydrogen resulted in the lowering of the thermocouple temperature indicating a decrease in the concentration of atomic hydrogen. The change in atomic hydrogen concentration at any particular distance from the filament can be roughly estimated assuming that the rate constant k_f in equation 4.8 does not change significantly upon the addition of methane. Using the data in Fig. 4.1, the decrease in atomic hydrogen concentration with 1% methane addition was calculated to be about 37% at a distance 10 mm from the filament. Celii and Butler [7] reported a similar effect of methane addition. Under conditions similar to our experiments, the REMPI intensity of the atomic hydrogen peak, 8 mm from the filament, decreased 33% as a result of the addition of 1% methane to hydrogen. Meier et al. [8] also reported a decrease in the atomic hydrogen concentration with methane addition. However, in their experiments, the filament temperature was not adjusted after methane addition. The changes in the concentration resulted due to a combined effect of changes in (a) filament temperature and, (b) gas composition due to methane addition. Unfortunately, their data cannot be used to obtain reliable quantitative effects of methane addition.
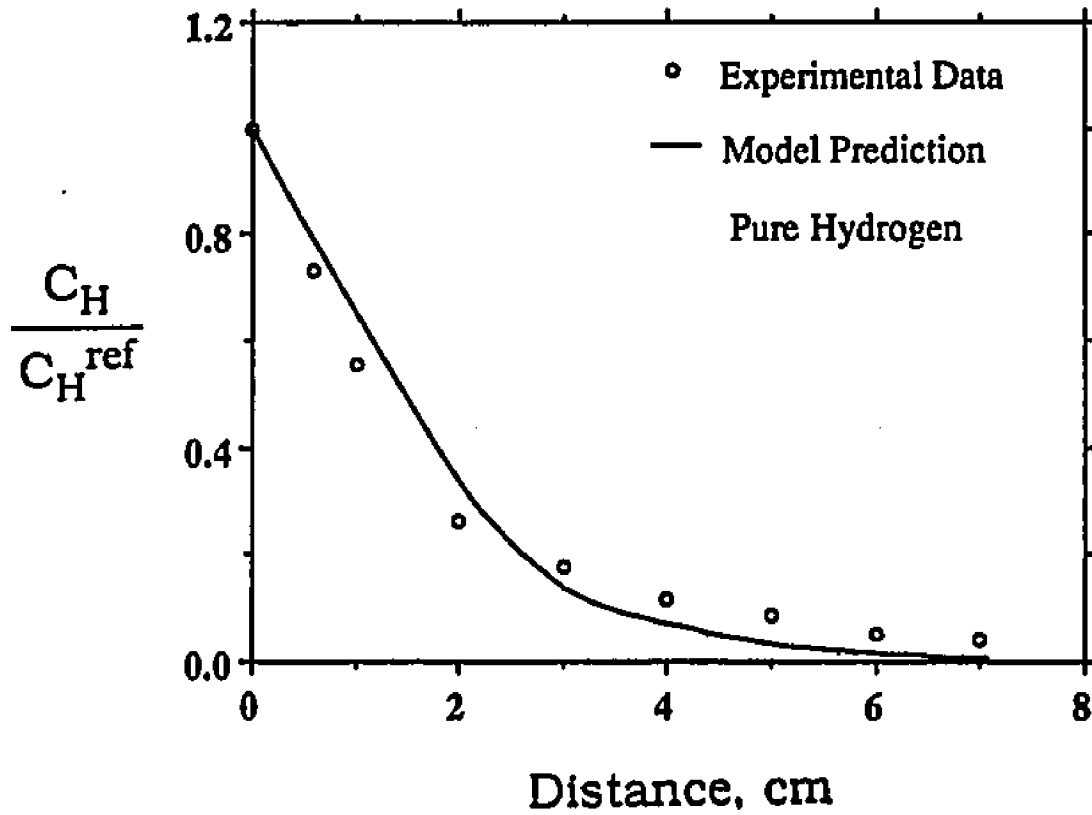
Fig. 4.7 Comparison of experimentally determined atomic hydrogen concentration profile in H_2 with the theoretically computed profile ignoring homogeneous chemical reactions of atomic hydrogen.

If the observed decrease in atomic hydrogen concentration is due to chemical reactions of atomic hydrogen with the hydrocarbon species, the experimentally observed atomic hydrogen concentration profile in a methane-hydrogen gas mixture would deviate from the profile predicted on the basis of diffusive mixing. However, if the generation of atomic hydrogen at the filament is reduced due to the addition of methane and homogeneous chemical reactions do not significantly alter the concentration of atomic hydrogen, good agreement should be achieved between the shapes of the experimental and the computed profiles. It is observed from Fig. 4.8 that the experimentally determined atomic hydrogen concentration profile in 1% CH_4-H_2 is in good agreement with the theoretically computed profile ignoring homogeneous chemical reactions of atomic hydrogen. In addition, the power required to heat the filament in a methane-hydrogen gas mixture was lower than that required to heat it in pure hydrogen, indicating a lower rate of generation of atomic hydrogen at the filament in the presence of methane. The presence of small quantities of methane reduces the concentration of atomic hydrogen in the reactor and diffusive mixing continues to be the most important factor in the establishment of the concentration field of atomic hydrogen.

Of the two possible reasons for the lowering of the atomic hydrogen concentration due to methane addition, i.e., possible gas phase reactions of atomic hydrogen and diminished generation of atomic hydrogen at the filament, convincing experimental evidence has been reported [8] in support of the later argument. In the experiments of Meier et al. [8], after the atomic hydrogen concentration dropped due to methane addition, the gas composition was immediately changed to pure hydrogen. If gas phase reactions were important, the atomic hydrogen concentration would change to its original value prior to methane addition. However, the results demonstrated that the concentration of atomic hydrogen generated
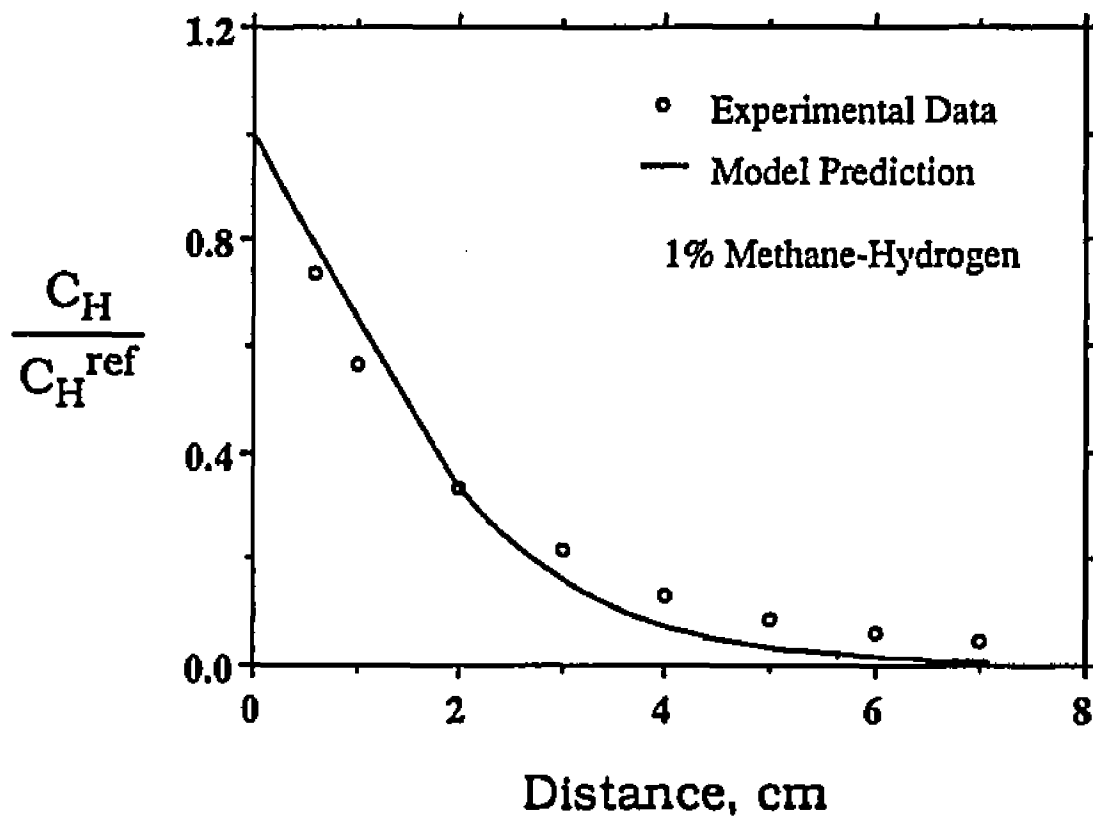
Fig. 4.8 Comparison of experimentally determined atomic hydrogen concentration profile in 1% CH_4-H_2 with the theoretically computed profile ignoring homogeneous chemical reactions of atomic hydrogen.

from the pure hydrogen feed stream, after withdrawal of methane, was the same as that observed when methane was present. Thus, the nature of the filament controlled the dissociation of hydrogen and gas phase reactions were not of significant importance. Since the rate of generation of atomic hydrogen is diminished due to a change in the nature of the filament, the addition of a small amount of methane can substantially change the atomic hydrogen concentration in the reactor. Further methane additions will only bring about progressively smaller changes in the atomic hydrogen concentration. The observed decrease in atomic hydrogen concentration in our experiments is in good agreement with the results of previous investigations [7,8].

4.3 Modeling of Substrate Surface Temperature

Since the quality, morphology and defect density of the diamond films are sensitive to temperature, a uniform surface temperature is crucial for the deposition of diamond films of uniform properties. Thus, the heat transfer to the substrate and the resultant substrate temperature distribution are important considerations in the design of reactors for coating large areas. Furthermore, a knowledge of the various factors that have a substantial influence on the substrate temperature distribution is crucial for reactor design and scale-up. An appropriate fluid flow and heat transfer model that accounts for substrate heating due to atomic hydrogen recombination in addition to conduction, convection and radiation, with adequate experimental verification, would be a useful for examining the role of various process parameters and reactor geometry on the substrate temperature.

4.3.1 Gas Phase Heat and Mass Transfer

The heat transfer and fluid flow phenomena in the reactor were modeled to obtain the velocity, temperature and atomic hydrogen concentration fields in the reactor. The velocity and temperature fields, computed for typical diamond deposition conditions, were used to examine the primary mechanisms for gas phase heat and mass transfer in the bell jar reactor. The computed velocity field for a filament temperature of 2473 K, reactor pressure of 30 Torr and a gas flow rate of 200 sccm is presented in Fig. 4.9. The average convective velocities in the reactor were of the order of 0.6 cm/s. The relative importance of mass transport by convection and diffusion in the bell jar reactor was examined from the Peclet number for mass transfer, Pe. An order of magnitude calculation of the Peclet number, which is the ratio of the mass transfer by convection to mass transfer by diffusion, yielded a value of 0.01, indicating diffusion, not convection, to be the dominant mechanism for mass transport in the bell jar reactor. Earlier it was shown that diffusion is the primary mechanism of species transport in the tubular hot filament reactor. DebRoy et al. [9,10] presented experimental evidence which indicated that in typical hot filament reactors for diamond deposition, diffusion is the dominant mechanism of mass transfer. Thus, the low value of Peclet number for this system is consistent with experimental observations.

Fig. 4.10(a) and (b) show the temperature fields in the HFCVD reactor for gas flow rates of 200 and 600 sccm, respectively. If convection were a significant mode of heat transfer, a change in the gas flow rate should result in a substantial change in the temperature field. However, as can be seen from Fig. 4.10(a) and (b), increasing the gas flow rate by a factor of three did not change the temperature field significantly. This indicates that convection is unimportant in determining the temperature distribution and conduction is the primary

Axis —

Reactor
Wall

Filament — ×
Substrate —

1.0 cm/s

30 mm
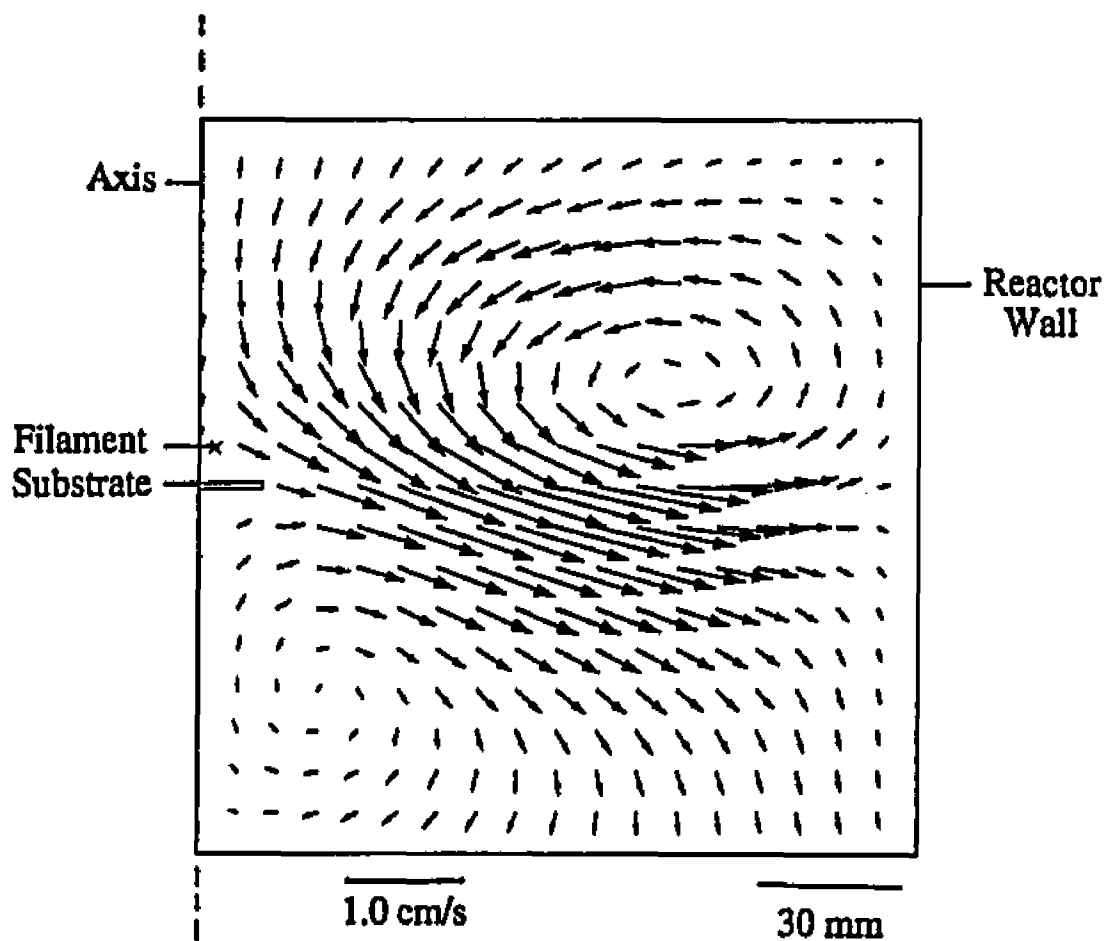
Fig. 4.9 Computed velocity field in the bell jar type hot filament reactor for a filament temperature of 2473 K, reactor pressure of 30 Torr, and a gas flow rate of 200 sccm. The spacing between the two filaments was 6 mm and the filament to substrate distance was 7 mm.
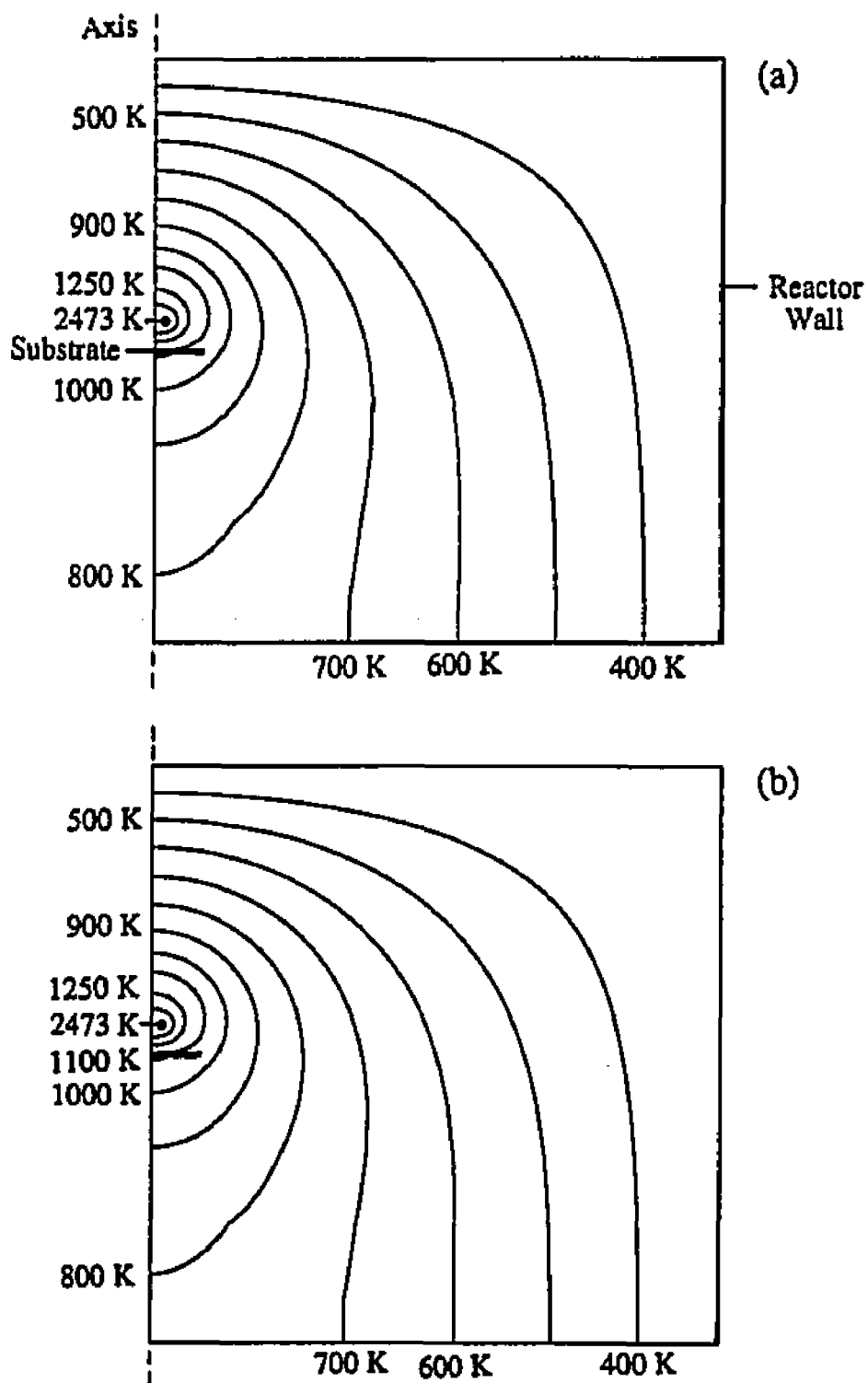
Fig. 4.10 Computed temperature fields in the bell jar type hot filament reactor for a filament temperature of 2473 K, reactor pressure of 30 Torr, and a gas flow rate of (a) 200 sccm and (b) 600 sccm.The spacing between the two filaments was 6 mm and the filament to substrate distance was 7 mm.

factor in establishing the temperature profiles in the gas phase. The ratio of convective heat transport to conductive heat transport, the Peclet number for heat transfer, is given by, $\rho u L C_p/k$, where L is the characteristic length for the system, u is the average velocity and ρ, C_p and k are the density, specific heat and thermal conductivity of the gas, respectively. For this system the Peclet number for heat transfer is of the order of 0.02. Thus the insignificant influence of flow rate on the temperature field is consistent with the low value of Peclet number, and indicates that conduction, and not convection, is the dominant mechanism of heat transfer in the gas phase.

The computed atomic hydrogen concentration fields in the reactor are presented in Fig. 4.11. The values of the contours represent atomic hydrogen concentrations as fractions of its concentration at the filament. Since homogeneous recombination of atomic hydrogen does not significantly alter its concentration in the reactor, as established earlier, the concentration profiles were calculated based only on mixing of atomic hydrogen with the surrounding gas. Furthermore, since the Peclet number for mass transfer is very small, the concentration field in Fig. 4.11 is established primarily by diffusion, and convection does not play an important role in determining the local concentrations of atomic hydrogen in the reactor. Fig. 4.11 shows that the concentration of atomic hydrogen at various locations on the substrate surface is different, indicating that the flux of atomic hydrogen at the substrate surface is spatially non-uniform. Thus, the hydrogen recombination effect is spatially non-uniform, and can contribute to significant spatial variation in the substrate temperature.
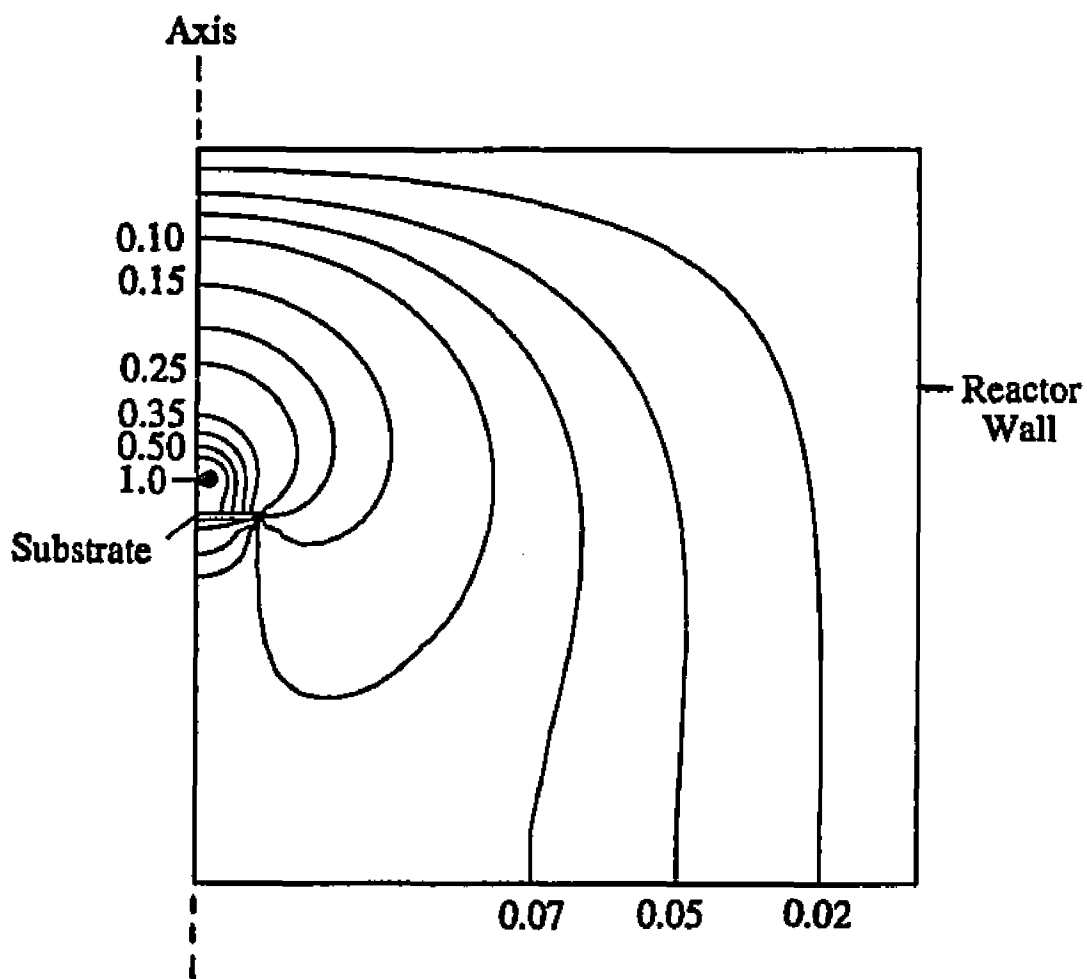
Fig. 4.11 Computed atomic hydrogen concentration field for a filament temperature of 2473 K, reactor pressure of 30 Torr, and a gas flow rate of 200 sccm. The spacing between the two filaments was 6 mm and the filament to substrate distance was 7 mm.

4.3.2 Role of Process Parameters

Experiments were conducted in a bell jar type hot filament reactor, shown in Fig. 3.2, to examine the effect of gas flow rate, filament temperature and reactor pressure in determining the substrate temperature. The experimental results were used to verify the model predictions of the effect of process parameters on the substrate temperature. The model includes substrate heating due to atomic hydrogen recombination in addition to conduction, convection and radiation. In order to accurately account for the effect of atomic hydrogen recombination on substrate temperature, the concentration of atomic hydrogen at the filament for various process conditions needs to be properly prescribed. Preliminary calculations, assuming that the atomic hydrogen concentration at the filament increases in the same proportion as the equilibrium concentration, did not yield the observed trends in the variation of substrate temperature with filament temperature and pressure. Therefore, experiments were conducted to examine the effect of process parameters on the atomic hydrogen generation rate.

4.3.2.1 Atomic Hydrogen Generation

The power required to heat the filament to a particular filament temperature at a particular reactor pressure was measured in helium and hydrogen atmospheres. In helium, the power dissipated by the filament is representative of the heat lost due to conduction, convection and radiation. In hydrogen, the power dissipated by the filament is representative of the heat required to dissociate molecular hydrogen into atoms in addition to heat losses due to conduction convection and radiation. Since heat losses due to conduction, convection and radiation are approximately same in hydrogen and helium, the difference in the power

dissipated by the filament in helium and hydrogen is a measure of the power required to dissociate hydrogen. If ΔE is the difference in the power dissipated in hydrogen and helium atmospheres, the generation rate of atomic hydrogen, r_H, in moles/cm^2 s, is given by

$$r_H = \frac{\Delta E}{2 \pi r_f L \Delta H} \qquad \qquad 4.9$$

where r_f is the radius of the filament, L is the length of the filament and ΔH is the enthalpy of formation of one mole of hydrogen atoms.

Experiments were conducted to determine the generation rate of atomic hydrogen using tungsten and tantalum filaments. Fig. 4.12 shows the generation rate of atomic hydrogen at various filament temperatures. It is observed, from Fig. 4.12, that the atomic hydrogen generation rate increases with filament temperature for both tantalum and tungsten wires. However, it can be seen that in the temperature range of 2100 K to 2473 K the rate of generation of atomic hydrogen was higher when tungsten wires were used than when tantalum wires were used. The results indicate that the atomic hydrogen generation rate is sensitive to the filament material and that the dissociation of hydrogen using refractory metal filaments is a surface reaction controlled process. Furthermore, it is also observed from Fig. 4.12 that the temperature sensitivity of the atomic hydrogen generation rate is different for tantalum and tungsten wires. Fig. 4.13 is a plot of the natural logarithm of the atomic hydrogen generation rate and the reciprocal of the filament temperature. The activation energies for the dissociation of hydrogen molecules, calculated from the slope of the Arrhenius plot, shown in Fig. 4.13, are 46.8 kcal/mole and 33.1 kcal/mole for tantalum and tungsten, respectively. The lower activation energy for the dissociation of molecular
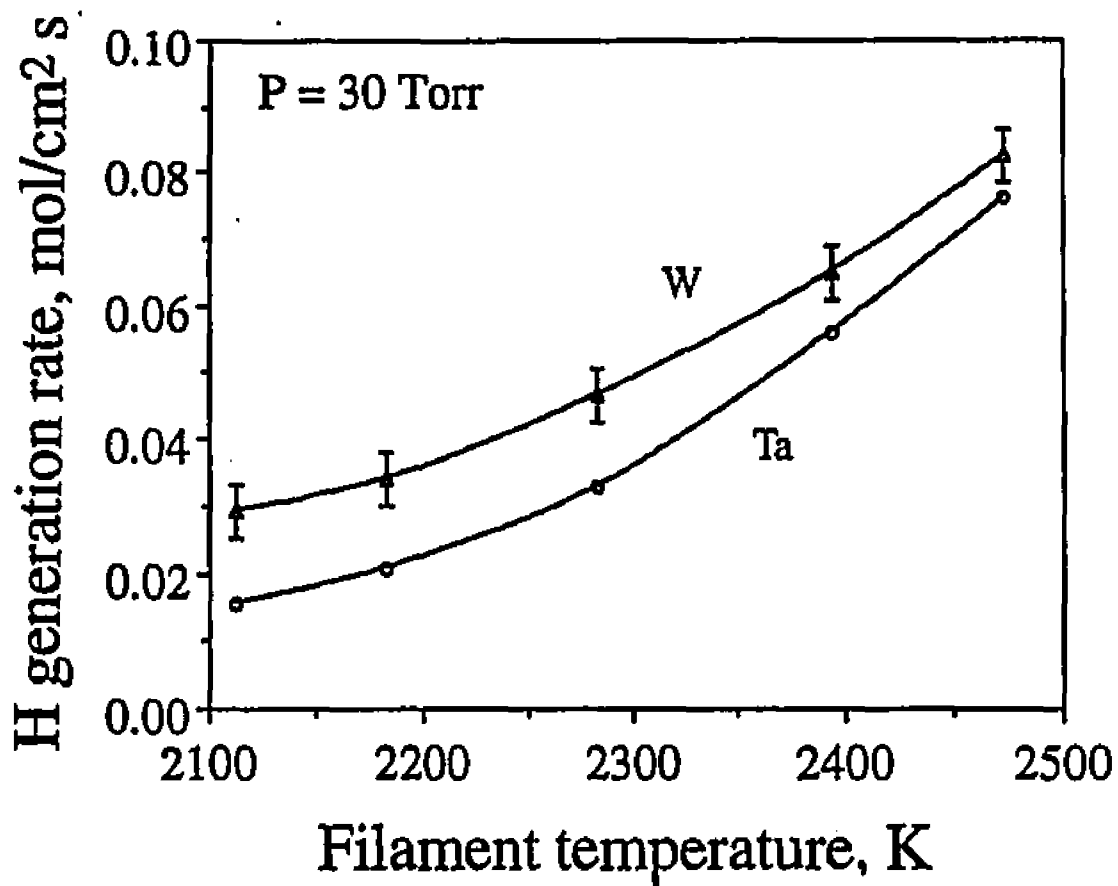
Fig. 4.12 Atomic hydrogen generation rates at tantalum and tungsten filaments for a reactor pressure of 30 Torr and a gas flow rate of 200 sccm. The filaments were 0.25 mm in diameter.
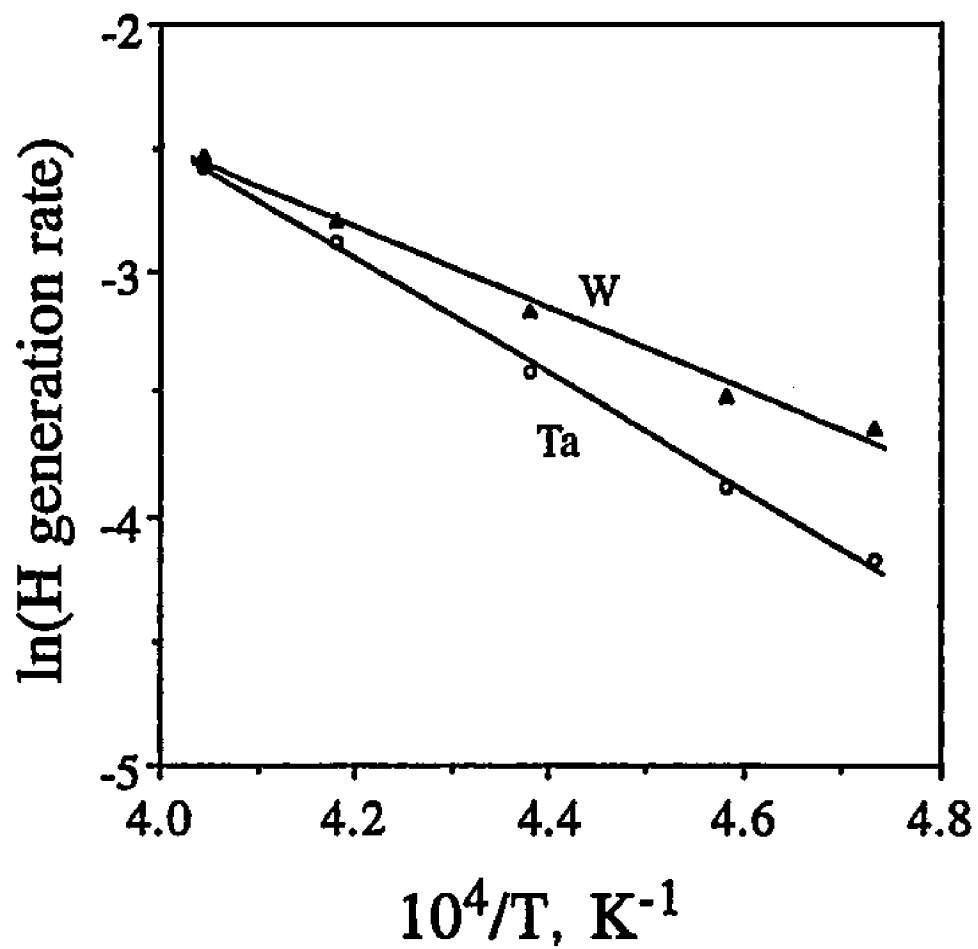
Fig. 4.13 Arrhenius plot for calculating the activation energy for dissociation of atomic hydrogen at tantalum and tungsten filaments.

hydrogen on tungsten compared to tantalum indicates that tungsten is a better catalyst for the dissociation of hydrogen in the temperature range examined in this study.

In order to examine if the dissociation of hydrogen attains equilibrium at the filament under typical hot filament diamond deposition conditions, the proportion in which the atomic hydrogen generation rate and the equilibrium concentration of atomic hydrogen increase with filament temperature were compared, as shown in Fig. 4.14. It is observed from the figure that the increase in atomic hydrogen generation rate at a tungsten filament deviates significantly from proportion in which the equilibrium concentration of atomic hydrogen increases with filament temperature. The result indicates that equilibrium is not attained at a tungsten filament. Although the atomic hydrogen generation rate at a tantalum filament increases in about the same proportion as the equilibrium concentration, Fig. 4.12 shows that the generation rate at a tantalum filament is lower than that at a tungsten filament indicating that the concentration of atomic hydrogen at a tantalum filament is less than at a tungsten filament. Thus, an equilibrium concentration of atomic hydrogen is not generated at the tantalum filament. The results indicate that during modeling of hot filament deposition reactors, an equilibrium concentration of atomic hydrogen can not be assumed to be present at the filament.

It is clear from the above results that a prescription of equilibrium atomic hydrogen concentration at the filament under hot filament diamond deposition conditions will not yield accurate estimates of the flux of atomic hydrogen at the substrate surface, and consequently, result in inaccurate prediction of the trends in the variation of substrate temperature with filament temperature and pressure. Langmuir [11-13] in his study of the dissociation of hydrogen on tungsten filaments developed a relation between the power
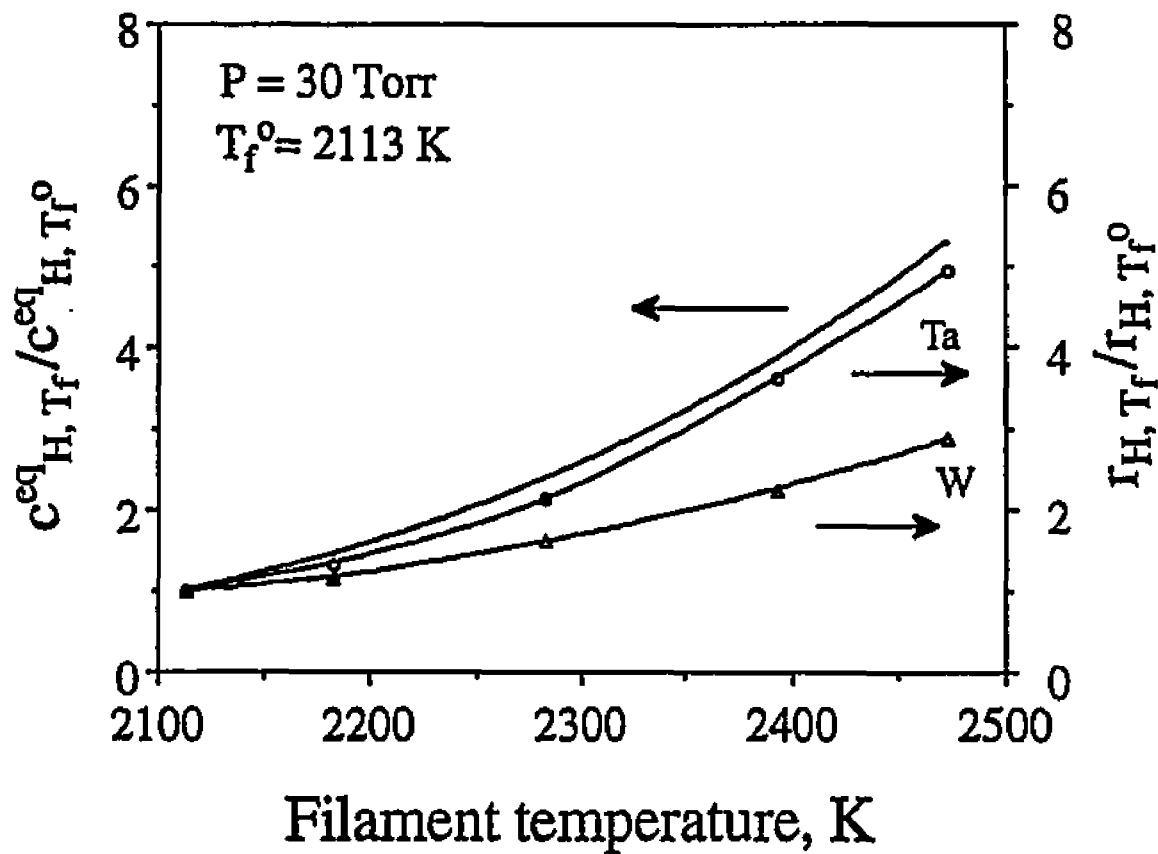
Fig. 4.14 Comparison of the proportion in which the atomic hydrogen generation rate and equilibrium concentration of atomic hydrogen increase with filament temperature.

dissipated by the filament due to dissociation of hydrogen molecules and the concentration of atomic hydrogen at the filament. The relation can be used for obtaining the proportion in which the atomic hydrogen concentration at the filament changes with filament temperature and pressure.

Consider a filament, of radius a, loosing heat to a film of gas, of radius b. From the laws of heat conduction the power dissipated by the wire, Q in watts/cm of wire, in a non-dissociating gas, such as helium, is given by

$$Q_{He} = -\frac{2\pi}{\ln b/a} \int_{T_2}^{T_1} k dT + Q_{rad} + Q_{conv} \qquad 4.10$$

where T_2 is the filament temperature, T_1 is the temperature at the outer surface of the film of gas, k is the conductivity of the gas, and Q_{rad} and Q_{conv} are the heat losses due to radiation and convection, respectively.

Let us now consider heat conduction in a dissociating gas, such as hydrogen. The heat flow due to ordinary conduction across a unit area is given by $-k dT/dx$. In a dissociating gas, besides this ordinary heat conduction we have heat transported by hydrogen atoms which are generated at the filament and recombine at a remote location. If C_H is the concentration of hydrogen atoms and D is the diffusivity of hydrogen atoms in hydrogen, the heat carried by hydrogen atoms across a unit area is given by $-D\Delta H dC_H/dx$, where ΔH is the heat of formation of hydrogen molecules from one mole of hydrogen atoms, i.e. for the reaction $H = 1/2 H_2$. Hence, the total heat transported across a unit area by conduction and transport of hydrogen atoms is given by

$$-\left(k + D\Delta H\frac{dC_H}{dT}\right)\frac{dT}{dx} \qquad 4.11$$

Thus, the effect of dissociation of hydrogen at the filament and recombining at a remote location can be viewed as an increase in the heat conductivity by an amount given by $D\Delta H dC_H/dT$. Substituting $(k + D\Delta H dC_H/dT)$ for k in equation 4.10 we get

$$Q_{H_2} = -\frac{2\pi}{\ln(b/a)}\int_{T_2}^{T_1}\left(k + D\Delta H\frac{dC_H}{dT}\right)dT + Q_{rad} + Q_{conv} \qquad 4.12$$

On integrating and taking C_H to be C_H^{fil} at T_2 and zero at T_1 we obtain

$$Q_{H_2} = Q_{cond} + s\, D\, \Delta H\, C_H^{fil} + Q_{rad} + Q_{conv} \qquad 4.13$$

where Q_{cond} is the heat lost by conduction, s is $2\pi/\ln(b/a)$, and C_H^{fil} is the atomic hydrogen concentration at the filament. Thus, the heat lost due to dissociation of hydrogen is given by

$$Q_{chem} = Q_{H_2} - Q_{He} = s\, D\, \Delta H\, C_H^{fil} \qquad 4.14$$

Substituting $C_H = p_H/RT$ and $D = D_0\,(T/298)^{3/2}\,(760/P)$, where R is the gas constant, T is the filament temperature, p_H is the partial pressure of atomic hydrogen, P is the total pressure and D_0 is the diffusion coefficient of atomic hydrogen in molecular hydrogen at room temperature and atmospheric pressure, we get

$$Q_{chem} = s\,\Delta H\,D_0\left(\frac{T}{298}\right)^{3/2}\left(\frac{760}{P}\right)\frac{p_H}{RT} \qquad\qquad 4.15$$

The proportion in which the partial pressure of atomic hydrogen at the filament increases can be obtained from the ratio of the heat lost due to dissociation of hydrogen and is given by

$$\frac{Q_{chem}}{Q^0_{chem}} = \sqrt{\frac{T}{T^0}}\left(\frac{p_H/P}{p_H^0/P^0}\right) \qquad\qquad 4.16$$

where, Q^0_{chem} is the heat lost due to dissociation of hydrogen and p_H^0 is the partial pressure

of atomic hydrogen at the filament for a reference pressure P^0 and a filament temperature T^0.

The effect of pressure on the atomic hydrogen generation rate was determined by measuring the power required to heat a filament to a particular temperature at various pressures in helium and hydrogen atmospheres. Fig. 4.15 shows the variation of atomic hydrogen generation rate with reactor pressure. It is observed from Fig. 4.15 that the generation rate of atomic hydrogen increases to a maximum at about 25 Torr and then decreases with increasing pressure. A similar variation in atomic hydrogen generation rate was reported by Langmuir [12], with the maximum in generation rate occurring between 25 to 50 Torr. Using equation 4.16 and the measured heat lost due to dissociation of hydrogen at various pressures the proportion in which the atomic hydrogen concentration increases with pressure was derived. In Fig. 4.16 the proportion in which the observed atomic
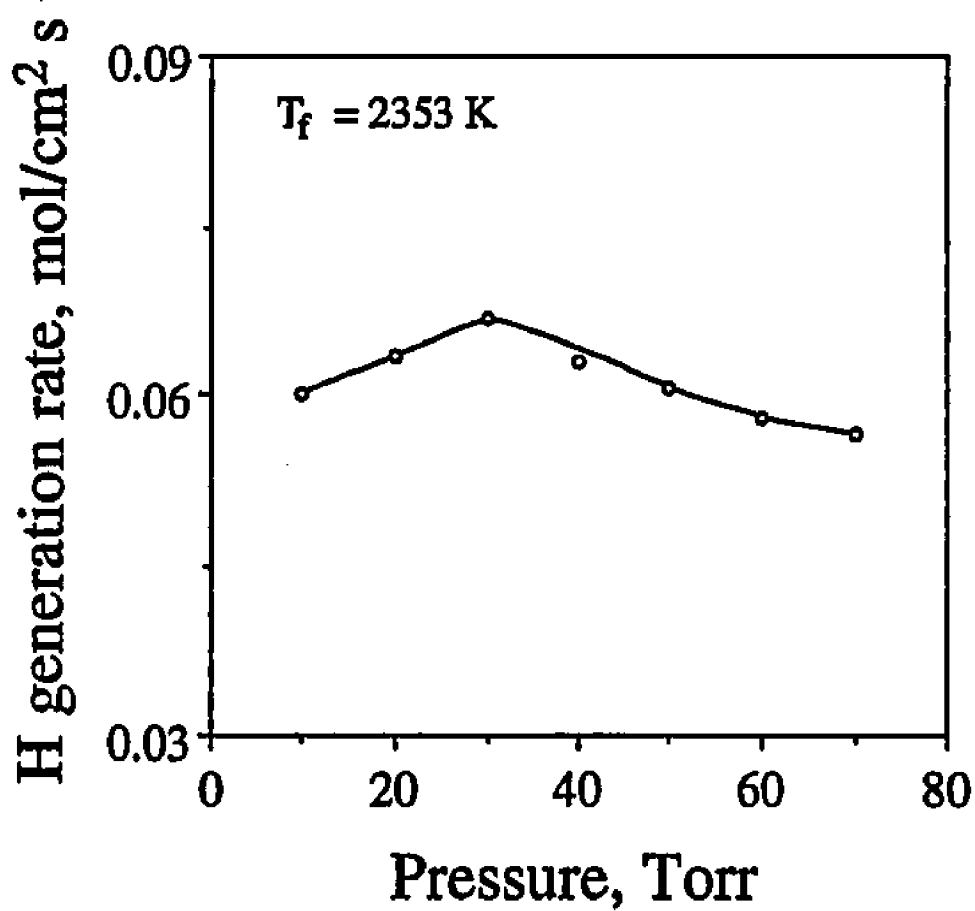
Fig. 4.15 Atomic hydrogen generation rate at a tungsten filament for a filament temperature of 2353 K and a gas flow rate of 200 sccm. The filament diameter was 0.25 mm.
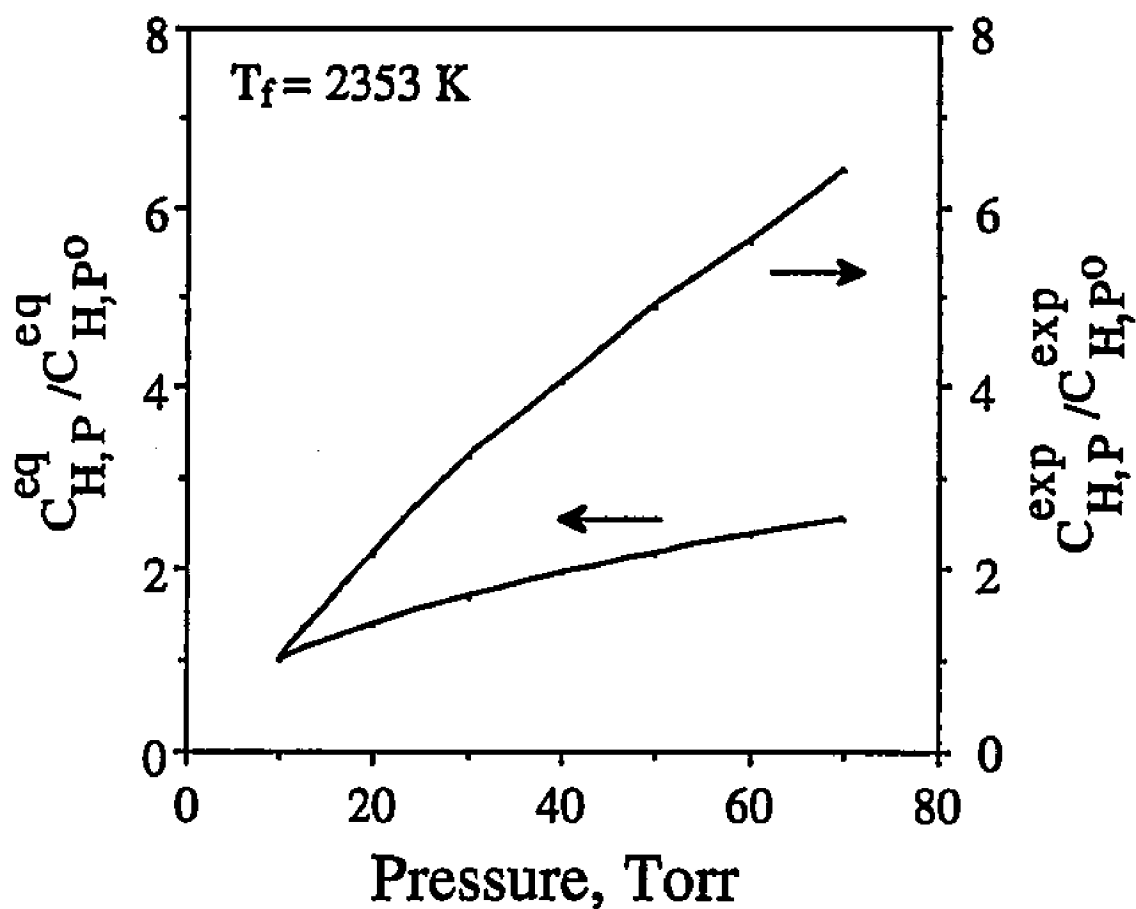
Fig. 4.16 Comparison of the proportion in which the experimentally determined atomic hydrogen concentration, right ordinate, and the equilibrium concentration of atomic hydrogen, left ordinate, increase with pressure.

hydrogen concentration at the filament increases with pressure is compared with the proportion in which the equilibrium concentration of atomic hydrogen increases with pressure. Fig. 4.16 shows that the pressure dependence of experimentally derived atomic hydrogen concentration and the equilibrium atomic hydrogen concentration are significantly different indicating that equilibrium is not attained at the filament.

4.3.2.2 Substrate Temperature

Experiments were conducted to examine the influence of gas flow rate, filament temperature and pressure on the substrate temperature. Fig. 4.17 shows the effect of total gas flow rate on the substrate temperature at 30 Torr pressure and two filament temperatures. It is observed from the figure that in the range of flow rates studied, the flow rate has an insignificant effect on the substrate temperature indicating that convection does not play an important role in substrate heating under typical hot filament deposition conditions. It was shown earlier that convection is not a major factor in determining the spatial distribution of species in the reactor. Thus, the location of the gas inlet and outlet manifolds and the nature of the gas flow patterns in the reactor are not important in the design of hot filament reactors for diamond deposition. Furthermore, it observed from Fig. 4.17 that the model predictions, solid lines, of the effect of flow rate on the substrate temperature are in good agreement with the experimental observations, indicated by circles and triangles.

The effect of filament temperature on the substrate temperature in helium and hydrogen, atmospheres, indicated by triangles and circles respectively, is presented in Fig. 4.18. The data show that at any given filament temperature the substrate temperature in hydrogen is
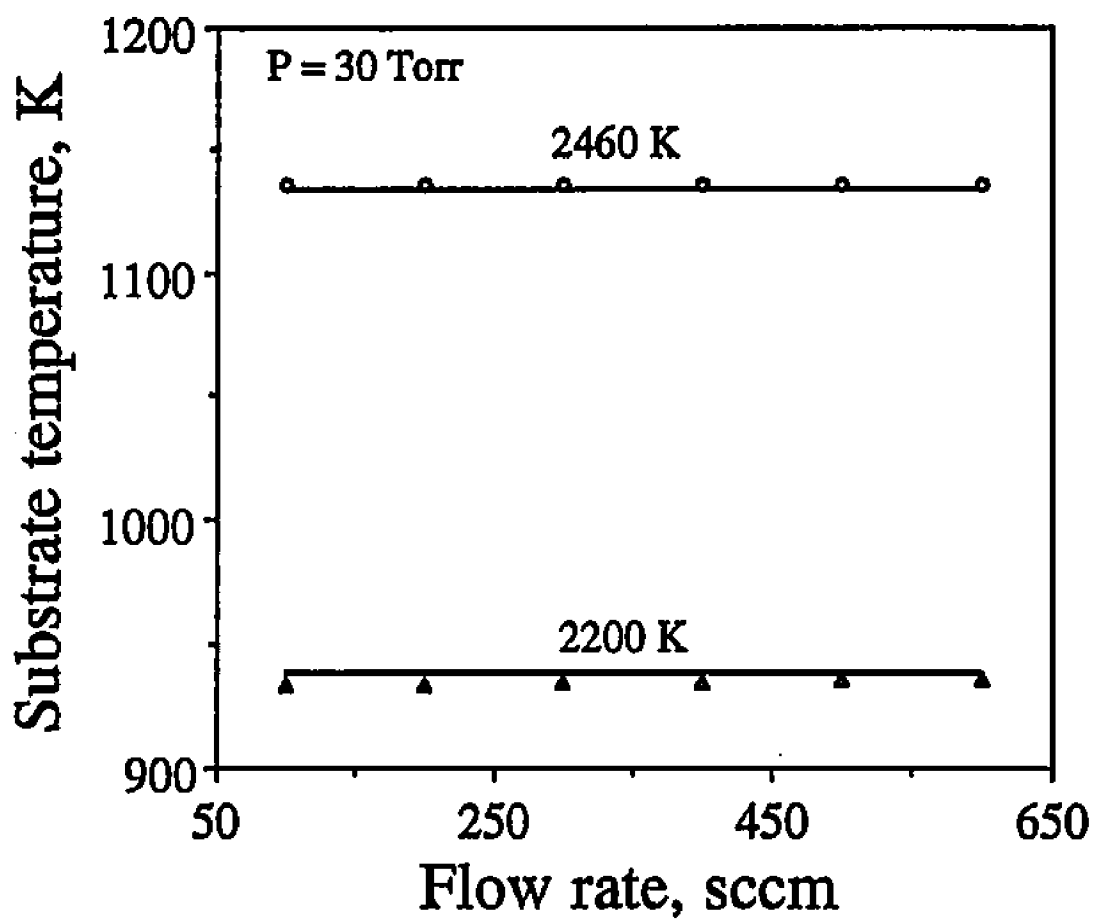
Fig. 4.17 Effect of flow rate on substrate temperature for a reactor pressure of 30 Torr. The circles and triangles represent experimental data and the solid lines represent the model predictions.
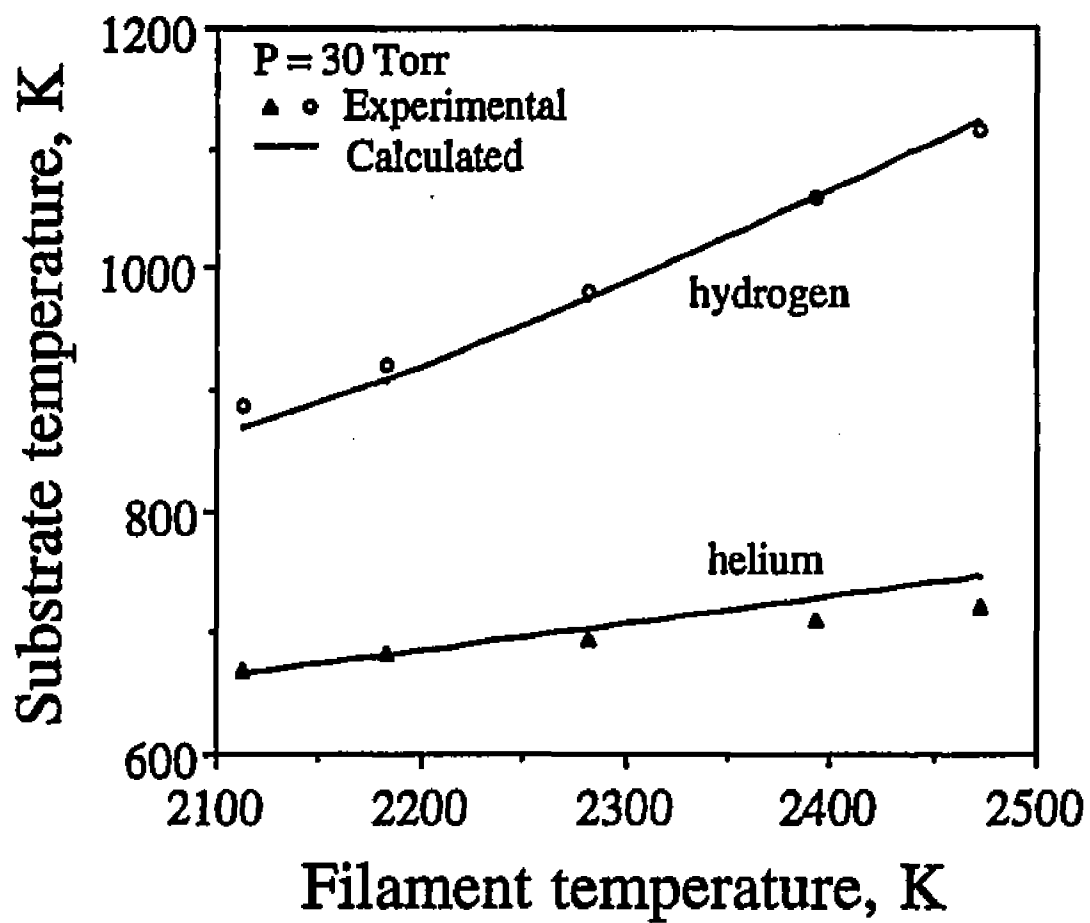
Fig. 4.18 Effect of filament temperature on the substrate temperature for a reactor pressure of 30 Torr and a gas flow rate of 200 sccm.

significantly higher than that in helium. The results indicate that the exothermic recombination of atomic hydrogen to form molecular hydrogen, equation 4.2, is a significant factor in substrate heating. It is also observed from Fig. 4.18 that the substrate heating due to atomic hydrogen recombination is enhanced at higher filament temperatures. The results are consistent with enhanced generation of atomic hydrogen at the filament as shown in Fig. 4.12. It is observed from the figure that the model predictions, solid line, of the effect of filament temperature on the substrate temperature in helium are in good agreement with experimental results. Preliminary calculations using equilibrium concentration of atomic hydrogen at the filament yielded a much higher increase in the difference between substrate temperatures in helium and hydrogen with filament temperature than that observed experimentally. Thus, prescribing equilibrium concentration of atomic hydrogen at the filament over-estimated the effect of atomic hydrogen recombination at higher filament temperatures. Since the atomic hydrogen concentration at the filament does not increase in the same proportion as the equilibrium concentration, as discussed from Fig. 4.14, the atomic hydrogen concentration at the filament at various filament temperatures was derived from equation 4.16 using experimental data of the heat lost due to dissociation of hydrogen. A reference condition of 30 Torr pressure and 2113 K filament temperature was used in equation 4.16. The atomic hydrogen concentration for this reference condition was assumed to be the equilibrium concentration. Fig 4.18 shows that when the experimentally derived atomic hydrogen concentrations, instead of equilibrium concentrations, were used in the model, good agreement was obtained between model predictions and experimental data.

Fig. 4.19 shows the effect of reactor pressure on the substrate temperature at two filament temperatures. It is observed from the figure that the substrate temperature increases with
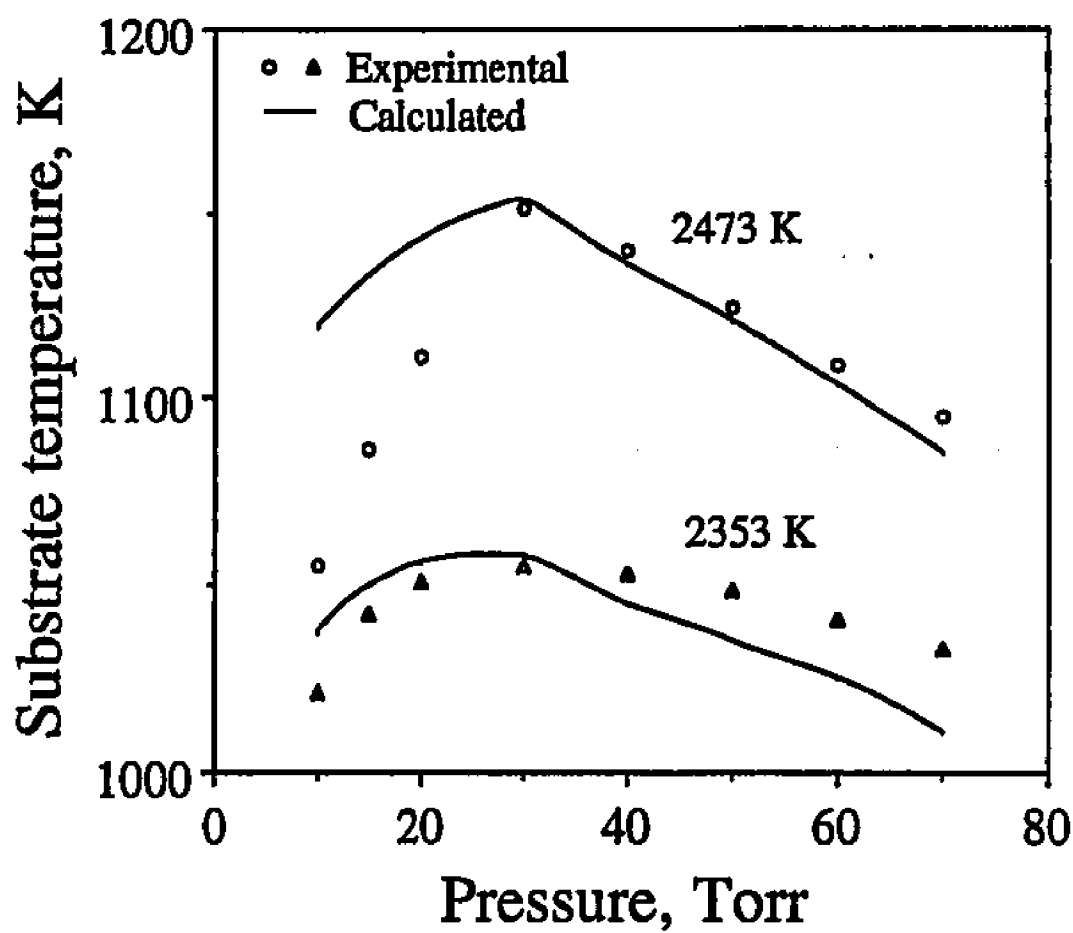
Fig. 4.19 Effect of reactor pressure on the substrate temperature for filament temperatures of 2353 K and 2473 K, and a gas flow rate of 200 sccm.

pressure initially and then decreases with further increase in pressure. It is also seen that the effect of changing pressure on the substrate temperature is more pronounced at higher filament temperatures. The observed variation in substrate temperature with pressure can be explained on the basis of changes in the concentration of atomic hydrogen at the filament and the diffusion coefficient of atomic hydrogen in molecular hydrogen. The flux of atomic hydrogen at the substrate surface, J_H in moles/cm^2, is given by

$$J_H = -D \frac{dC_H}{dx} \qquad . \qquad 4.17$$

where D is the diffusion coefficient of H in H_2 and C_H is the atomic hydrogen concentration. The concentration of atomic hydrogen at the filament increases with pressure, as can be observed from Fig. 4.16, but the diffusion coefficient decreases linearly with pressure. A combination of these two opposing effects results in an initial increase followed by a decrease in the atomic hydrogen flux at the substrate, and hence the substrate temperature, with increasing pressure. The proportion in which the atomic hydrogen concentration at the filament increases with pressure was derived from equation 4.16 and used in the model. The model predictions, shown by the solid lines in Fig. 4.19, show that although the model is unable to predict the exact substrate temperatures, it is capable of predicting the trend in the variation of substrate temperature with pressure.

4.3.3 Effect of Reactor Geometry

The above results indicate that the model predictions of the substrate temperature are reliable. The model can therefore be used to examine the influence of reactor geometry,

such as filament to substrate distance and spacing between filaments, and other parameters such as filament and substrate emissivities on the substrate surface temperature distribution.

Fig. 4.20 shows the effect of spacing between filaments on the substrate surface temperature distribution. The results indicate that the spacing between the filaments is an important factor in determining the temperature distribution. Jansen et al. [14] conducted experiments to examine the effect of filament spacing on the uniformity of the films. They observed that the thickness uniformity of the diamond films was sensitive to the separation between the filaments. The filament spacing can significantly influence the spatial distribution of the nutrient species at the substrate surface, and hence, the local growth rates. The results presented in Fig. 4.20 indicate that the changes in the surface temperature distribution can also play an important role in determining film uniformity.

Previous investigations [15] indicated that the growth rate of diamond films can be significantly improved by decreasing the filament to substrate distance. However, the enhanced growth rates were often accompanied by film non-uniformity and even graphitic deposits [16]. The effect of filament to substrate distance on the substrate temperature is presented in Fig. 4.21. The results indicate that the substrate temperature can be controlled by adjusting the filament to substrate distance. The thickness non-uniformity and graphitic deposits obtained at small filament to substrate distances can largely be attributed to excessive heating of the substrate by both atomic hydrogen recombination and conventional heat transfer mechanisms, particularly radiation from the filament.

Several types of refractory metal filaments [15], viz. Ta, W and Re, and carbon filaments [2], have been used to deposit diamond films over a variety of substrates. The effects of
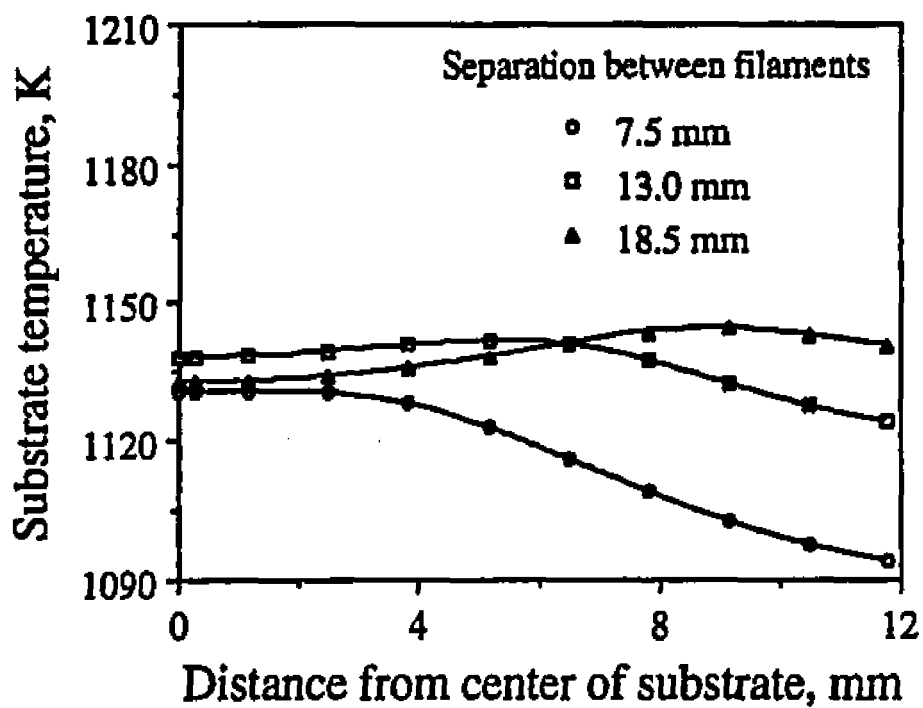
Fig. 4.20 Computed substrate temperature distributions for different filament spacings at a filament temperature of 2500 K, reactor pressure of 30 Torr and filament to substrate distance of 10 mm.
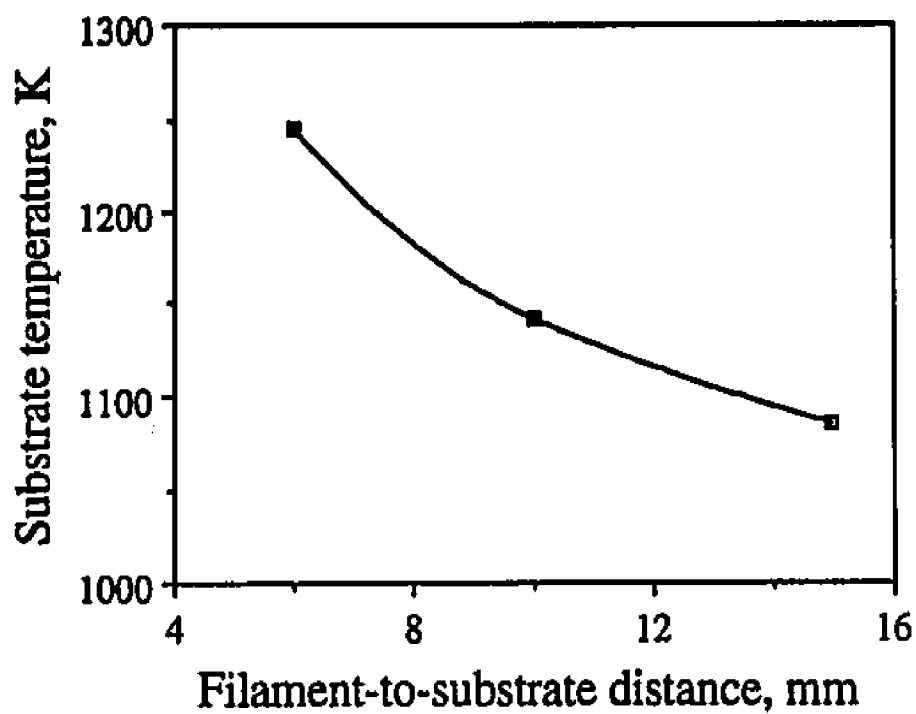
Fig. 4.21 Computed substrate temperatures for different filament to substrate distances at 2500 K filament temperature, 30 Torr pressure and 13 mm separation between the filaments.

filament and substrate emissivities on the substrate temperature distribution were examined. Fig. 4.22(a) shows that changes in substrate emissivity during nucleation and initial stages of diamond film growth may alter the substrate temperature. Furthermore, appropriate changes in process conditions may be required for coating substrates with different emissivities. The filament emissivity is also an important in determining the temperature of the substrate, as can be seen from Fig. 4.22(b). The use of different filament materials can result in significantly different substrate temperatures. Furthermore, changes in filament emissivity due to carburization of the filament during initial stages of the deposition can result in substantial changes in substrate temperature.

4.4 Stability of Diamond and Graphite Surfaces

Fig. 1.2 shows that the diamond growth using chemical vapor deposition techniques takes place under conditions where graphite is the stable phase. The phase diagram shown in Fig. 1.2 is obtained for a single component system, viz. carbon, using free energies of formation of bulk diamond and graphite. In chemical vapor deposition, diamond growth occurs at the gas-solid interface in the carbon-hydrogen system. The vapor growth process does not involve just elemental carbon, the one component in the phase diagram presented in Fig. 1.2, but also involves hydrogen. Furthermore, the composition and structure of the diamond surface is significantly different from that of the bulk. Thus, the stability of diamond and graphite surfaces, rather than the bulk forms, should be examined to understand diamond growth by CVD processes.

In Fig. 2.3, the stacking of diamond (111) and graphite (0001) planes has been shown with hydrogen atoms satisfying the dangling sp^3 bonds of the carbon atoms at the diamond
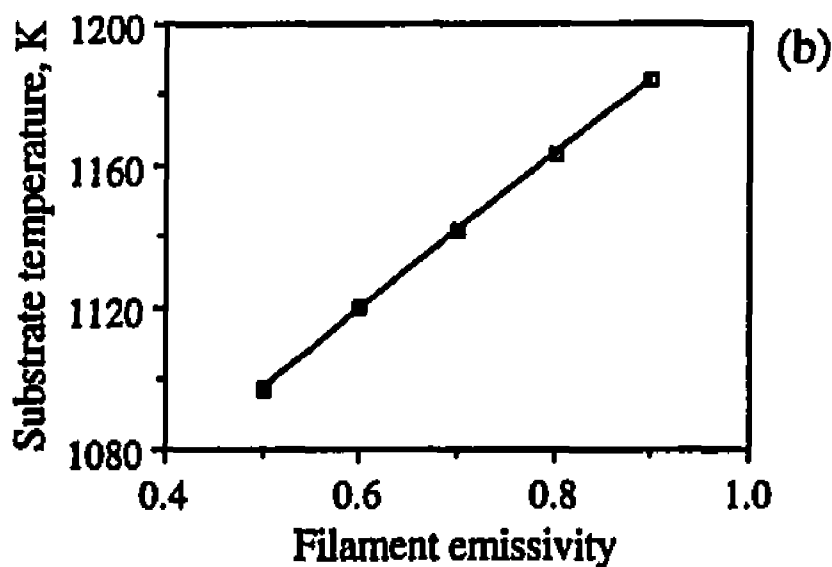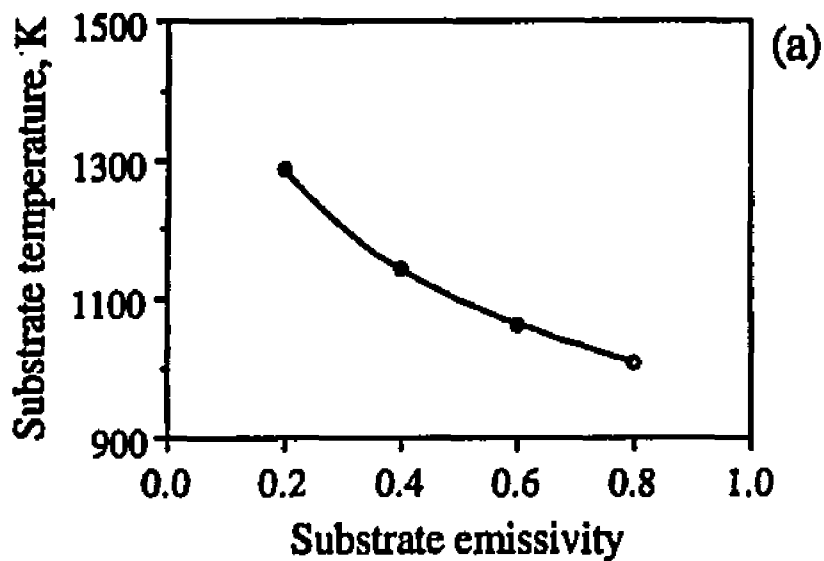
Fig. 4.22 Effect of (a) substrate emissivity, and (b) filament emissivity on the substrate temperature for a filament temperature of 2500 K, reactor pressure of 30 Torr, and a filament to substrate distance of 10 mm.

(111) surface. In the absence of the hydrogen atoms maintaining the sp^3 character of the surface carbon atoms, it is easy to imagine the diamond (111) plane collapsing into the more stable planar graphite like structure. Thus, the role of atomic hydrogen in influencing the relative stability of diamond and graphite can be studied using diamond (111) and graphite (0001) as an example.

The role of atomic hydrogen in influencing the relative stability of diamond (111) and graphite (0001) can be examined from the following reaction

$$C \text{ [graphite (0001)]} + H = CH \text{ [diamond (111)]} \qquad 4.18$$

From the enthalpies and entropies of formation of diamond (111) and graphite (0001), estimated using bond energy contributions, and the free energy of formation data for atomic hydrogen tabulated in JANAF tables [17] the free energy change for reaction 4.18 is calculated to be

$$\Delta G_R^0 = -54505 + 27.5\, T\, \text{cal/mole} \qquad 4.19$$

Similarly, using enthalpies and entropies of formation data, estimated from group additivity principles using the procedure suggested by Yarbrough [18], the free energy change for the reaction analogous to equation 4.18 is

$$\Delta G_R^0 = -53500 + 29.0\, T\, \text{cal/mole} \qquad 4.20$$

It is observed from equations 4.19 and 4.20 that the data calculated from bond energy contributions are in fairly good agreement with the data obtained using group additivity principles.

Fig. 4.23 shows the activity of atomic hydrogen in equilibrium with graphite (0001) and diamond (111) at various substrate temperatures, calculated from equation 4.18 and the data in 4.19 and 4.20. It is seen from equation 4.18 that when the activity of atomic hydrogen is higher than the equilibrium value, diamond (111) planes are stable, while graphite (0001) planes are stable at lower activities. Based on this information, the regions of stability of diamond (111) and graphite (0001) are marked on Fig. 4.23. It is observed from Fig. 4.23 that there is good agreement between the diamond and graphite stability regions predicted from bond energy data and group additivity data.

The activity of atomic hydrogen in equilibrium with molecular hydrogen in a closed system at various temperatures is also plotted in Fig. 4.23. It is observed from the data in the figure that super-equilibrium concentrations of atomic hydrogen are required at the substrate surface to stabilize diamond relative to graphite. Thus, the chemical vapor deposition of diamond requires gas phase activation, by a hot filament or a plasma, to generate significant concentrations of atomic hydrogen. By placing the substrate close to the atomic hydrogen source substantial amounts of atomic hydrogen can be transported to the substrate and a super-equilibrium concentration can be maintained near the growth surface to stabilize diamond growth. Fig. 4.23 also shows that the activity of atomic hydrogen required to stabilize diamond decreases with decreasing substrate temperature. Yarbrough et al. [19] showed that when diamond was deposited on substrates placed remote from a microwave plasma, where the concentration of atomic hydrogen reaching the
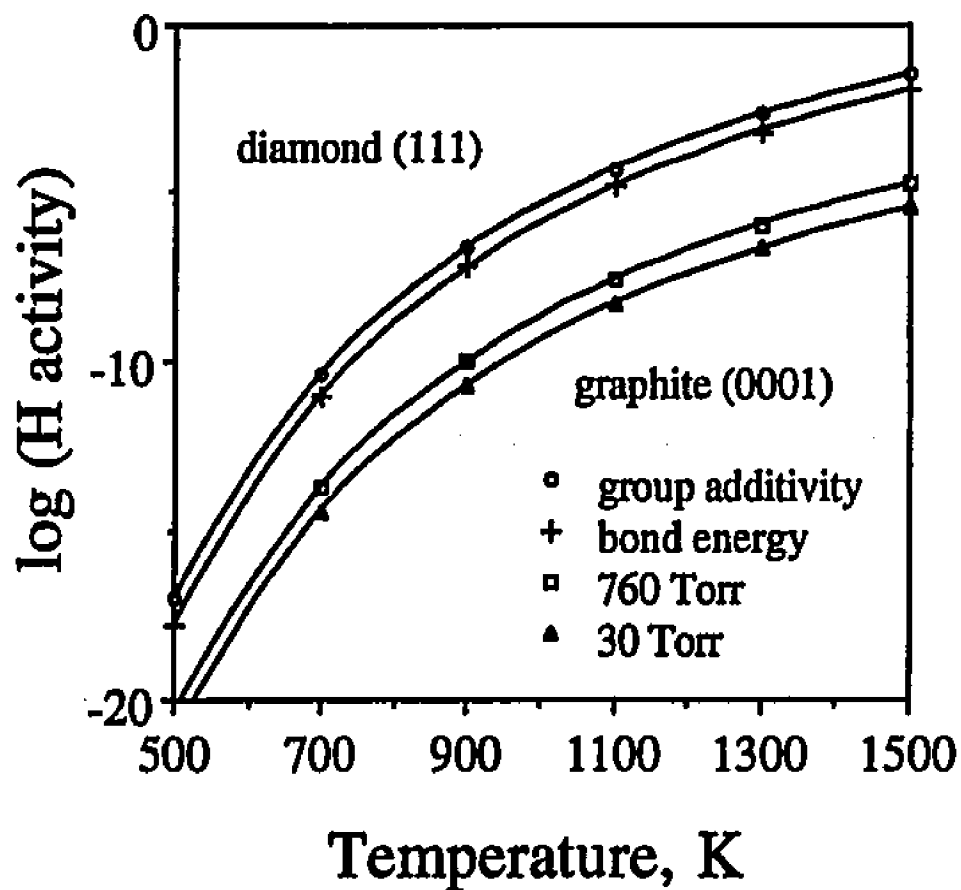
Fig. 4.23 Atomic hydrogen activity, in equilibrium with hydrogenated diamond (111) and graphite (0001) surfaces, at various temperatures. Curves are plotted for surface free energies estimated using principles of group additivity (o) and bond energy contributions (+). Activity of atomic hydrogen in equilibrium with molecular hydrogen in a closed system at 30 Torr (Δ) and 760 Torr (□).

substrate is low, reducing the substrate temperature resulted in deposits with substantially less graphitic components. Thus, the prediction is consistent with low temperature deposition of diamond [19].

In order to examine if the atomic hydrogen concentration near the substrate is sufficient to stabilize the diamond (111) surface relative to graphite (0001) surface, the heat transfer and fluid flow phenomena in a tubular hot filament reactor for diamond deposition were modeled to obtain the velocity, temperature and atomic hydrogen concentration fields in the reactor. The spatial distribution of velocities, temperature and atomic hydrogen concentration calculated for typical hot filament diamond deposition conditions of 2500 K filament temperature, 30 Torr pressure, 200 sccm gas flow rate and a filament to substrate distance of 10 mm are presented in Fig. 4.24. The calculations were done using spatial variation of thermophysical properties. It has been demonstrated earlier that the homogeneous recombination of atomic hydrogen in the gas phase does not significantly alter the atomic hydrogen concentration profile in the reactor. Therefore, the spatial distribution of atomic hydrogen in the reactor was calculated considering only convective and diffusive mixing of atomic hydrogen with molecular hydrogen.

The activity of atomic hydrogen near the substrate, obtained from the computed concentration field, for different substrate temperatures is presented along with the activity of atomic hydrogen in equilibrium with diamond (111) and graphite (0001) in Fig. 4.25. It is observed from the figure that under typical hot filament diamond deposition conditions the atomic hydrogen concentrations at the substrate are sufficient to stabilize diamond (111) surface relative to graphite (0001) up to a temperature of about 1300 K. At temperatures above 1300 K the activity of atomic hydrogen at the substrate is not sufficient to stabilize
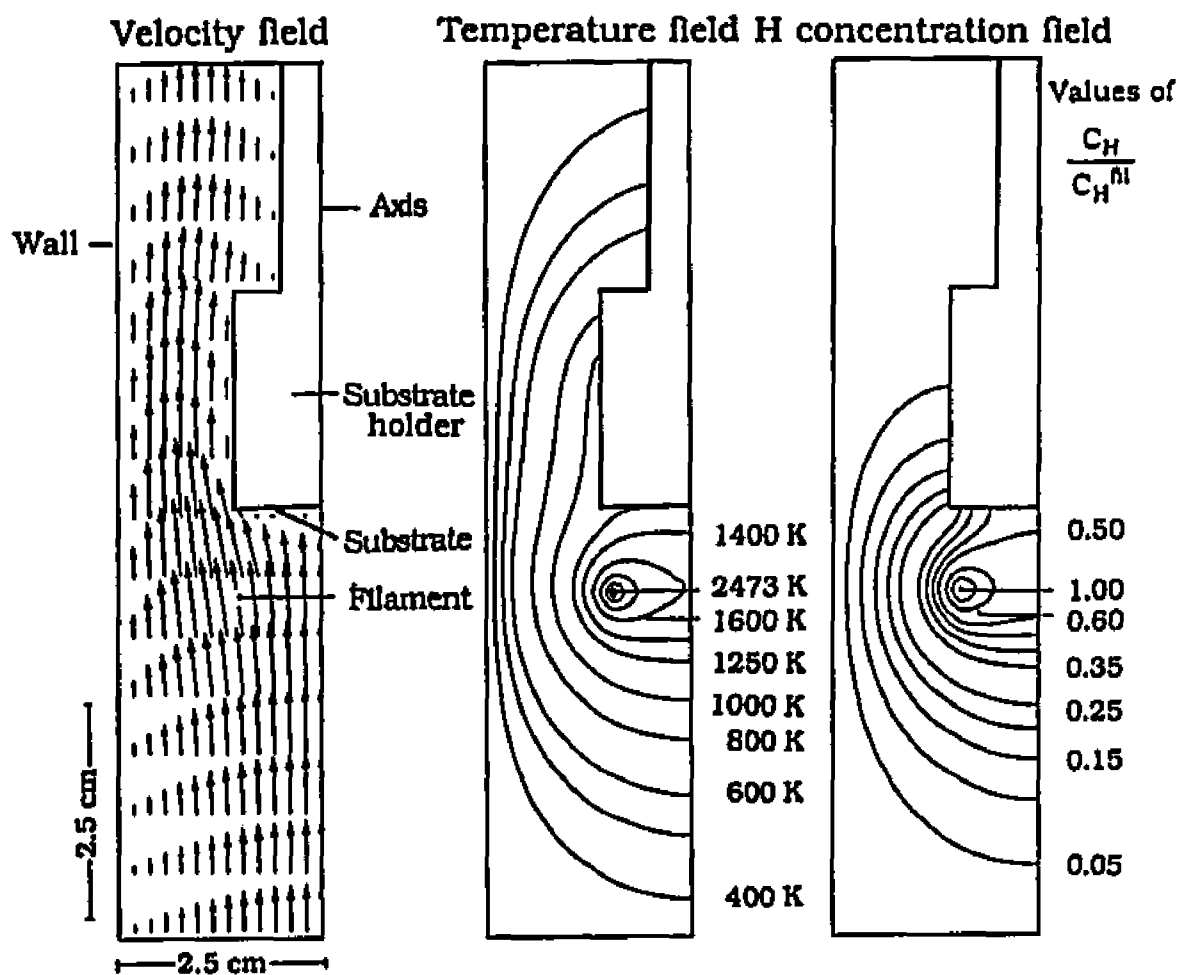
Fig. 4.24 Computed velocity, temperature and atomic hydrogen concentration fields in a tubular hot filament reactor for a filament temperature of 2473 K, reactor pressure of 30 Torr, gas flow rate of 200 sccm and a filament to substrate distance of 10 mm.

diamond (111) planes and graphite (0001) planes are expected to be stable. The results are consistent with the common observation that in hot filament reactors where substrate temperatures are maintained in excess of about 1100 °C the deposits are primarily graphitic in nature.

Fig. 4.25 predicts that at any given atomic hydrogen activity there exists a upper limit to the temperature at which diamond can be deposited. However, it is seen that the curve representing the activity of atomic hydrogen in equilibrium with diamond (111) and graphite (0001) flattens out at higher substrate temperatures indicating that the high temperature limit for diamond growth can be substantially increased by a small increase in the partial pressure of atomic hydrogen reaching the substrate surface. Recently diamond films were reported to have been deposited at temperatures about 1400 to 1500 °C in microwave reactors at high powers [20]. The use of high microwave powers may have resulted in a higher activity of atomic hydrogen in the plasma, and consequently a higher temperature limit for diamond growth. Thus, the predictions are consistent with the high temperature deposition of diamond films.

The results on the influence of atomic hydrogen on the relative stability of diamond and graphite surfaces indicate that the deposition of diamond at low pressures and relatively low temperatures occurs not necessarily due to any kinetic competition between diamond and graphite but because the diamond surface is more stable than the graphite surface in the presence of sufficient quantities of atomic hydrogen. An important implication of the result is that there is no fundamental limitation to the quality of the diamond films that can be deposited by chemical vapor deposition for optical and electronic applications.
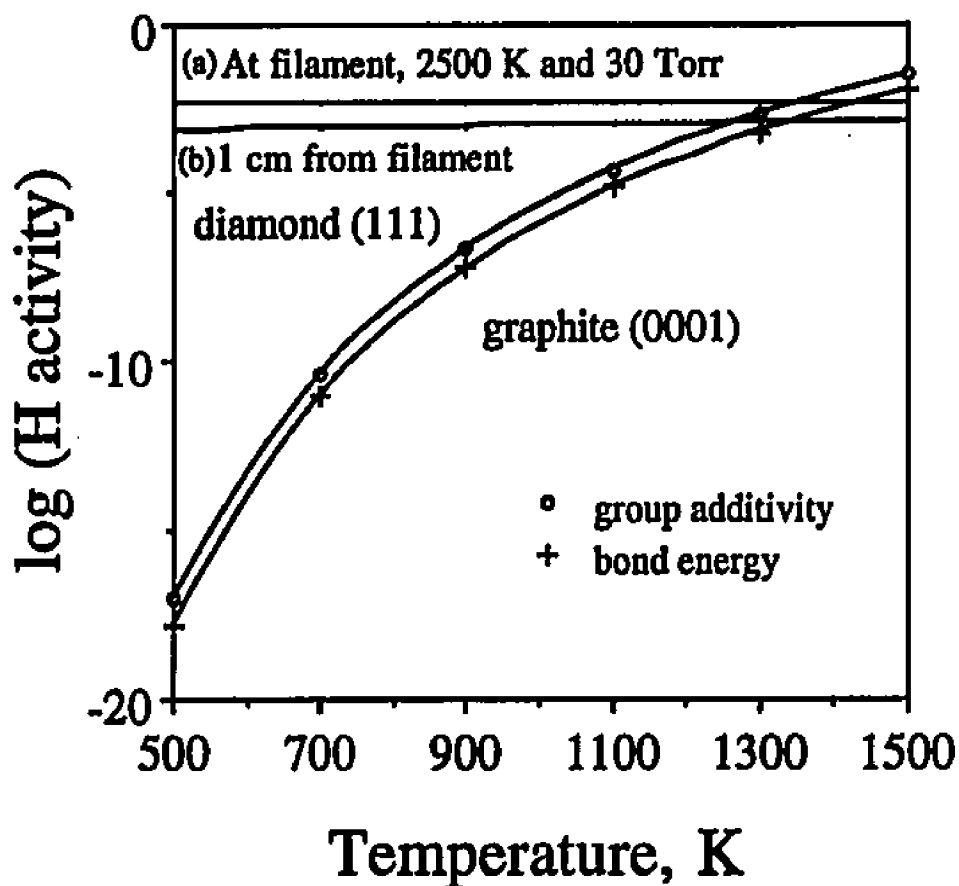
Fig. 4.25 Atomic hydrogen activity, in equilibrium with hydrogenated diamond (111) and graphite (0001) surfaces, at various temperatures calculated using surface free energies estimated from principles of group additivity (o) and bond energy contributions (+). Curve (a) represents equilibrium atomic hydrogen activity for a temperature of 2500 K and a pressure of 30 Torr. Curve (b) represents atomic hydrogen activities at the substrate placed 1 cm from the filament, calculated from principles of heat transfer and fluid flow, for a filament temperature of 2500 K, reactor pressure of 30 Torr and gas flow rate of 200 sccm.

4.5 References

1. G. H. Geiger and D. R. Poirier, Transport Phenomena in Metallurgy (Addison-Wesley, MA, 1973).

2. M. Mecray, M.S. Thesis, The Pennsylvania State University, 1991.

3. F. Jansen, I. Chen, and M. A. Machonkin, J. Appl. Phys. 66, 5749 (1989).

4. M. Sommer and F. W. Smith, J. Mater. Res. 5, 2433 (1990).

5. D. G. Goodwin and G. G. Gavillet, J. Appl. Phys. 68, 6393 (1990).

6. P. W. Atkins, Physical Chemistry (Oxford University Press, Oxford, 1987).

7. F. G. Celli and J. E. Butler, Appl. Phys. Lett. 54, 1031 (1989).

8. U. Meier, K. Kohse-Hoinghaus, L. Schafer, and C. -P. Klages, Appl. Optics 29, 4993 (1990).

9. T. DebRoy, K. Tankala, W. A. Yarbrough, and R. Messier, J. Appl. Phys., 68(5), 2424 (1990).

10. T. DebRoy, K. Tankala, W. A. Yarbrough, and H. Li, in New Diamond Science and Technology, eds. R. Messier, J. T. Glass, J. E. Butler, and R. Roy, p. 359 (MRS Publications, Pittsburgh, PA, 1991).

11. I. Langmuir, J. Am. Chem. Soc., 34, 860 (1912).

12. I. Langmuir and G. M. J. Mackay, J. Am. Chem. Soc., 36, 1708 (1914).

13. I. Langmuir, J. Am. Chem. Soc., 36, 417 (1914).

14. F. Jansen, M. A. Machonkin, and D. E. Kuhman, J. Vac. Sci. Technol., A8(5), 3785 (1990).

15. S. Matsumoto, Y. Sato, M. Tsutsumi, and N. Setaka, J. Mater. Res., 17, 3106 (1982).

16. K. Suzuki, A. Sawabe, H. Yasuda, and T. Inuzuka, Appl. Phys. Lett., 50, 728 (1987).

17. JANAF Thermochemical Tables, Vol. 14, 3rd ed., American Institute of Physics, New York, 1985.

18. W. A. Yarbrough, MRS Symp. Proc., 162, 75 (1990).

19. W. A. Yarbrough, A. R. Badzian, D. Pickrell, Y. Liou, and A. Inspektor, J. Cryst. Growth, **99**, 1177 (1990).

20. Y. Tseng, paper presented at Tri-service Diamond Dome and Window Research and Development Program Review, Naval Surface Warfare Center, Silver Springs, MD, Sept. 22-23, 1993.

Chapter 5

SUMMARY AND CONCLUSIONS

The role of atomic hydrogen in heat transfer during hot filament assisted chemical vapor deposition of diamond was investigated experimentally and theoretically. Temperatures and atomic hydrogen concentration profiles in a hot filament reactor were determined using a specially designed hydrogen atom probe. The temperatures recorded in helium were significantly less than those in pure hydrogen and 1% methane-hydrogen atmospheres, indicating that the hetrogeneous recombination of hydrogen atoms at the substrate surface results in significant substrate heating. Thus, the endothermic generation of hydrogen atoms at the filament and its subsequent transport to the substrate surface, where it recombines exothermically to form molecular hydrogen, serves as an important mechanism of heat transport in hot filament reactors.

Since the hetrogeneous recombination of atomic hydrogen is important in substrate heating, the spatial distribution of atomic hydrogen in the reactor is important for determining the substrate temperature distribution. The factors influencing the spatial distribution of atomic hydrogen in the reactor were examined by comparing experimentally determined atomic hydrogen concentration profile with the theoretically computed profile ignoring homogeneous chemical reactions. A good agreement between the experimental and computed profiles indicated that homogeneous chemical reactions of atomic hydrogen do not significantly alter its concentration profile in the reactor and diffusive mixing of atomic hydrogen with molecular hydrogen and other gaseous species is the primary factor in determining the spatial distribution of atomic hydrogen. The observed lower substrate

temperatures in 1% methane-hydrogen atmosphere compared to pure hydrogen atmosphere is attributed to a lower atomic hydrogen generation rate at the filament in the presence of small amounts of methane. The homogeneous gas phase reactions of atomic hydrogen with hydrocarbon species do not significantly alter the local concentration of atomic hydrogen in the reactor.

A mathematical model was developed to calculate heat transfer, fluid flow and the substrate surface temperatures. The model accounts for substrate heating due to atomic hydrogen recombination at the substrate surface, in addition to conduction, convection and radiation from the filament. The calculated velocity and temperature fields in a typical hot filament reactor were used to examine the mechanism of heat and mass transfer in the gas phase. The results indicate that diffusion, not convection, is the primary mechnism of species transport in the reactor. Furthermore, conduction is the most important factor in establishing the temperature profiles in the gas phase. Convective heat transfer does not play an important role under typical hot filament deposition conditions.

Experiments were conducted to examine the effect of process parameters on the atomic hydrogen generation rates and the substrate temperatures. The generation of atomic hydrogen at a tungsten filament was higher than at a tantalum filament, indicating that the generation of atomic hydrogen is surface reaction controlled. The activation energy for generation of atomic hydrogen at tungsten and tantalum filaments was found to be 47 kcal/mole and 33 kcal/mole, respectively. Comparison of the proportion in which the equilibrium concentration and the experimentally observed concentration of atomic hydrogen at the filament change with filament temperature and pressure indicate that, under

typical hot filament conditions, the dissociation of molecular hydrogen into atomic hydrogen does not attain equilibrium at the filament.

Substrate temperature measurements under various conditions of gas flow rate, filament temperature and reactor pressure indicate that filament temperature and pressure are the most important process parameters in determining the substrate temperature. The insignificant influence of gas flow rate on the substrate temperature indicated that convection is not important in determining the substrate temperature. The nature of the gas flow patterns and the location of the gas inlet and outlet manifolds are not important in the design of hot filament reactors to obtain uniform substrate temperatures over large areas.

The model predictions of the effect of gas flow rate, filament temperature and pressure were in fairly good agreement with experimental observations. The model was used to examine the effect of reactor geometry on the substrate temperature distribution. The results indicate that the spacing between the filaments, and the filament-to-substrate distance are important parameters in determining the substrate temperature distribution. Thus, filament temperature, pressure and reactor geometry are important in the design of hot filament reactors to obtain uniform substrate temperatures, and hence films of uniform quality and thickness, over large areas.

The enthalpies and entropies of formation of various principal surfaces of diamond and graphite were estimated using principles of group additivity and bond energy contributions. The influence of atomic hydrogen on the relative stability of diamond (111) surface and graphite (0001) surface was examined. The results indicate that a super-equilibrium concentration of atomic hydrogen is required to stabilize diamond (111) surface relative to

graphite (0001) surface. Atomic hydrogen activity at the substrate, computed from principles of heat transfer and fluid flow, indicates that diamond (111) surface is the expected stable surface under typical hot filament diamond deposition conditions. The predicted stability of the diamond surface is consistent with experimentally observed trends in low pressure synthesis of diamond.

Appendix A

ADAPTATION ROUTINE FOR THE CALCULATION OF HEAT

TRANSFER AND FLUID FLOW IN THE TUBULAR REACTOR

The following adaptation routine was used along with a generally available commercial program, MicroCompact version 1.1, Innovative Research, Inc., MN, for the solution of equations of conservation of momentum, energy and concentration of hydrogen atoms in the tubular hot filament reactor.

```
        subroutine adapt
c-----definitions of terms used in the program---------------------
c       amu:        array for storing viscosity
c       ak:         array for storing thermal conductivity
c       amutav:     viscosity of hydrogen at an average temperature
c       aktav:      thermal conductivity of hydrogen at an average temperature
c       c:          array for storing atomic hydrogen concentrations
c       cmax:       atomic hydrogen concentration at the filament
c       cp:         array for storing specific heat data
c       cstr:       axial concentration at i expressed as a fraction c(i,2)/c(ihot,2)
c       dist:       axial distance from filament
c       flowar:     cross-sectional area of flow
c       flor:       gas flow rate
c       ihot:       index for x-direction location of filament
c       jhot:       index for y-direction location of filament
c       last:       number of iterations to be executed
c       ni:         number of grids in x-direction
c       nj:         number of grids in y-direction
c       pcth:       percent dissociation of hydrogen
c       press:      reactor pressure
c       re:         reynolds number
c       rhotav:     density of hydrogen at an average temperature
c       t:          array for storing temperatures
c       tdiffh:     array for storing diffusion coefficient of H in H2
c       tfil:       filament temperature
```

```
c       tkav:           average temperature defined as (tfil + tkin)/2
c       tkin:           temperature of inlet gas
c       tstr:           axial temperature at i expressed as a fraction t(i,2)/t(ihot,2)
c       uav:            average inlet velocity
c       xfil:           x-direction location of filament
c       xl:             x-direction length of computation domain
c       yfil:           y-direction location of filament
c       yl:             y-direction length of computation domain
c-----end of definition of terms------------------------------------
        parameter(ni=50,nj=25,nfmax=6)
        include '/u/mundra/MICCOM/adpt.f'
come here to specify dimensions of arrays
        dimension t(ni,nj),amu(ni,nj),cp(ni,nj),c(ni,nj),tdiffh(ni,nj)
        equivalence (f(1,1,5),t(1,1))
        equivalence (f(1,1,6),c(1,1))
        entry grid
c prhcon is the print file to examine convergence
        open(unit=7,file='prhcon')
        header='flow in diamond CVD'
c specify value of right boundary grid line, l1, and top boundary grid line
c mode set equal to 2 for calculation in cylindrical coordinates
        call inta3(l1,ni,m1,nj,mode,2)
c specify dimensions of computational domain
        call data3(xl,16.,yl,2.5,r(1),0.)
c specify inlet gas temperature, filament temperature and pressure,flow rate
        call data4(tkin,300.,tfil,2473.,press,30.,flor,3.33)
c specify filament location and percent dissociation of hydrogen
        call data4(xfil,6.,yfil,0.9,pcth,10.57,grea,1.0e10)
c specify coordinates of filament
        call inta2(ihot,20,jhot,9)
c specify relaxation parameters for u and v velocities
        call data2(relax(1),0.7,relax(2),0.7)
c grx1, grx2, gry1 and gry2 are exponents used to generate non-uniform grids
        call data4(grx1,1.5,grx2,.75,gry1,1.,gry2,.75)
come here to generate grids
        xu(2)=0.
        do 1 i=3,ihot
1       xu(i)=xu(2)+xfil*(1.-(float(ihot-i)/float(ihot-2))**grx1)
```

```
        ihotp1=ihot+1
        do 2 i=ihotp1,ni
2       xu(i)=xu(ihot)+(xl-xfil)*(1-(float(ni-i)/float(ni-ihot))**grx2)
        yv(2)=0.
        do 3 j=3,jhot
3       yv(j)=yv(2)+yfil*(1.-(float(jhot-j)/float(jhot-2))**gry1)
        jhotp1=jhot+1
        do 4 j=jhotp1,nj
4       yv(j)=yv(jhot)+(yl-yfil)*(1.-(float(nj-j)/float(nj-jhot))**gry1)
        return
c end grid generation here
c-------------------------------------------------------------------
        entry begin
c plhcon is the plot file for viewing the profiles of different variables
        plotf='plhcon'
c sthconc file is generated to save results of x iterations and start
c calculations with x+1 iterations
        startf='sthconc'
        title(5)='Temperature '
        title(6)='Concentration'
        write(6,*)'How many iterations?'
        read(5,*)last
calculate thermophysical properties for an average temperature
        tkav=0.5*(tkin+tfil)
        rhotav=2.*press/(82.03*tkav*760.)
        amutav=(2.434e-6)*(tkav**0.636)
        aktav=(0.8e-04)+(0.86e-6)*tkav
calculate equilibrium H concentration for 2473 K and 30 Torr
        cmax=(pcth/100.)*(press/(82.03*tfil*760.))
calculate average inlet gas velocity
        flowar=3.1416*(yv(m1)**2)
        uav=flor*760./(flowar*press)
come here to specify inlet velocity profile
        do 5 j=1,m1
        u(2,j)=uav*2.*(1.-(y(j)/yl)**2)
5       continue
c specify initial H concentration, velocity and temperature in reactor
        do 100 i=1,11
```

```
        do 100 j=1,ml
        c(i,j)=0.
100     t(i,j)=tkin
        do 110 j=1,ml-1
        do 110 i=3,l1
        u(i,j)=uav
110     continue
        do 120 nff=1,nfmax
        ksolve(nff)=1
        kplot(nff)=1
120     kprint(nff)=1
c calculate reynolds number, re
        re=rhotav*uav*2.*yl/amutav
        write(6,*)'type 1 to continue calculations'
c if the input is 1 calculations will start with initial values
c as output of last x iterations
        read(5,*)ichange
        if(ichange.ne.1)go to 125
        call tools(start)
125     continue
c write pressure, flow rate, filament temperature, reynolds number
c average velocity, and average thermophysical properties
        do 124 iunit=6,kdisk+6
        write(iunit,82)press,flor,tfil
        write(iunit,85) re,uav
        write(iunit,88)amutav,aktav,rhotav
124     continue
82      format(2x,'press=',f7.1,2x,'flor=',f7.1,2x,'tfil=',f7.1)
85      format(2x,'Re=',1pe11.2,2x,'uav=',1pe11.2)
88      format(2x,'mutav=',1pe11.3,2x,'aktav=',2x,1pe11.3,2x,
      1 'rhotav=',1pe11.2)
        return
c-------------------------------------------------------------
        entry dense
come here to define spatially variable thermophysical properties
        do 200 j=1,ml
        do 200 i=1,l1
        amu(i,j)=(2.434e-6)*(t(i,j)**0.636)
```

```
        cp(i,j)=(3.34+(3.46e-4)*t(i,j))
        tdiffh(i,j)=1346.*((t(i,j)/1672.)**1.5)*(30./press)
        rho(i,j)=2.*press/(82.03*t(i,j)*760.)
200     continue
        return
c------------------------------------------------------------
        entry output
        if(iter.ne.0) go to 300
come here to write output during run
        do 350 iunit=6,kdisk+6
        write(iunit,301)
350     continue
301     format(1x,'iter',4x,'rsmax',5x,'smax',5x,'ssum',
       1 4x,'u(15,9)',3x,'u(25,9)',3x,'t(24,9)',3x,'c(24,9)')
300     continue
        do 351 iunit=6,kdisk+6
        write(iunit,303) iter,rsmax,smax,ssum,u(15,9),u(25,9),
       1 t(24,9),c(24,9)
351     continue
303     format(2x,i3,1p7e10.3)
c stop solving for velocities and temperature after 60 iterations
        if(iter.le.60)go to 305
        do 304 nff=1,5
304     ksolve(nff)=0
305     if(iter.ne.last)return
create print file prhcon and save output in sthconc
        call tools(print)
        call tools(save)
c write input parameters and out put in a file
        open(unit=8,file='conout')
        do 360 iunit=6,kdisk+7
        write(iunit,*)'pressure=',press,' torr',' 	     tfil=',tfil,' K'
        write(iunit,*)' flow rate=',flor,' cc/sec'
        write(iunit,*)'distance',' temperature',' t/tfil',' 	     ch',
       1 ' 	         ch/chfil'
        do 359 i=ihot,ni-2,4
        tstr=t(i,2)/tfil
        dist=x(i)-x(ihot)
```

```
          cstr=c(i,2)/cmax
359    write(iunit,361)dist,t(i,2),tstr,c(i,2),cstr
360    continue
361    format(2x,f7.4,2x,f10.4,2x,f6.4,2x,e11.4,2x,e11.4)
c save atomic hydrogen concentrations as fraction of concentration
c at filament for ploting
          do 358 i=1,ll
          do 358 j=1,ml
          c(i,j)=c(i,j)/cmax
358    continue
create plot file plhcon for examining contours of variables
          call tools(plot)
          return
c---------------------------------------------------------------
          entry outflo
          return
c---------------------------------------------------------------
          entry phi
          if(nf.gt.2) go to 504
          if(nf.ne.1) go to 488
c define source term for natural convection
          do 486 j=jst,ml-1
          do 486 i=ist,ll-1
486    sc(i,j)=-rho(i,j)*981.
488    continue
c define diffusion coefficient for velocity
          do 500 j=2,ml
          do 500 i=2,ll
          gam(i,j)=amu(i,j)
500    continue
504    continue
come here to define diffusion coefficient and source term for temperature
          if(nf.ne.5) go to 603
          do 602 i=1,ll
          do 602 j=1,ml
          gam(i,j)=((0.86e-6)*t(i,j)+(0.8e-4))/cp(i,j)
602    continue
come here to specify filament temperature
```

```
            sc(ihot,jhot)=tfil*grea
            sp(ihot,jhot)=-grea
            do 605 j=1,ml
            t(11,j)=t(11-1,j)
605     continue
603     continue
come here to specify source term and diffusion coefficient for concentration
            if(nf.ne.6) go to 950
            do 902 i=1,11
            do 902 j=1,ml
902     gam(i,j)=rho(i,j)*tdiffh(i,j)
come here to specify H concentration at the filament
            sc(ihot,jhot)=cmax*grea
            sp(ihot,jhot)=-grea
            do 905 j=1,ml
            c(11,j)=c(11-1,j)
905     continue
950     continue
come here to specify the source terms for v-velocity----------------
            if(nf.ne.2) go to 507
            do 505 j=jst,m2
            do 505 i=ist,12
505     sp(i,j)=-amutav/rv(j)**2
            go to 509
507     continue
come here to specify boundary conditions---------------------------
            if (nf .eq. 2) go to 509
c at the axis gradient of u-velocity, temperature and concentration is 0
            do 508 i=2,11
508     kbcj1(i)=2
509     continue
c at the exit u-velocity, temperature and concentration are fully
c developed, and v-velocity is zero
            do 550 j=2,ml
            u(11,j)=u(11-1,j)
            v(11,j)=0.
            t(11,j)=t(11-1,j)
            c(11,j)=c(11-1,j)
```

```
550     continue
        return
c----------------------------------------------------------------
        entry lc
        return
caution: -- do not delete or alter the following statement
        include '/u/mundra/MICCOM/finish.f'
        end
```

Appendix B

ADAPTATION ROUTINE FOR THE CALCULATION OF HEAT

TRANSFER AND FLUID FLOW IN THE BELL JAR REACTOR

The following adaptation routine was used along with a generally available commercial program, MicroCompact version 1.1, Innovative Research, Inc., MN, for the solution of equations of conservation of momentum, energy and concentration of hydrogen atoms in the bell jar type hot filament reactor. The program includes substrate heating due to atomic hydrogen recombination in addition to conduction, convection and radiation to calculate the substrate temperature distribution.

```
         subroutine adapt
c-----definitions of terms used in the program----------------------
c      amu:        array for storing viscosity
c      ak:         array for storing thermal conductivity
c      akeq:       equilibrium constant for formation of H at 2113 K
c      ajh:        array for storing flux of atomic hydrogen at the substrate
c      amutav:     viscosity of hydrogen at an average temperature
c      aktav:      thermal conductivity of hydrogen at an average temperature
c      anet:       heat accumulated in the silicon wafer
c      arad:       radiation heat intercepted by an element
c                  on the substrate surface
c      c:          array for storing atomic hydrogen concentrations
c      cmax:       atomic hydrogen concentration at the filament
c      cp:         array for storing specific heat data
c      cptav:      specific heat of hydrogen at an average temperature
c      dbf:        distance between filaments
c      dens1:      array for storing density data
c      dens5:      array for storing product of density and specific heat
c      diffh:      array for storing diffusion coefficient of H in H2
c      dfs:        filament to substrate distance
c      etawaf:     emissivity of substrate
c      etawir:     emissivity of filament
c      f:          view factor for radiation
```

c	factrt:	factor by which atomic hydrogen concentration increases
c		with filament temperature. Derived from equation 4.16
c	factrp:	factor by which atomic hydrogen concentration increases
c		with pressure. Derived from equation 4.16
c	flowar:	cross-sectional area of flow
c	flor:	gas flow rate
c	hri:	effective heat transfer coefficient for radiation
c	ihot:	index for x-direction location of filament
c	jhot:	index for y-direction location of filament
c	last:	number of iterations to be executed
c	molfr:	mole fraction of atomic hydrogen at the filament
c	nedge:	index for edge of silicon wafer
c	ni:	number of grids in x-direction
c	nj:	number of grids in y-direction
c	nw:	number of filaments
c	ny1:	index for bottom surface of silicon wafer
c	ny2:	index for top surface of silicon wafer
c	ph:	partial pressure of atomic hydrogen in equilibrium with
c		molecular hydrogen at 2113 K and 30 Torr total pressure
c	press:	reactor pressure
c	qcell:	chemical heat gained by an element on the substrate surface
c	qrad:	net radiative heat gained by the wafer
c	qcond:	net conductive heat gained by the wafer
c	radin:	array for storing chemical heat and radiation heat
c	rf:	radius of filament
c	rhotav:	density of hydrogen at an average temperature
c	srina:	radiative heat gained by top surface of wafer
c	srlosa:	radiative heat lost from top surface of wafer
c	srlosb:	radiative heat lost from side of wafer
c	srlosc:	radiative heat lost from bottom surface of wafer
c	srneta:	net radiative heat gained by top surface of wafer
c	suma:	conductive heat gained by top surface of wafer
c	sumb:	conductive heat lost from the side of wafer
c	sumc:	conductive heat lost from the bottom of wafer
c	sumch:	chemical heat gained by the wafer
c	sumta:	net heat gained by top surface of wafer
c	sumtb:	net heat lost from the side of wafer
c	sumtc:	net heat lost from the bottom surface of wafer

```
c     t:           array for storing temperatures
c     tfil:        filament temperature
c     tkav:        average temperature defined as (tfil + tkin)/2
c     tkin:        temperature of inlet gas
c     tstr:        radial substrate surface temperature as fraction of
c                  temperature at the center of wafer
c     vav:         average inlet velocity
c     vmax:        maximum inlet velocity
c     xl:          x-direction length of computation domain
c     yl:          y-direction length of computation domain
c-----end of definition of terms-----------------------------------
      parameter(ni=40,nj=40,nfmax=6,ny2=12,nedge=12)
      include '/u/mundra/MICCOM/adpt.f'
come here to specify dimensions of arrays
      dimension t(ni,nj),amu(ni,nj),cp(ni,nj),c(ni,nj),ak(ni,nj),
     1 diffh(ni,nj),ajh(nedge),radin(nedge),dens1(ni,nj),dens5(ni,nj)
      equivalence (f(1,1,5),t(1,1))
      equivalence (f(1,1,6),c(1,1))
c-----------------------------------------------------------------
      entry grid
c prtsys is the file to examine convergence and results of calculations
      open(unit=7,file='prtsys')
      header='heat transfer and fluid flow in diamond cvd'
c specify value of right boundary grid line, 11, and top boundary grid line
c mode set equal to 1 for calculation in cartesian coordinates
      inta3(11,ni,m1,nj,mode,1)
      call data2(xl,15.,yl,15.)
c ny1,ny2,ny3 and ny4 are indices used for obtaining non-uniform
c grid spacing in the y-direction
      call inta3(ny1,8,ny3,18,ny4,25)
c grx0, grx1, gr1, gr2, gr3 and gr4 are values of exponents
c used for obtaining non-uniform grid spacing
      call data6(grx0,1.,grx1,0.75,gr1,1.5,gr2,1.,gr3,1.,gr4,0.5)
      call data5(press,30.,tfil,2473.,flor,3.33,tkin,300.,grea,1.0e15)
      call data5(rf,0.0125,etawaf,.8,etawir,.27,dfs,.7,dbf,0.6)
      call data4(relax(1),0.7,relax(2),0.7,relax(6),0.9,greac,1.0e28)
      relax(5)=.99
      write(6,*)'filament temperature,pressure,factrt,factrp,flow rate'
```

```
      read(6,*)tfil,press,factrt,factrp,flor
come here to specify coordinates for the filaments
      call inta2(ihot,4,jhot,18)
c the following statements generate grids in x direction---------------
      xu(3)=.05
      xu(4)=0.5*dbf-0.01
      xu(5)=xu(4)+0.02
      do 4 i=6,nedge
4     xu(i)=xu(5)+(1.25-xu(5))*(1.-(float(nedge-i)/
     1 float(nedge-5))**grx0)
      nedgep1=nedge+1
      do 5 i=nedgep1,ni
5     xu(i)=xu(nedge)+(xl-1.25)*(1.-(float(ni-i)/float(ni-nedge))**grx1)
c the following statements generate grids in y direction---------------
      yv(3)=0.05
      do 10 i = 4,ny1
10    yv(i)=yv(3)+7.45*(1.-(float(ny1-i)/float(ny1-3))**gr1)
      ny1p1=ny1+1
      do 20 i=ny1p1,ny2
20    yv(i)=yv(ny1)+0.05*(1.-(float(ny2-i)/float(ny2-ny1))**gr2)
      ny2p1=ny2+1
      do 30 i=ny2p1,ny3
30    yv(i)=yv(ny2)+dfs*(1.-(float(ny3-i)/float(ny3-ny2))**gr3)
      ny3p1=ny3+1
      yv(ny3p1)=yv(ny3)+0.022
      ny3p2=ny3p1+1
      do 35 i=ny3p2,ny4
35    yv(i)=yv(ny3p1)+dfs*(1.-(float(ny4-i)/float(ny4-ny3p1))**gr3)
      ny4p1=ny4+1
      do 40 i=ny4p1,nj
40    yv(i)=yv(ny4)+(yl-7.572-2.*dfs)*
     1 (1.-(float(nj-i)/float(nj-ny4))**gr4)
      return
c---------------------------------------------------------------------
      entry begin
c pltsys is plot file for viewing the profiles of different variables
      plotf='pltsys'
c startf file is generated to save results of x iterations and start
```

calculations from x+1 iterations
```
      startf='hfreactor'
      title(5)='temperature'
      title(6)='concentration'
      write(6,*)'how many iterations?'
      read(5,*)last
      write(6,*)'type 1 to consider chemical heat'
      read(5,*)ichem
      tkav=0.5*(tkin+tfil)
      amutav=(2.434e-6)*(tkav**0.636)
      aktav=(0.8e-04)+(0.86e-6)*tkav
      rhotav=2.*press/(82.03*tkav*760.)
      cptav=(3.34+(3.46e-4)*tkav)
52    continue
```
come here to calculate atomic hydrogen concentration at the filament
```
      akeq=exp((-225878.+59.635*2113.)/(8.314*2113.))
      ph=(-akeq**2.+sqrt(akeq**4.+4.*(30./760.)*akeq**2.))/2.
      molfr=factrt*factrp*ph/(30./760.)
      cmax=1.*press*molfr/(760*82.03*tfil)
      write(6,*)'cmax=',cmax
```
come here to calculate average and maximum inlet gas velocity
```
      flowar=3.1416*(xl**2)
      vav=-flor*760./(flowar*press)
      vmax=-2.*flor*760./(press*3.1416*(xu(ni)**2))
```
come here to define input velocity field
```
      do 101 i=1,11
      u(i,m1)=0.
      v(i,m1)=vmax*(1-(xu(i)/xu(ni))**2.)
101   continue
      do 110 nff=1,nfmax
      ksolve(nff)=1
      kplot(nff)=1
110   kprint(nff)=1
      if(ichem.ne.1)ksolve(6)=0
```
come here to define initial velocity, H concentration, and temperature
```
      do 115 i=1,11
      do 115 j=1,m1
      u(i,j)=0.
```

```
            c(i,j)=0.
115         t(i,j)=tkin
            do 120 j=2,ml-1
            do 120 i=2,ll-1
            v(i,j)=vav
120         continue
come here to specify velocities in the sample----------------------
            do 123 i=1,nedge-1
            do 123 j=ny1,ny2
            v(i,j)=0.
123         continue
            write(6,*)'type 1 to continue calculations'
c if the input is 1 calculations will start with initial values
c as output of last x iterations
            read(5,*)ichange
            if(ichange.ne.1) goto 125
            call tools(start)
125         continue
            do 130 iunit=6,kdisk+6
            write(iunit,82)press,flor,vav
            write(iunit,84)rhotav,amutav,cptav,aktav
130         continue
82          format(2x,'pressure=',f7.1,2x,'flor=',f7.1,2x,'vav=',1pe11.2)
84          format(2x,'rho=',1pe11.2,2x,'mu=',1pe11.2,2x,'cp=',1pe11.2,
            1 2x,'aktav=',2x,1pe11.3)
            return
c------------------------------------------------------------------
            entry dense
come here to specify temperature dependent thermophysical properties
            do 200 i=1,ll
            do 200 j=1,ml
            amu(i,j)=(2.434e-6)*(t(i,j)**0.636)
            ak(i,j)=0.8*(1.84e-4 + 4.85e-7*t(i,j))
            cp(i,j)=1.1*(3.34+(3.46e-4)*t(i,j))
            diffh(i,j)=1346.*((t(i,j)/1672.)**1.5)*(30./press)
            dens1(i,j)= 2.*press/(82.03*t(i,j)*760.)
            dens5(i,j)=dens1(i,j)*cp(i,j)
200         continue
```

```
come here define thermophysical properties for the substrate
      do 201 i=1,nedge-1
      do 201 j=ny1,ny2-1
      dens1(i,j)=2.33
      ak(i,j)=0.0564
      cp(i,j)=0.27
      dens5(i,j)=dens1(i,j)*cp(i,j)
201   continue
      return
c------------------------------------------------------------------
      entry output
c write output on screen and in print file during run
      if(iter.ne.0) go to 300
      do 350 iunit=6,kdisk+6
      write (iunit,301)
350   continue
300   continue
      do 351 iunit=6,kdisk+6
      write(iunit,303) iter,rsmax,smax,ssum,v(7,14),u(7,14),
     1 t(2,11),c(7,12)
351   continue
301   format(1x,'iter',4x,'rsmax',5x,'smax',5x,'ssum'
     1,4x,'v(7,14)',3x,'u(7,14)',3x,'t(2,11)',3x,'c(7,12)')
303   format(2x,i3,1p7e10.3)
      if(ichem.ne.1) goto 355
come here to calculate H flux on the surface of sample
      do 360 i=1,nedge-1
      j=ny2-1
      ajh(i)=-diffh(i,j+1)*((0.-c(i,j+1))/(0.5*ycv(j+1)))
360   continue
347   format(2x,1p8e10.3)
c write on the screen the H flux on substrate after every 50 iterations
      if((iter/50)*50.eq.iter)then
      write(6,*)'H flux for i=2 to nedge-1'
      write(6,347)(ajh(i),i=1,nedge-1)
      endif
355   continue
c stop solving for velocities after 250 iteration
```

```fortran
      if(iter.gt.250) ksolve(1)=0
      if(iter.ne.last)return
      call tools(print)
      call tools(save)
c save concentrations as fraction of concentration at the filament
      do 358 i=1,11
      do 358 j=1,m1
      c(i,j)=c(i,j)/cmax
358   continue
      call tools(plot)
c write conditions and output of calculations in a file
      open(unit=8,file='temp')
      write(8,*)'tfil=',tfil,'   press=',press,'  Cfil=',cmax
      write(8,*)'flowrate=',flor,'  etawaf=',etawaf,'  etawir=',etawir
      write(8,*)
      do 365 iunit=6,kdisk+7
      do 364 i=1,nedge-1
      j=ny2-1
      tstr=t(i,ny2-1)/t(1,ny2-1)
364   write(iunit,370)i,j,ajh(i),t(i,j),tstr
365   continue
370   format(2x,'i=',i2,2x,'j=',i2,2x,'fluxH=',e11.4,2x,
     1 2x,'temp=',2f9.4)
come here to check heat balance for substrate
      do 356 i=1,nedge-1
      fe=0.5*ycv(ny2-1)/ydif(ny2)
      akav=1./((1-fe)/ak(i,ny2)+fe/ak(i,ny2-1))
      suma= suma+akav*xcv(i)*(t(i,ny2)-t(i,ny2-1))/ydif(ny2)
      fe=0.5*ycv(ny1-1)/ydif(ny1)
      akav=1./((1-fe)/ak(i,ny1)+fe/ak(i,ny1-1))
      sumc=sumc+akav*xcv(i)*(t(i,ny1)-t(i,ny1-1))/ydif(ny1)
356   continue
      do 357 j=ny1,ny2-1
      i=nedge
      fe=0.5*xcv(i)/xdif(i)
      akav=1./((1-fe)/ak(i-1,j)+fe/ak(i,j))
      sumb=sumb+akav*ycv(j)*(t(i-1,j)-t(i,j))/xdif(i)
357   continue
```

```
      sumta=srina+sumch-srlosa+suma
      sumtb=srlosb+sumb
      sumtc=srlosc+sumc
      qrad=srina-srlosa-srlosb-srlosc
      qcond=suma-sumb-sumc
      anet=sumta-sumtb-sumtc
      smeta=srina-srlosa
c write heat gained and heat lost terms in a file
      write(8,*)
      write(8,*)'radiative heat gain at top= ',srina
      write(8,*)'radiative heat loss from top= ',srlosa
      write(8,*)'net radiative heat gain at top=',smeta
      write(8,*)'chemical heat at top= ',sumch
      write(8,*)'conductive heat into top surface = ',suma
      write(8,*)'radiative heat loss from side= ',srlosb
      write(8,*)'conductive heat out of side= ',sumb
      write(8,*)'radiative heat loss from bottom= ',srlosc
      write(8,*)'conductive heat out of bottom= ',sumc
      write(8,*)'net heat gained by top surface= ',sumta
      write(8,*)'net heat lost from the side= ',sumtb
      write(8,*)'net heat lost from the bottom= ',sumtc
      write(8,*)'heat accumulated in silicon= ',anet
      write(8,*)'qrad= ',qrad
      write(8,*)'qcond= ',qcond
c end checking of heat balance for substrate
      return
c----------------------------------------------------------------
      entry outflo
c adjust out flow velocities to ensure overall mass conservation
      if(iter.ne.0) goto 705
      flow=0.
      do 711 i=1,ni
711   flow=flow+dens1(i,m1)*v(i,m1)*xcv(i)
705   fl=0.
      vmin=0.
      ars=0.
      do 706 i=1,12
      ar=dens1(i,1)*xcv(i)
```

```
        ars=ar+ars
        fl=fl+ar*v(i,2)
        if(v(i,2).gt.0.) vmin=amin1(vmin,-v(i,2))
706     continue
        factor=flow/(fl+ars*vmin-1.e-35)
        do 707 i=1,l2
707     v(i,2)=(v(i,2)+vmin)*factor
        return
c-------------------------------------------------------------------
        entry phi
c define diffusion coefficient for velocities
        if(nf.gt.2) go to 504
        do 500 j=1,ml
        do 500 i=1,l1
        rho(i,j)=dens1(i,j)
        gam(i,j)=amu(i,j)
500     continue
c define diffusion coeffecient in sample assembly
        do 503 i=1,nedge-1
        do 503 j=ny1,ny2-1
503     gam(i,j)=grea
come here to specify boundary conditions for u velocities------------
        if (nf .ne. 1) go to 611
c  left boundary is a symmetry plane hence u velocity is 0.
        do 612 j=1,ml
        kbcil(j)=1
612     u(2,j)=0.
c right boundary is a rigid wall with no slip hence u velocity is 0.
        do 613 j=1,ml
        kbcll(j)=1
613     u(l1,j)=0.
c top boundary is the input boundary with zero u velocity
        do 614 i=1,l1
        kbcm1(i)=1
614     u(i,m1)=0.
c bottom boundary is an outflo boundary with zero u velocity gradient
        do 615 i=1,l1
615     kbcj1(i)=2
```

```
611    continue
c   come here to specify boundary conditions for v velocities ------------
        if (nf .ne. 2) go to 621
c   left boundary is a symmetry plane hence gradient of v velocity is 0.
        do 622 j=1,ml
622    kbcil(j)=2
c   right boundary is a rigid wall with no slip hence v velocity is 0.
        do 623 j=1,ml
        kbcl1(j)=1
623    v(l1,j)=0.
c   top boundary has a prescribed input v velocity
        do 624 i=1,l1
        kbcm1(i)=1
        v(i,m1)=vmax*(1-(xu(i)/xu(ni))**2.)
624    continue
c   bottom boundary is an outflo boundary and gradient of v velocity is 0.
        do 625 i=1,l1
625    kbcj1(i)=2
621    continue
c   prescribe u and v velocities inside the sample assembly
        do 511 i=1,nedge
        do 511 j=ny1,ny2-1
511    u(i,j)=0.
        do 513 i=1,nedge-1
        do 513 j=ny1,ny2
513    v(i,j)=0.
504    continue
c   define diffusion coefficient and source term for temperature ----------
        if(nf.ne.5) go to 603
        do 602 i=1,l1
        do 602 j=1,ml
        rho(i,j)=dens5(i,j)
602    gam(i,j)=ak(i,j)
c   source term for temperature at the filament
        sc(ihot,jhot)=tfil*grea
        sp(ihot,jhot)=-grea
c   come here to specify source term for surface cells of sample and holder
        call  wafer(t,radin,ny1,ny2,ajh,xcv,ycv,ichem,rlosab,
```

```
      1 etawaf,etawir,iter,tfil,rf,dbf,dfs,last,srina,srlosa,sumch)
        sigma=1.355e-12
        do 690 i=2,nedge-1
        j=ny2-1
        sc(i,j)=radin(i)/(xcv(i)*ycv(j))
        sp(i,j)=0.
690   continue
c come here to specify source terms for vertical face of sample
        srlosb=rlosab
        do 694 j=ny1,ny2-2
        hri=sigma*etawaf*(t(nedge-1,j)**2+300.**2)*(t(nedge-1,j)+300.)
        rlosb=hri*ycv(j)*(t(nedge-1,j)-300.)
        srlosb=srlosb+rlosb
        if(j.eq.ny1)then
        rlosbc=hri*xcv(nedge-1)*(t(nedge-1,j)-300.)
        rlosb=rlosb+rlosbc
        endif
        sc(nedge-1,j)=-rlosb/(xcv(nedge-1)*ycv(j))
694   sp(nedge-1,j)=0.
c come here to specify source terms for bottom surface of sample
        srlosc=rlosbc
        do 695 i=2,nedge-2
        hri=sigma*etawaf*(t(i,ny1)**2+300.**2)*(t(i,ny1)+300.)
        rlosc=hri*xcv(i)*(t(i,ny1)-300.)
        srlosc=srlosc+rlosc
        sc(i,ny1)=-rlosc/(xcv(i)*ycv(ny1))
695   sp(i,ny1)=0.
c come here to specify boundary conditions for temperature --------------
c left boundary is a symmetry plane hence gradient of temperature is 0.
        do 652 j=1,ml
        kbcil(j)=2
652   continue
c right boundary is the reactor wall at room temperature
        do 653 j=1,ml
        kbcll(j)=1
653   t(l1,j)=300.
c top boundary represents input gas and top wall at room temperature
        do 654 i=1,l1
```

```
        kbcml(i)=1
654    t(i,ml)=300.
c bottom boundary has fully developed temperature field hence temperature
c gradient is 0.
        do 656 i=2,11
656    kbcjl(i)=2
603    continue
c define diffusion coefficient and source term for atomic H concentration----
        if(nf.ne.6) go to 950
        do 902 i=1,11
        do 902 j=1,ml
        rho(i,j)=densl(i,j)
        gam(i,j)=rho(i,j)*diffh(i,j)
902    continue
come here to specify H conc at filament
        sc(ihot,jhot)=cmax*grea
        sp(ihot,jhot)=-grea
come here to specify H conc in sample
        do 901 i=1,nedge-1
        sc(i,ny2-1)=c(i,ny2)*greac
        sp(i,ny2-1)=-greac
        do 901 j=ny1,ny2-2
        sc(i,j)=0.
        sp(i,j)=-greac
901    continue
come here to define boundary conditions for atomic hydrogen concentration
c left boundary is a symmetry plane hence gradient of concentration is 0
        do 662 j=1,ml
        kbcil(j)=2
662    continue
c right boundary is the reactor wall hence H concentration is 0.
        do 663 j=1,ml
        kbcll(j)=1
663    c(11,j)=0.
c top boundary is the input boundary hence H concentration is 0.
        do 664 i=1,11
        kbcml(i)=1
664    c(i,ml)=0.
```

```
c bottom boundary has fully developed concentration field hence
c gradient of H concentration is 0.
      do 665 i=1,11
665   kbcj1(i)=2
950   continue
      return
c--------------------------------------------------------------
      entry lc
      return
caution: -- do not delete or alter the following statement
      include '/u/mundra/MICCOM/finish.f'
      end
c--------------------------------------------------------------
c the subroutine wafer calculates chemical heat and radiation heat
c gained by the substrate surface
      subroutine wafer(t,radin,ny1,ny2,ajh,xcv,ycv,ichem,rlosab,
     1 etawaf,etawir,iter,tfil,rf,dbf,dfs,last,srina,srlosa,sumch)
      parameter(ni=40,nj=40,nedge=12,nw=2)
come here to define dimensions of arrays used in the subroutine wafer
      dimension radin(nedge),t(ni,nj),arad(nedge,nw),dist(nw),
     1 ajh(nedge),xcv(ni),ycv(nj)
come here to calculate radiation view factor
      do 2 l=1,nw
2     dist(l)=-0.5*dbf+float(l-1)*dbf
3     sigma=1.355e-12
      do 100 j=1,nw
      sumdx=0.
      do 100 i=2,nedge-1
      sumdx=sumdx+xcv(i-1)
      a=sumdx+dist(j)
      b=a+xcv(i)
      x=dfs/rf
      y=a/rf
      z=b/rf
      f12=(atan(z/x)-atan(y/x))/(z-y)
      f=f12*xcv(i)/(3.14*rf*2.)
c end calculation of view factor
come here to calculate radiation heat intercepted by the substrate
```

```
       arad(i,j)=etawir*sigma*(tfil**4)*3.14*rf*2.*f
100    continue
       srina=0.
       srlosa=0.
       sumch=0.
       sum=0.
       do 106 i=2,nedge-1
       k=ny2-1
       radin(i)=0.
       do 102 j=1,nw
102    radin(i)=radin(i)+arad(i,j)
       srina=srina+radin(i)
come here to calculate chemical heat to the substrate
       if(ichem.ne.1)goto 104
       qcell=ajh(i)*52340.*xcv(i)
       radin(i)=radin(i)+qcell
       sumch=sumch+qcell
104    continue
calculate radiation heat loss and net heat gained by top surface of sample
       hri=sigma*etawaf*(t(i,k)**2+300.**2)*(t(i,k)+300.)
       rlosa=hri*xcv(i)*(t(i,k)-300.)
       srlosa=srlosa+rlosa
       if(i.eq.nedge-1)then
       rlosab=hri*ycv(k)*(t(i,k)-300.)
       rlosa=rlosa+rlosab
       endif
       radin(i)=radin(i)-rlosa
       sum=sum+radin(i)
106    continue
19     format(2x,6e12.3)
       if((iter/50)*50.eq.iter)write(6,20) sum
20     format(2x,'Net heat intercepted in cal/sec per cm of wire',f7.3)
c   This is the end of statements--------------------------------
       return
       end
```

Appendix C

ESTIMATION OF ENTHALPIES AND ENTROPIES OF FORMATION OF DIAMOND AND GRAPHITE SURFACES

The procedure for the estimation of enthalpies and entropies of formation of diamond and graphite surfaces using Laidler parameters for bond energy contributions has been discussed in chapter 3. The enthalpies and entropies of formation of diamond (111) and graphite (0001) surfaces were calculated to illustrate the procedure. The calculation of enthalpies and entropies of formation of other principal surfaces of diamond and graphite is presented here.

C.1 Hydrogenated Diamond (110) Surface

Fig. C.1(a) shows a plan view of the hydrogenated diamond (110) surface. The large open circles represent surface carbon atoms and the hashed circles represents carbon atoms below the surface. The small open circles represent hydrogen atoms bonded to the surface carbon atoms. Fig. C.1(b) shows the bonding configuration of the carbon atom on the diamond (110) surface. A carbon atom at the surface of a hydrogenated diamond (110) surface makes three bonds with carbon atoms in the diamond lattice and one bond with a hydrogen atom. Since each C-C bond is shared by two carbon atoms, the energy associated with the surface C atom is 3/2 E(C-C). Thus, the heat of dissociation of a mole of hydrogenated surface carbon atoms on diamond (110) to gaseous carbon and hydrogen atoms, henceforth referred to as heat of atomization, is given by

(a)

H Atom

Surface
C Atom

C Atom Below
Surface

(b)

H
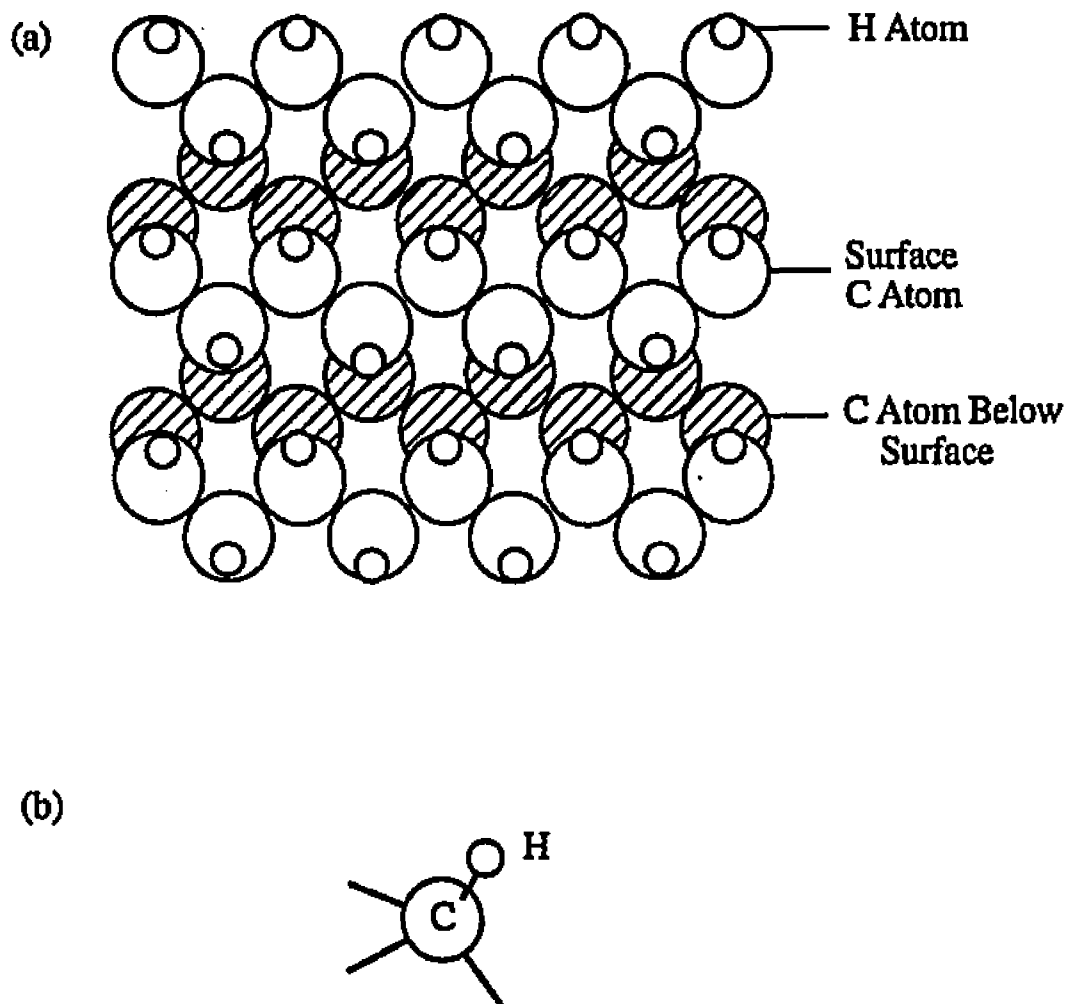
Fig. C.1 Schematic diagram of (a) hydrogenated diamond (110) surface and (b) bonding configuration of carbon atom on the surface.

$$\Delta H_a \text{ [diamond (110)]} = \frac{3}{2}E(C\text{-}C) + E(C\text{-}H)_t \qquad\qquad A.1$$

where $E(C\text{-}C)$ is the carbon-carbon bond energy in diamond and $E(C\text{-}H)_t$ is the bond energy for a hydrogen atom bonded to a tertiary carbon atom. Using values of Laidler parameters for bond energies [1] presented in Table 3.6, the heat of atomization of surface carbon atoms on diamond (110) is calculated to be 224.75 kcal/mole. i.e.,

$$\Delta H_a \text{ [diamond (110)]} = \frac{3}{2} \cdot 85.48 + 96.53 = 224.75 \text{ kcal/mole} \qquad A.2$$

$$CH \text{ [diamond (110)]} = C(g) + H(g) \qquad \Delta H_a = 224.75 \text{ kcal/mole} \qquad A.3$$

Furthermore, from the data in JANAF tables [2] we have

$$C(\text{graphite}) = C(g) \qquad\qquad \Delta H_a = 171.29 \text{ kcal/mole} \qquad A.4$$

$$\frac{1}{2}H_2(g) = H(g) \qquad\qquad \Delta H_a = 52.103 \text{ kcal/mole} \qquad A.5$$

From reactions A.3 through A.5 we get

$$C(\text{graphite}) + \frac{1}{2}H_2 = CH \text{ [diamond (110)]} \qquad \Delta H_f^0 = -1.357 \text{ kcal/mole} \qquad A.6$$
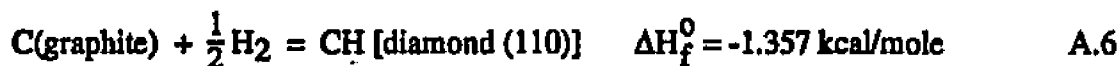
where ΔH_f^0 is the heat of formation of diamond (110) surface at 298 K. Since the bond entropy is inversely proportional to bond energy [3], a proportionality constant, K_D, was calculated in chapter 3 from the entropy of bulk diamond and the C-C bond energy in

diamond. The value of K_D is assumed to be same for the surface C-H bond. The entropy of hydrogenated diamond (110) surface, using the value of the proportionality constant K_D calculated in chapter 3, is given by

$$S^0_{298}[\text{diamond (110)}] = \frac{3}{2}\frac{K_D}{E(C\text{-}C)} + \frac{K_D}{E(C\text{-}H)_t}$$

$$= \frac{3}{2} \times \frac{25003}{85480} + \frac{25003}{96530} = 0.698 \text{ cal/mole-K} \qquad \text{A.7}$$

C.2 Unreconstructed Hydrogenated Diamond (100) Surface

Fig. C.2(a) is a schematic diagram of the plan view of the unreconstructed hydrogenated diamond (100) surface. The large open circles represent surface carbon atoms and the shaded circles represents carbon atoms at different levels below the surface. The small open circles represent hydrogen atoms bonded to the surface carbon atoms. Fig. C.2(b) shows the bonding configuration of the carbon atom on the diamond (100) surface. A carbon atom at the surface of a unreconstructed hydrogenated diamond (100) surface makes two bonds with carbon atoms in the diamond lattice and one bond each with two hydrogen atoms. Thus, the heat of atomization of a mole of surface carbon atoms on diamond (100), using values presented in Table 3.6, is given by

$$\Delta H_a [\text{diamond (100)}] = 2\frac{1}{2}E(C\text{-}C) + 2.E(C\text{-}H)_t$$

$$= 2\frac{1}{2}(85.48) + 2(96.53) = 280.02 \text{ kcal/mole} \qquad \text{A.8}$$

(a)

C Atoms Below
Surface

H Atom

Surface C Atom

(b)
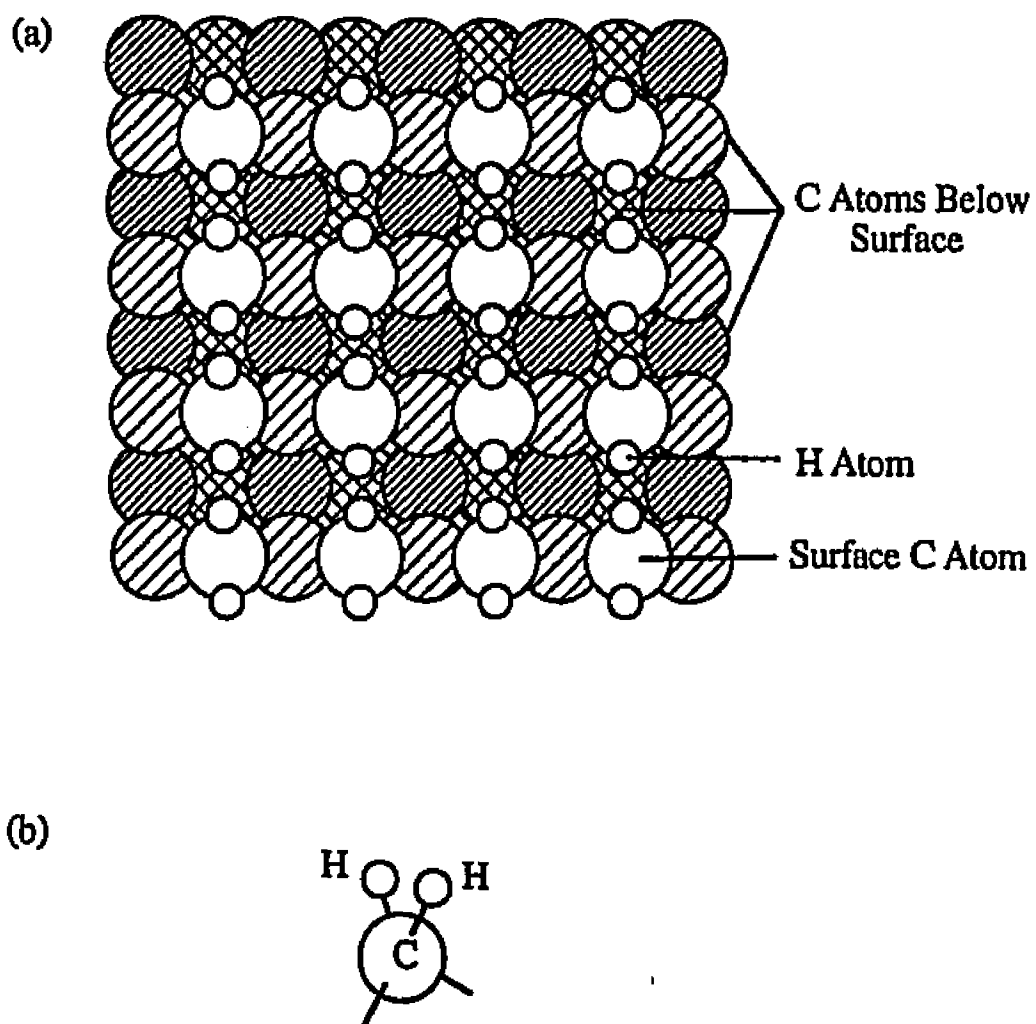
Fig. C.2 Schematic diagram of (a) unreconstructed hydrogenated diamond (100) surface
and (b) bonding configuration of a carbon atom on the (100) surface.

It should be noted that the steric hinderence between hydrogen atoms on the surface has not been accounted for in this calculation. The atomization of surface carbon atoms on diamond (110) using bond energy contributions is given by

$$CH_2 \, [\text{diamond (100)}] = C(g) + 2H(g) \qquad \Delta H_a = 280.02 \, \text{kcal/mole} \qquad \text{A.9}$$

From reactions A.4, A.5 and A.9 we get

$$C(\text{graphite}) + H_2 = CH_2 \, [\text{diamond (100)}] \qquad \Delta H_f^0 = -4.524 \, \text{kcal/mole} \qquad \text{A.10}$$
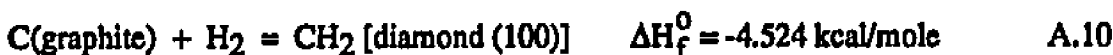
where ΔH_f^0 is the heat of formation of diamond (100) surface at 298 K. The entropy of hydrogenated diamond (100) surface is given by

$$S_{298}^0 [\text{diamond (100)}] = 2 \cdot \frac{1}{2} \cdot \frac{K_D}{E(C\text{-}C)} + 2 \cdot \frac{K_D}{E(C\text{-}H)_t}$$

$$= 2 \cdot \frac{1}{2} \cdot \frac{25003}{85480} + 2 \cdot \frac{25003}{96530} = 0.8066 \, \text{cal/mole-K} \qquad \text{A.11}$$

C.3 Hydrogenated Graphite (10$\bar{1}$0) Surface

A schematic diagram of the plan view of hydrogenated graphite (10$\bar{1}$0) surface is presented in Fig C.3(a). The large open circles represent surface carbon atoms and the small circles represent hydrogen atoms. The shaded circles represent carbon atoms at different levels below the surface. Fig C.3(b) and (c) show the bonding configurations of hydrogenated carbon atoms near the surface. As can be seen from Fig. C.3(a) half the hydrogenated carbon atoms near the surface have a configuration shown in Fig. C.3(b) while the other
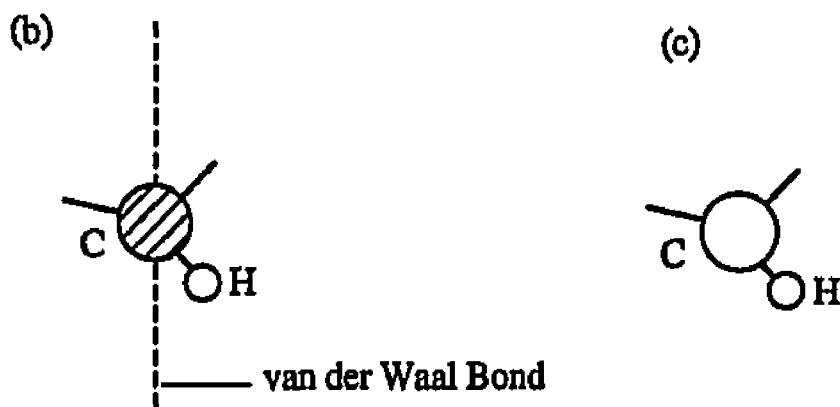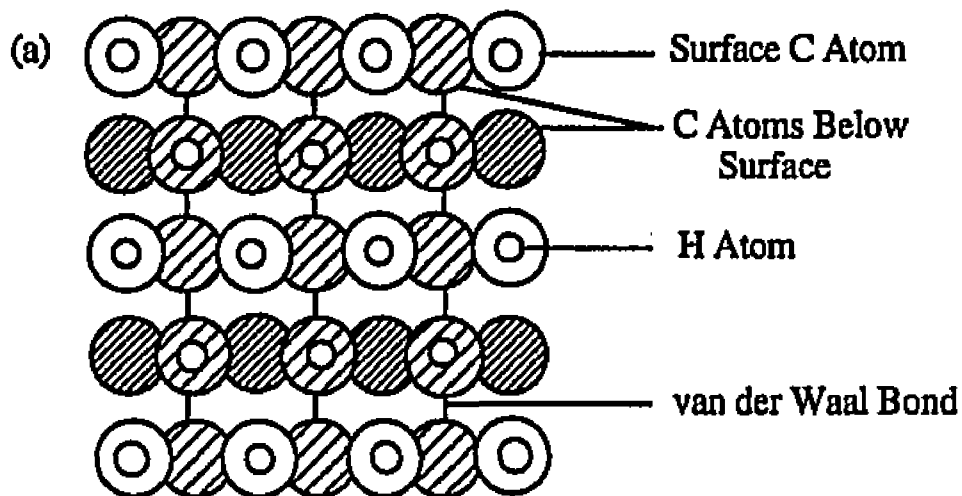
Fig. C.3 Schematic diagram of(a) hydrogenated graphite (10Ī0) surface and bonding configuration of a surface carbon atom that (b) makes van der Waal bonds and (c) does not make van der Waal bonds.

half have a configuration corresponding to Fig. C.3(c). The sp^2 hybridized surface carbon atom on the hydrogenated graphite $(10\bar{1}0)$ makes carbon-carbon bonds with two other sp^2 hybridized carbon atoms in the graphite lattice and one bond with a surface hydrogen atom. From Fig. C.3(b) and (c) it is observed that the C-C bond is of the type ^{H}>C-C< and the C-H bond is of the type >C-H. In addition to the C-C and C-H bonds, every other carbon atom on the surface makes van der Waal bonds with carbon atoms in adjacent (0001) planes. Since each C-C bond is shared by two carbon atoms, the energy associated with the surface carbon atom due to C-C bonds is 2 (1/2) E(^{H}>C-C<). Furthermore, for every mole of surface carbon atoms 1/2 a mole of carbon atoms make one van der Waal bond each with two carbon atoms in adjacent (0001) planes. Since each van der Waal bond is shared by two carbon atoms, the energy associated with a mole of the surface carbon atoms due to van der Waal bonds is 2 (1/2) (1/2) $E_{v.b}$. Thus, the heat of atomization of a mole of carbon atoms on the graphite $(10\bar{1}0)$ surface, using values presented in Table 3.6, is given by

$$\Delta H_a \text{ [graphite } (10\bar{1}0]] = 2.\frac{1}{2} E(^H\text{>C-C<}) + E(\text{>C-H}) + \frac{1}{2} E_{v.b}$$

$$= 114.3 + 100.53 + 0.5 \ (4.18) = 216.92 \text{ kcal/mole} \qquad A.12$$

Thus, the atomization of carbon atoms on graphite $(10\bar{1}0)$ surface is given by

$$CH \text{ [graphite } (10\bar{1}0)] = C(g) + H(g) \qquad \Delta H_a = 216.92 \text{ kcal/mole} \qquad A.13$$

From reactions A.4, A.5 and A.13 we get

$$C(\text{graphite}) + \frac{1}{2}H_2 = CH \text{ [graphite (10$\bar{1}$0)]} \qquad \Delta H_f^0 = 6.473 \text{ kcal/mole} \qquad A.14$$

where ΔH_f^0 is the heat of formation of graphite (10$\bar{1}$0) surface at 298 K. The entropy of graphite (10$\bar{1}$0) surface, using the value of $K_G = 10322$ cal^2/mole^2 K calculated in chapter 3, is given by

$$S_{298}^0[\text{graphite (10$\bar{1}$0)}] = 2\cdot\frac{1}{2} \frac{K_G}{E(^H{>}C\text{-}C{<})} + \frac{K_G}{E({>}C\text{-}H)} + \frac{1}{2} \frac{K_G}{E_{v.b}}$$

$$= \frac{10322}{114300} + \frac{10322}{100530} + \frac{1}{2}\cdot\frac{10322}{4180} = 1.428 \text{ cal/mole-K} \qquad A.15$$

C.4 Hydrogenated Graphite (11$\bar{2}$0) Surface

Fig. C.4(a) presents a schematic diagram of the plan view of the graphite (11$\bar{2}$0) surface. The large open circles are surface carbon atoms and the small circles are hydrogen atoms bonded to the surface carbon atoms. The hashed circles are carbon atoms below the surface. The bonding configuration of surface carbon atoms, shown in Fig C.4(b), indicates that the sp^2 hybridized surface carbon atom on the hydrogenated graphite (11$\bar{2}$0) makes a carbon-carbon bond with a sp^2 hybridized carbon atoms in the graphite lattice, a carbon-carbon bond with an adjacent surface carbon atom and one bond with a hydrogen atom. Furthermore, every other carbon atom on the surface makes van der Waal bonds with carbon atoms in adjacent (0001) planes. The C-C bond between surface carbon atoms is a $^H{>}C\text{-}C{<}^H$ type bond. The C-C bond between a surface carbon atom and a carbon atom in the graphite lattice is $^H{>}C\text{-}C{<}$ type. Since each C-C bond is shared by two C atoms, only half the energy of each type of bond is associated with a surface carbon atom.
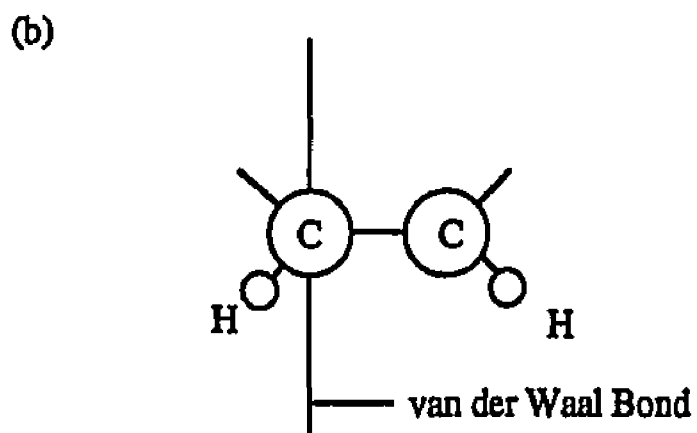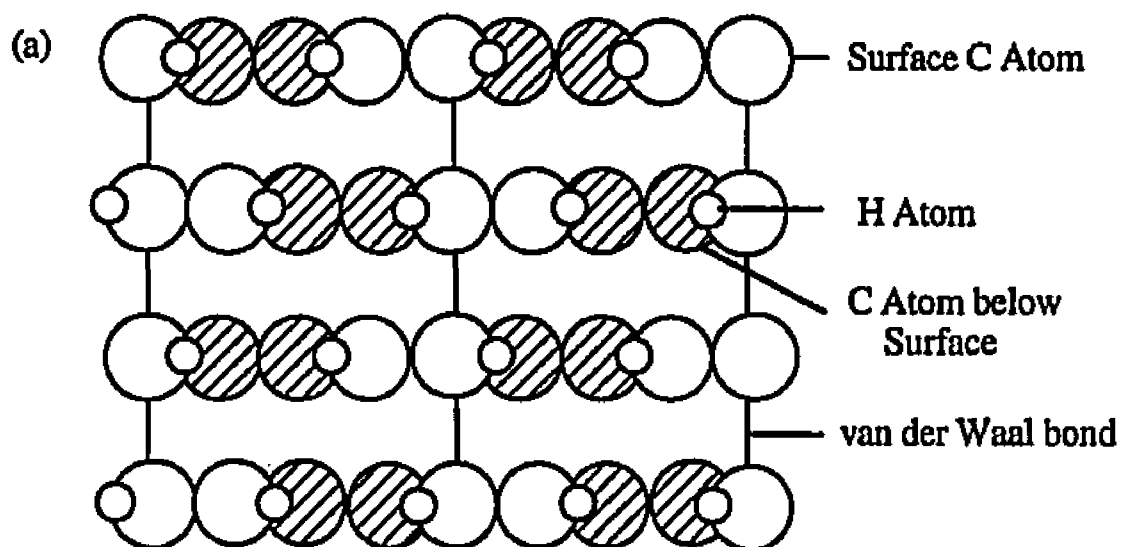
Fig C.4 Schematic diagram of (a) hydrogenated graphite $(11\overline{2}0)$ surface and (b) bonding configuration of carbon atoms on the surface.

On the graphite (11$\bar{2}$0) surface, like in the case of graphite (10$\bar{1}$0) surface, one out of every two surface carbon atoms makes two van der Waal bonds, one each with a carbon atom in an adjacent (0001) plane. Thus, the energy associated with a mole of surface carbon atoms due to van der Waal bonds is 0.5 $E_{v,b}$. The heat of atomization of a mole of carbon atoms on the graphite (11$\bar{2}$0) surface, using values presented in Table 3.6, is given by

$$\Delta H_a \text{ [graphite (11}\bar{2}\text{0)]} = \frac{1}{2} E(^H{>}C\text{-}C{<}) + \frac{1}{2} E(^H{>}C\text{-}C{<}^H) + E({>}C\text{-}H) + \frac{1}{2} E_{v,b}$$

$$= \frac{1}{2}(114.30) + \frac{1}{2}(119.17) + 100.53 + \frac{1}{2}(4.18) = 219.36 \quad \text{A.16}$$

Thus, the atomization of surface carbon atoms on graphite (11$\bar{2}$0) is given by

$$\text{CH [graphite (11}\bar{2}\text{0)]} = C(g) + H(g) \qquad \Delta H_a = 219.36 \text{ kcal/mole} \qquad \text{A.17}$$

From reactions A.4, A.5 and A.16 we get

$$C(\text{graphite}) + \frac{1}{2} H_2 = \text{CH [graphite (11}\bar{2}\text{0)]} \quad \Delta H_f^0 = 4.038 \text{ kcal/mole} \qquad \text{A.18}$$
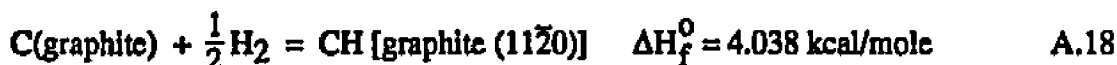
where ΔH_f^0 is the heat of formation of graphite (11$\bar{2}$0) surface at 298 K. The entropy of hydrogenated graphite (11$\bar{2}$0) surface, calculated using the value of the proportionality constant K_G calculated in chapter 3, is given by

$$S_{298}^0 \text{[graphite (11}\bar{2}\text{0)]} = \frac{1}{2} \cdot \frac{K_G}{E(^H{>}C\text{-}C{<})} + \frac{1}{2} \cdot \frac{K_G}{E(^H{>}C\text{-}C{<}^H)} + \frac{K_G}{E({>}C\text{-}H)} + \frac{1}{2} \frac{K_G}{E_{v,b}}$$

$$= \frac{1}{2} \cdot \frac{10322}{114300} + \frac{1}{2} \cdot \frac{10322}{119170} + \frac{10322}{100530} + \frac{1}{2} \cdot \frac{10322}{4180}$$

$$= 1.426 \, \text{cal/mole-K} \hspace{4cm} \text{A.19}$$

C.5 References

1. J. D. Cox and G. Pilcher, *Thermochemistry of Organic and Organometallic Compounds* (Academic Press, New York, NY, 1970).

2. JANAF Thermochemical Tables, vol. 14, 3rd ed., (American Institute of Physics, New York, NY, 1985).

3. R. A. Swalin, *Thermodynamics of Solids* (Wiley, New York, NY, 1967).

VITA

Kanishka Tankala was born in Mandapeta, India, on 22 July 1964. After completion of his high school education in 1982, he joined Hindu College, Delhi University, Delhi, India, and graduated with a B. Sc.(H) degree in Physics in 1985. He then obtained a B.E. degree in Metallurgy from the Indian Institute of Science, Bangalore, India, in 1988. He was awarded the K. K. Malik gold medal for being adjudged the best B. E. student in the Department of Metallurgy in 1988. He then joined The Pennsylvania State University to pursue graduate studies in Metals Science and Engineering. He obtained his M.S. degree in 1991, and was awarded the Xerox Research Achievement Award for his work. He continued his graduate study at The Pennsylvania State University leading to a Ph.D. degree in Metals Science and Engineering. He was a winner of The American Vacuum Society student prize in 1992. He is a member of Materials Research Society, American Vacuum Society and Tau Beta Pi engineering honors society. He is a author/co-author of eleven publications. The following is a selected list of his publications.

1. K. Tankala and T. DebRoy, "Transport Phenomena in the Scale-up of Hot Filament Assisted Chemical Vapor Deposition Reactors," *Surface and Coatings Technology*, 62, 349 (1993).

2. K. Tankala, T. DebRoy, W. A. Yarbrough and C. J. Robinson, "Modeling of Substrate Surface Temperature Distribution during Hot Filament Assisted Chemical Vapor Deposition of Diamond," *Diamond and Related Materials*, 1, 1177 (1992).

3. K. Tankala and T. DebRoy, "Modeling of the Role of Atomic Hydrogen during Hot Filament Assisted Chemical Vapor Deposition of Diamond," *J. Appl. Phys.*, 72(2), 712 (1992).

4. W. A. Yarbrough, K. Tankala, M. Mecray and T. DebRoy, "Hydrogen Assisted Heat Transfer during Diamond Growth using Carbon and Tantalum Filaments," *Appl. Phys. Lett.*, 60(17), 2068 (1992).

5. W. A. Yarbrough, K. Tankala and T. DebRoy, "Diamond Growth with Locally Supplied Methane and Acetylene," *J. Mater. Res.*, 7(2), 379 (1992).

6. K. Tankala, M. Alam and T. DebRoy, "Oxidation of Diamond Films Synthesized by Hot Filament Assisted Chemical Vapor Deposition," *J. Mater. Res.*, 5(11), 2483 (1990).

7. T. DebRoy, K. Tankala, W. A. Yarbrough and R. Messier, "Role of Heat Transfer and Fluid Flow in the Chemical Vapor Deposition of Diamond," *J. Appl. Phys.*, 68(11), 2424 (1990).